Heavy Ion Physics

I) Quantum chromodynamics: the deconfinement/chiral transition.

Quantum chromodynamics is believed to be a well established theory of strong interactions.

QCD is:

i) a non-abelian gauge fiedd theory whose gauge groups is $SU(3)$ (color)

ii) It has $(N^2-1) \equiv (3^2-1) = 8$ gauge bosons called gluons

iii) Matter particles are 1/2 spin quarks appearing in six different flavors:

$$\begin{pmatrix} u \\ d \end{pmatrix} ; \begin{pmatrix} c \\ s \end{pmatrix} ; \begin{pmatrix} t \\ b \end{pmatrix}$$

iv) the current masses of quarks are

$m_0 = 1.5$ To 3.3 MeV

tilibra

$m_d = 3.5$ To 6.0 MeV

$m_s = 104^{+26}_{-34}$ MeV

$m_c = 1.27^{+0.07}_{-0.11}$ GeV

$m_b = 4.20^{+0.17}_{-0.07}$ GeV

$m_t = 171.2 \pm 2.1$ GeV.

- Masses of u, d and s quarks are estimates of the so called current quark masses in the mass independent subtraction scheme $\overline{MS}$ at the scale $\mu \cong 2$ GeV.

- Masses of the c, b quarks are the running masses in the $\overline{MS}$ scheme

- These are not constituent quark masses!

In any case, note that whereas the masses of quarks u, d and s are of the order of some MeV's, masses of quarks c, b and t are of the order of some GeV's until some of the order of hundred of GeV's.
Then, while the u, d and s quarks are considered as light, the other

tilibra

three are heavy and will not play any role in the discussion along their course because their masses are much larger than the energy scale of a few hundred of MeV's in which we are interested.

The quarks u and d will be often considered as massless

- Quantum Chromodynamics is a renormalizable field theory and, as in all field theories of this kind, the coupling constant g is a function of the energy scale!

$$g \equiv g(Q)$$

- QCD has the remarkable property of asymptotic freedom:

$$\lim_{Q \to \infty} g(Q) = 0$$

Thus, perturbation theory can be used in all processes involving a large momentum transfer, the so called "hard processes". That aspect of QCD has been extensively tested, being

tilibra

the cleanest test the deep Inelastic Scattering (DIS) of leptons on nucleons.

- QCD has been extensively tested both from the theoretical as well as the experimental point of view and there is almost no doubt that QCD reproduces all the observed patterns of strong interactions.

However, the accuracy of the comparison is no better than a few percent, due to theoretical and experimental uncertainties

- When the energy scale decreases, the counterpart of asymptotic freedom is that the coupling constant increases, leading to a breakdown of perturbation theory as a series expansion in powers of $g^2(Q)$

- Processes with small momentum transfer (low Q) are called as "soft processes" and this name includes small momentum transfer processes as well as low energy properties of hadrons. The reason for the last is that (assuming massless quarks to simplify the discussion) all the hadron masses, for example, must

be proportional to the QCD scale Λ:

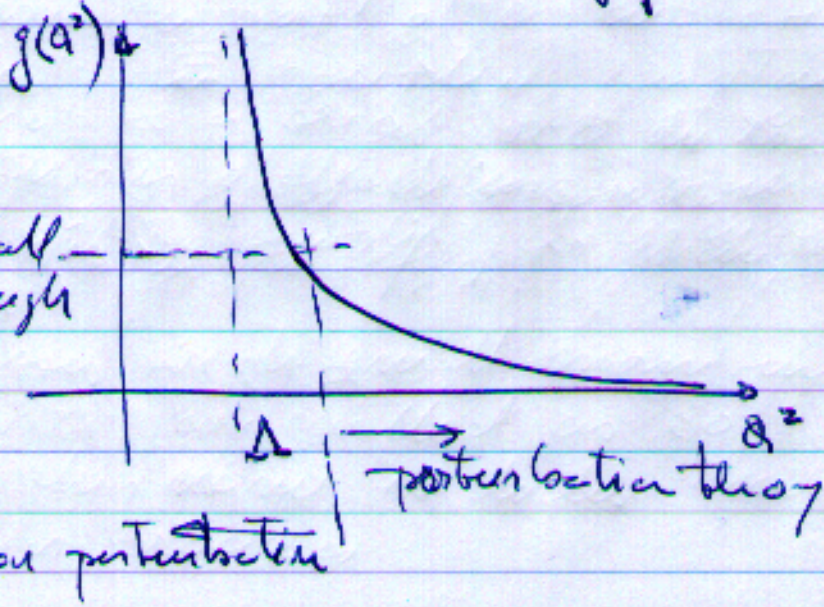
$$\Lambda = \lim_{Q\to\infty} Q\, e^{-\frac{1}{2}\beta_0 g^2(Q^2)} \left[\beta_0 g^2(Q^2)\right]^{-\beta_1/2\beta_0^2}$$

where g is the running coupling constant and β_0, β_1 are the first two coefficients of the renormalization group β-function.

Clearly, the expression for Λ is non perturbative.

In summary:

i) The coupling constant of QCD depends on the energy scale as



ii) the perturbative regime of QCD has been extensively tested

iii) In the non-perturbative regime, two main possibilities exist:

a) Low energy models which attempt to include some of the QCD Lagrangian features

b) Lattice QCD

a) Low energy models

The most interesting model is the effective chiral Lagrangian. It is based on the existence of the pion which is presumably a Goldstone boson that would be massless in the case of massless u and d quarks

The corresponding broken symmetry is the chiral $SU(2) \times SU(2)$ symmetry. The chiral Lagrangian model uses this property as the starting point.

In spite of its success, this model cannot be used in any serious comparison between QCD and experiment.

tilibra

b) Lattice QCD

In principle limited only by computing power. Lattice QCD has been decisive in convincing the physicists that a phase transition should occur at sufficiently high temperatures or densities.

At $T=0$ and for densities of the order of nuclear density, quarks and gluons are confined in hadrons.

For $T_c \simeq 150$ MeV one may obtain a gas of almost free quarks and gluons, the so called Quark-Gluon-Plasma (QGP)

The same situation may occur at $T=0$ for sufficiently high densities (or better, large chemical potential)

The occurrence of the phase transition is conceptually important:

i) it implies a new state of matter

ii) in the standard cosmology this state of matter should prevail during the beginning of the universe, until a time

of order $10^{-6} - 10^{-5}$ s after the Big-Bang

iii) It could also occur in the core of heavy neutron stars and also be produced in heavy ion collisions at large energy.

- Additional comments

i) at high Temperature, the only available scale is temperature itself.

ii) the coupling constant goes as

$$g(T) \sim \frac{1}{\ln(T/\Lambda)}$$

and for large T the QGP is close to an ideal gas.

iii) There are, however, several scales which can spoil the above simple picture by infrared divergencies!

$l_p = 1/T$ → perturbative scale

$l_{el} = 1/gT$ → electric or Debye scale

$l_{mag} = 1/g^2T$ → magnetic scale

tilibra

leading to a hierarchy of scales.

- Example of deconfinement/chiral transition: the bag model

The bag model is a simple model which incorporates, in a crude way, two of the main features of QCD: asymptotic freedom and confinement.

Hadrons in the bag model are bubbles of perturbative vacuum (bags) in a confining medium. Inside the bag, quarks move freely and in the simplest approximation, there is no interactions among quarks.

Outside the bag, quarks and gluons cannot appear as free particles. This is achieved by assuming a constant energy density B for the vacuum which keeps quarks and gluons confined.

Assuming a spherical bag, the energy of the hadron is

$$E_H = \frac{4\pi}{3} R^3 B + \frac{C}{R}$$

where the first term is associated with

tilibra

volume of the bag and the second is the kinetic energy

The radious of the bag is found by minimizing the energy E_H with respect to R:

$$R = \left(\frac{C}{4\pi B}\right)^{1/4},$$

the hadron mass is

$$M = \frac{16\pi}{3} R^3 B$$

and the pressure P is

$$P = -\frac{\partial E_H}{\partial V} = -B + \frac{C}{4\pi R^4}$$

In equilibrium the total pressure vanish by balancing the vacuum with the kinetic energy contributions.

In order to derive the condition for a deconfinement phase transition, we have to compare the thermodynamical function.

tilibra

Interlude: Quantum Statistical Mechanics

1) Ensembles

In equilibrium statistical mechanics one encounters three types of ensemble:

1) Microcanonical ensemble:

Describes an isolated system which has fixed energy E, fixed particle number N and fixed volume V

2) Canonical ensemble

used to describe a system in contact with a heat reservoir at a temperature T. The system can freely exchange energy with the reservoir and T, N and V are fixed

3) Grand Canonical ensemble

used to describe a system which can exchange particles as well as energy with a reservoir. T, V and the chemical potential μ are fixed.

tilibra

In the case of a relativistic quantum system, where particles can be created and destroyed, it is straightforward to compute observables in the grand canonical ensemble. So we will concentrate the discussion on it along these lectures.

Consider a system described by a Hamiltonian H and a set of conserved number operators $\hat{N}_i$ (for instance, in relativistic QED, the number of electrons minus the number of positrons, which is a conserved number)

The number operators $\hat{N}_i$ must be hermitian and must commute with H, as well as with each other.
The number operators must also be extensive in the sense that the usual thermodynamic limit can be taken.

The statistical density matrix is

$$\hat{\rho} = \exp\left[-\beta\left(H - \mu_i \hat{N}_i\right)\right]$$

$$\beta = T^{-1} \qquad (\text{we use } k_B = 1)$$

where a summation over i is implicit.

tilibilia

The ensemble average of an operator $\hat{A}$ is given by

$$A = \frac{\mathrm{Tr}\,\hat{\rho}\hat{A}}{\mathrm{Tr}\,\hat{\rho}}$$

and the grand canonical partition function is defined as

$$Z = \mathrm{Tr}\,\hat{\rho}$$

From the function Z, all other standard thermodynamical properties may be determined, for example

$$P = T\frac{\partial \ln Z}{\partial V} \quad ; \quad N_i = T\frac{\partial \ln Z}{\partial \mu_i}$$

$$S = \frac{\partial (T \ln Z)}{\partial T} \quad ; \quad E = -PV + TS + \mu_i N_i$$

II) One bosonic degree of freedom

Consider a time-independent single-particle quantum mechanical state which can be occupied by bosons.

Each boson in this state has the same energy ω. There may be $0, 1, 2, \ldots$ or any number of bosons in that state.

tilibra

Call the state of the system as $|n\rangle$, meaning that there are n particles in the state. The state $|0\rangle$ is the vacuum.

The properties of the states are:

i) $\langle n|n'\rangle = \delta_{nn'}$ orthogonality

ii) $\sum_{n=0}^{\infty} |n\rangle\langle n| = 1$ completeness

$\langle n|$ and $|n'\rangle$ are row and column vectors in a infinite-dimensional vector space. The operation in i) is the inner product and ii) is an infinite dimensional unit matrix

We introduce also the creation and annihilation operators by

$$a^+|n\rangle = (n+1)^{1/2}|n+1\rangle$$

$$a|n\rangle = n^{1/2}|n-1\rangle$$

with the properties

$$a|0\rangle = 0$$

$$\hat{N}|n\rangle = a^+a|n\rangle = n|n\rangle$$

tilibra

$$[a, a^+] = aa^+ - a^+a = 1$$

$$|n\rangle = \frac{1}{(n!)^{1/2}} (a^+)^n |0\rangle$$

The last property shows how to build all states $|n\rangle$ from the vacuum by repeated application of the creation operator.

Since each boson in the state has the same energy ω, the hamiltonian must be, up to an additive constant, ω times the number operator:

$$H = \frac{1}{2}\omega(aa^+ + a^+a) = \omega\left(a^+a + \frac{1}{2}\right)$$

$$= \omega\left(\hat{N} + \frac{1}{2}\right)$$

where the additive term $\frac{1}{2}\omega$ is the zero point energy. This term can be usually ignored, so we will take

$$H = \omega \hat{N}$$

States $|n\rangle$ are simultaneously number and energy eigenstates, therefore, we can assign a chemical potential to the particles.

tilibra

The partition function is

$$Z = \mathrm{tr}\, e^{-\beta(H-\mu\hat{N})} = \mathrm{tr}\, e^{-\beta(\omega-\mu)\hat{N}}$$

$$= \sum_{n=0}^{\infty} \langle n | e^{-\beta(\omega-\mu)\hat{N}} | n \rangle =$$

$$= \sum_{n=0}^{\infty} e^{-\beta(\omega-\mu)n} = \frac{1}{1-e^{-\beta(\omega-\mu)}}$$

The mean number of bosons is

$$N_i = T \frac{\partial \ln Z}{\partial \mu_i} = \frac{1}{e^{\beta(\omega-\mu)}-1}$$

and the mean energy is

$$E = \omega N$$

Note that N ranges continuously from zero to infinity

III) <u>One fermionic degree of freedom.</u>

The Pauli exclusion principle forbids the occupation of a single-particle state by more than one fermion. Then there are only two states in the system:

$|0\rangle$ and $|1\rangle$

tilibra

The action of the fermion creation and annihilation operators is as follows:

$$a^\dagger|0\rangle = |1\rangle \,, \quad a|1\rangle = |0\rangle$$

$$a^\dagger|1\rangle = 0 \,; \quad a|0\rangle = 0$$

and they have the property of nilpotency (ie, their square is zero)

$$aa = a^\dagger a^\dagger = 0$$

The number operator is $a^\dagger a$ and

$$\hat{N}|0\rangle = a^\dagger a|0\rangle = 0 \,; \quad \hat{N}|1\rangle = a^\dagger a|1\rangle = |1\rangle$$

They also satisfy the anti-commutation relation

$$aa^\dagger + a^\dagger a = \{a, a^\dagger\} = 1$$

The hamiltonian is taken as

$$H = \frac{1}{2}\omega\left(a^\dagger a - aa^\dagger\right) = \omega\left(\hat{N} - 1/2\right)$$

Notice that the zero point energy is equal in magnitude but opposite in sign to the bosonic case.

tilibra

The partition function is computed as in the previous case, except that the sum ends at $n=1$,

$$Z = \mathrm{Tr}\, e^{-\beta(H-\mu\hat{N})} = \sum_{n=0}^{1} \langle n| e^{-\beta(\omega-\mu)\hat{N}} |n\rangle$$

$$= 1 + e^{-\beta(\omega-\mu)}$$

The mean number of fermions is

$$N = \frac{1}{e^{\beta(\omega-\mu)}+1}$$

and the mean energy is ωN. Note that N ranges from 0 to 1.

IV) Non interacting particles in a box

Assume you have identical particles (either bosons or fermions) in a box with sides L. Assume also that they are non-interacting particles in equilibrium (for instance, you leave them to interact until equilibrium is reached, and then you turn-off all the interactions)

Imposing the condition that wave-functions vanish in the boundary means that an integral number of half wave lengths

fits in the distance L,

$$\lambda_x = 2L/l_x \; ; \; \lambda_y = 2L/l_y \; ; \; \lambda_z = 2L/l_z$$

with l_x, l_y, l_z positive integers.

The magnitude of each component of the momentum is

$$|p_i| = 2\pi/\lambda_i \qquad i = x, y, z$$

Quantum mechanics tell us that these relations hold for both non relativistic and relativistic motion, for both, bosons and fermions.

The hamiltonian is the sum of the hamiltonians for each mode:

$$H = \sum_i H_i \; ; \; N = \sum_i N_i \quad (i = x, y, z)$$

and the partition function is the product of the partition functions for each mode:

$$Z = \prod_i Z_i$$

or, equivalently

$$\ln Z = \sum_{l_x=1}^{\infty} \sum_{l_y=1}^{\infty} \sum_{l_z=1}^{\infty} \ln Z_{l_x, l_y, l_z}$$

tilibra

In the macroscopic limit, when $L \to \infty$, sums can be replaced by integrals ranging from 1 to ∞. As

$$dl_i = L\, d|p_i|/\pi$$

$$\left(|p_i| = 2\pi/\lambda_i = \frac{\pi}{L} l_i \Rightarrow \frac{d|p_i|}{dl_i} = \frac{\pi}{L} \right)$$

hence

$$\ln Z = \frac{L^3}{\pi^3} \int_0^\infty d|p_x| \int_0^\infty d|p_y| \int_0^\infty d|p_z| \ln Z_p$$

and dividing by 2 and extending the integrals to be between $-\infty$ and $+\infty$, we obtain

$$\ln Z = V \int_{-\infty}^{+\infty} \frac{d^3p}{(2\pi)^3} \ln Z_p \,.$$

Note that the total phase space integral $\int \frac{d^3p\, d^3x}{(2\pi)^3}$ has appeared in the definition of the partition function.

Recalling the previous results for bosons and fermions, we have

tilibra

$$\ln Z = V \int \frac{d^3p}{(2\pi)^3} \ln\left(1 \pm e^{-\beta(\omega-\mu)}\right)^{\pm 1} \quad (1)$$

where the (+) is for fermions and the (-) refers to bosons

From eq (1) we obtain

$$P = T \ln Z / V$$

$$N = V \int \frac{d^3p}{(2\pi)^3} \frac{1}{e^{+\beta(\omega-\mu)} \pm 1}$$

$$E = V \int \frac{d^3p}{(2\pi)^3} \frac{\omega}{e^{+\beta(\omega-\mu)} \pm 1}$$

The dispersion relation $\omega = \omega(p)$ permits the connection between p and ω. For relativistic particles it is

$$\omega = \left(p^2 + m^2\right)^{1/2}$$

For bosons which carry non conserved charge as photons and π^0's, $\mu = 0$. For electrically charged bosons as π^+ or π^- we can associate a chemical potential with the electric charge. Thus π^+ has $\mu = +\mu$ and π^- has $\mu = -\mu$ (Antiparticles have chemical

tilibra

potential of opposite sign to particles)
The total screened charge is

$$Q = V\int \frac{d^3p}{(2\pi)^3}\left(\frac{1}{e^{\beta(\omega-\mu)}-1} - \frac{1}{e^{\beta(\omega+\mu)}-1}\right)$$

and the total energy is

$$E = V\int \frac{d^3p}{(2\pi)^3}\left(\frac{\omega}{e^{\beta(\omega-\mu)}-1} + \frac{\omega}{e^{\beta(\omega+\mu)}-1}\right)$$

In addition, if bosons have non zero spin, the phase space integrals must be multiplied by the spin degeneracy factor $(2s+1)$.

An analog discussion holds for fermions

- End of Interlude -

Let us now return to the beg model. In order to derive the conditions for a deconfinement phase transition we have to compare their thermodinamical properties.
Let us start by looking at the ground potential, which is defined as

illibia

$$\Omega_b = \frac{1}{\beta} \ln Z =$$

$$= VT \int_{-\infty}^{+\infty} \frac{d^3p}{(2\pi)^3} \ln\left(1 - e^{-\beta(\omega - \mu)}\right)$$

for an ideal boson gas with one degree of freedom. For massless bosons and $\mu = 0$, after an integration by parts we get

$$\Omega = \frac{VT^4}{6\pi^2} \int_0^\infty \frac{x^3 dx}{e^x - 1} = -\frac{\pi^2 V T^4}{90}$$

So, in general, for a boson ideal gas with ν_b degrees of freedom we obtain

$$\Omega_{\nu_b} = -\nu_b \frac{\pi^2 V T^4}{90}$$

Using that

$$P = -\frac{\partial \Omega}{\partial V}$$

and the relation $E = 3PV$ which is valid for a ultrarelativistic ideal gas (Note: $E = 3PV$ is the equipartition of energy theorem for an ideal gas whose equation of state is $PV = kT$)

we obtain for the pressure and energy density ε

$$P = \nu_b \frac{\pi^2 T^4}{90} \; ; \quad \varepsilon = \frac{E}{V} = 3\left(\frac{\pi^2 T^4}{90}\nu_b\right) = \frac{\pi^2 T^4}{30}\nu_b$$

The entropy density, for $\mu = 0$ is simply derived from

$$\Omega = E - TS$$

which leads to

$$s \equiv \frac{S}{V} = \frac{4}{3}\frac{\varepsilon}{T}$$

The particle density can also be calculated as

$$n = \frac{N}{V} = \int \frac{d^3p}{(2\pi)^3} \frac{1}{e^{\beta\omega} - 1} = \frac{T^3}{2\pi^2}\int_0^\infty \frac{x^2\,dx}{e^x - 1}$$

$$= \frac{T^3}{\pi^2}\,\zeta(3) \simeq 1.202\,\frac{T^3}{\pi^2}$$

with ζ the Riemann ζ-function, $\zeta(3) \approx 1.202$. Note also that for massless particles $\omega = p$!

tilibra

For fermions, the grand potential is

$$\Omega_f = -VT \int_{-\infty}^{+\infty} \frac{d^3p}{(2\pi)^3} \ln\left[1 + e^{-\beta(\omega-\mu)}\right]$$

↑ Note the signs! ↑

For massless fermions, and taking into account particles and antiparticles, we obtain

particles ↓ anti-particles ↓

$$\Omega_f = -\frac{VT^4}{6\pi^2} \int_0^\infty p^3 dp \left[\frac{1}{e^{\beta(\omega-\mu)}+1} + \frac{1}{e^{\beta(\omega+\mu)}+1}\right]$$

$$= -\frac{V}{6\pi^2}\left[\frac{7\pi^4 T^4}{60} + \mu^2\frac{\pi^2 T^2}{2} + \frac{\mu^4}{4}\right]$$

Let us examine the possibility of a phase transition with zero chemical potential. In that case the hadronic system must consist mainly of pi neutral pions. Neglecting also the pion mass and using $\nu = 3$ for the three charged states of pions, the pressure of the plasma phase is

tilibra

$$P = \nu_b \frac{\pi^2 T^4}{90} + \frac{\nu_f \tfrac{7}{8} \pi^2 T^4}{6 \times 60 \pi^2} - B$$

$$= \left(\nu_b + \frac{7}{4} \nu_f \right) \frac{\pi^2 T^4}{90} - B$$

where the first two terms are the contribution of bosonic and fermionic degrees of freedom and we have added a free energy of BV representing the energy of the perturbative vacuum inside the confining medium.

If we use that the number of bosonic degrees of freedom is $2(N^2-1)$, where N is the number of colors, while $\nu_f = 2 N N_f$ with N_f the number of flavors ($N_f = 2$ for u and d flavors) we obtain

$$P = \frac{37}{90} \pi^2 T^4 - B$$

The equality of the pressure in the plasma and hadron phases gives us the critical temperature

$$\frac{37}{90} \pi^2 T^4 - B = -B + \frac{C}{4\pi R^4}$$

$$\frac{37}{90}\pi^2 T^4 = \frac{+C}{4\pi R^4}$$

and using that $R^4 = \frac{C}{4\pi B}$,

$$\frac{37}{90}\pi^2 T^4 = B$$

Thus

$$T_c = \left(\frac{90B}{37\pi^2}\right)^{1/4} \simeq 140 \text{ MeV}$$

for a bag constant of $B^{1/4} = 200$ MeV.

The bag model can be used to determine the transition line between the hadronic and plasma phases in the whole (μ, T) plane. However the model is less convincing for non-zero μ, as is clear from considering the $\mu = 0$ situation.

The baryonic density n_B is related to the baryonic chemical potential μ_B and to the nucleon mass m_N by

$$n_B = \frac{2}{3\pi^2}\left(\mu_B^2 - m_N^2\right)^{3/2}$$

tilibra

The critical chemical potential can be determined by writing the equality of the pressures with $\mu_B = 3\mu$, where μ is the quark chemical potential.

The result of this exercise is that the transition can only happens for a narrow range of the bag constant values, which seems to be difficult to understand from a physical point of view. Thus, the bag model does not seems to give too much information in the $T=0$, $\mu \neq 0$ case.

However, it is useful to have in mind the following orders of magnitude:

for $n_B \simeq 0.15\ fm^{-3} \rightarrow \mu \simeq 0.26\ GeV$

$\downarrow \times 5$ $\qquad\qquad$ $\downarrow \times 1.2$

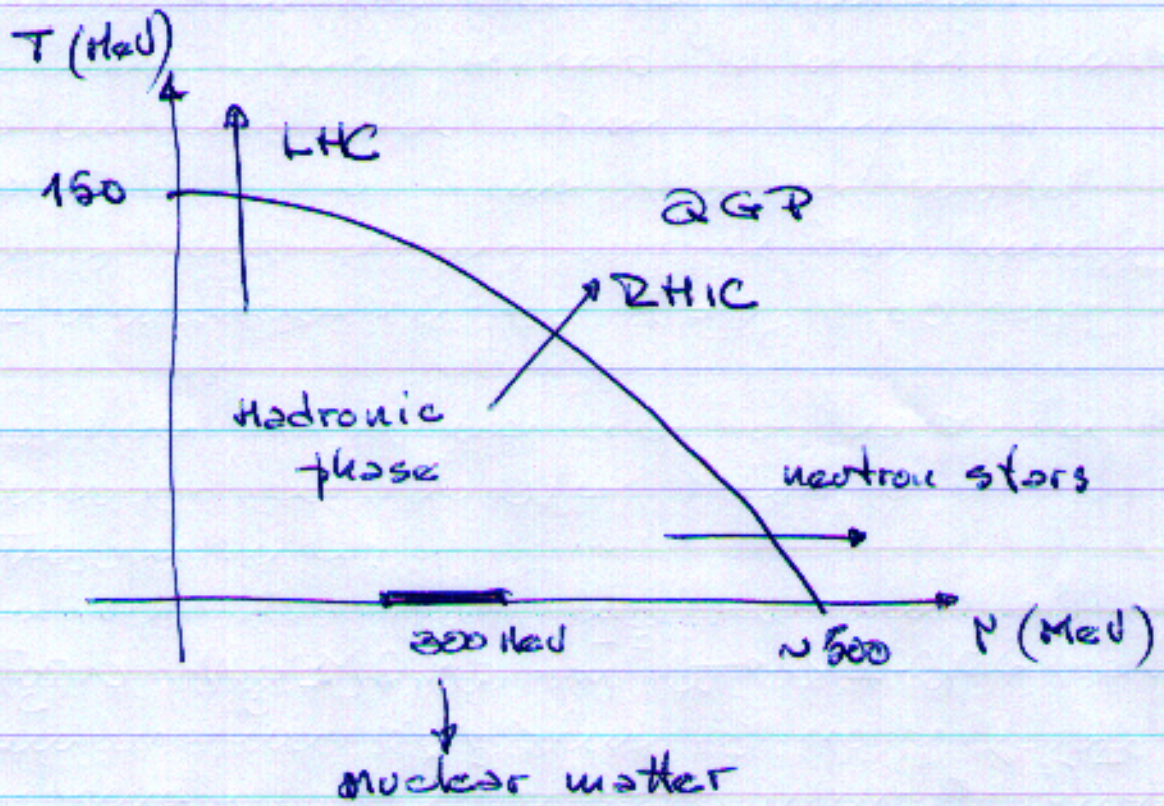
$n_B \simeq 0.75\ fm^{-3} \rightarrow \mu \simeq 0.45\ GeV$

where $n_B \simeq 0.15\ fm^{-3}$ is the ordinary nuclear density.

Lattice QCD confirms the value of $T_c \sim 190$ MeV for the critical temperature but there is no reliable estimation of the critical chemical potential

tilibra

In spite of the above, it is generally assumed that the transition should occur for a density of order 3 to 5 times the nuclear density. Thus the phase diagram in the (T, ρ) plane must be approximately as shown in the following figure:



Energy as a unit of temperature

$$\frac{1\,eV}{k_B} = \frac{1.6022 \times 10^{-19}\,J}{1.3806 \times 10^{-23}\,J/K} = 11604.50\,K$$

$$150\text{–}175\,MeV \sim (1.7\text{–}2.0) \times 10^{12}\,K$$

tilibra

II) Heavy Ion Collisions

One of the main reasons to be interested in hot QCD is the hope of production of QGP in collisions of ultrarelativistic heavy ions.

In the following we will show that, indeed, heavy ion collisions at sufficiently high energy are able to produce energy densities large enough for a phase transition to occur.

To start with, we shall give a short account of the thermal evolution of the collision.

In what follows, we will always view the collision in the center of mass frame; E_{cm} ($\sqrt{s}$) denotes the energy per nucleon in this frame, the z-axis is chosen along the collision axis and we will neglect transverse motion. Finally, for simplicity, we will restrict the discussion to collisions of identical nuclei with atomic number A.

The generally accepted picture for the collision of two ultrarelativistic

heavy nuclei rests on two concepts which are consistent with the present experimental data: i) Nuclear transparency and ii) inside-outside cascade.

i) Nuclear Transparency:

or leading particle effect, was first observed in nucleon-nucleon collisions: a large fraction (about 1/2) of the available energy is carried away by two secondary nucleons, which are called leading baryons

Similarly, in the collision of heavy nuclei, the baryonic number is carried away essentially by two systems of nucleons leaving the interaction region with large momentum in the center of mass.

Quantitatively,

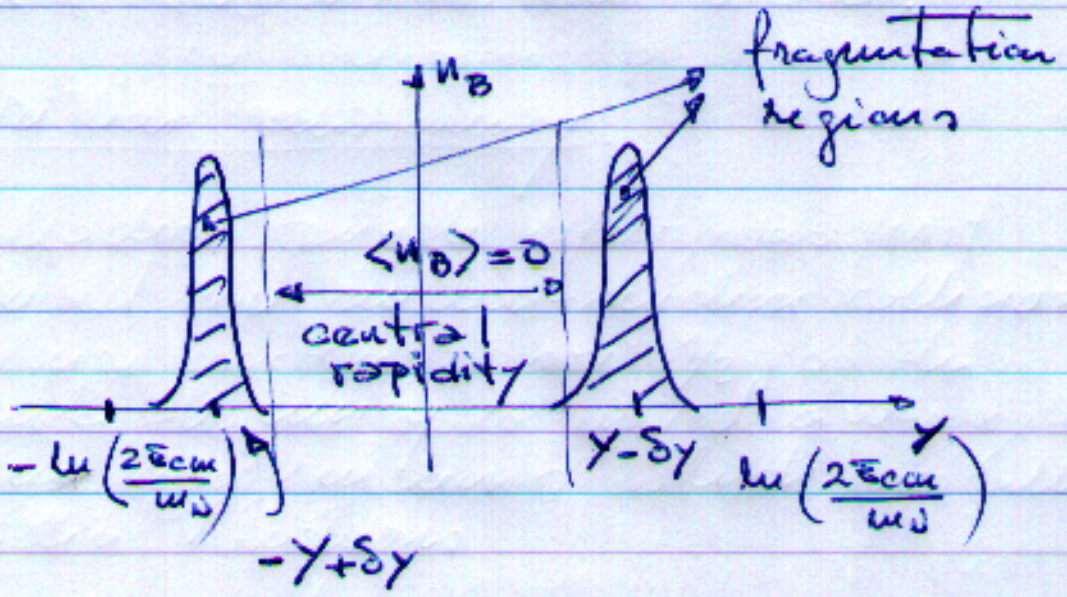
$$Y = \ln\left(\frac{2E_{cm}}{M_N}\right)$$

is the maximum rapidity in the collision. Recall that

$$Y = \frac{1}{2}\ln\left(\frac{E+P_z}{E-P_z}\right) = \ln\left(\frac{E+P_z}{M_T}\right)$$

tilibra

The rapidity distribution of the baryonic number is centered at $\pm (Y - \delta y)$



Nucleon - Nucleon collisions give $\delta y \sim 2$. For A-A collisions event generators suggest $\delta y \sim 3 - 3.5$

There is also a range $\cong \left[-(Y-2\delta y), +(Y-2\delta y)\right]$ where the baryonic number averages to zero. This is the so called central region, while the regions which carry the baryonic number are called as fragmentation regions

For a clean separation of the central and fragmentation regions one needs at least $Y \sim 5-6$, which implies $E_{cm} \gtrsim 100$ GeV.

ii) Inside - outside cascade:

in the rest frame an excited hadronic system decays in a characteristic time

$$\tau_0 \sim 1\ \text{fm}/c$$

However, in movement, the decay time of a hadronic system changes by the time dilation: slow systems disintegrate earlier than faster ones. This effect is the so called inside-outside cascade

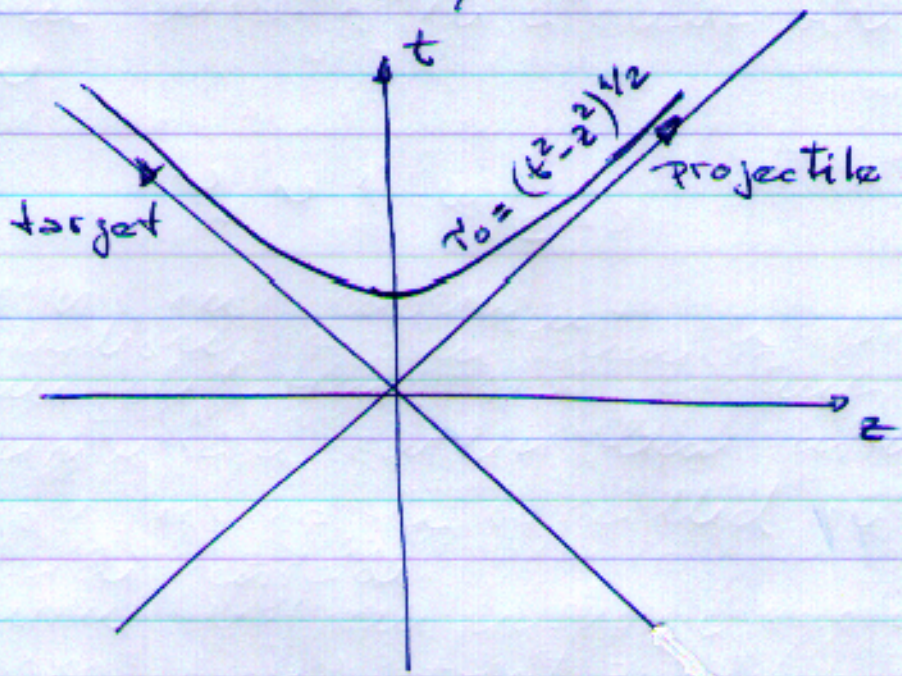
Assume that an hadronic system leaves the interaction point $z=0$ at time $t=0$ and moves freely with velocity v along the collision axes. Then, its proper time is

$$\tau = \left(t^2 - z^2\right)^{1/2} = t\left(1 - v^2\right)^{1/2}$$

A collection of hadronic systems created a $t=z=0$ will thus disintegrate on average on a hyperbola of constant proper time $\tau_0 = \left(t^2 - z^2\right)^{1/2}$; in a hydrodynamical description, the initial conditions for the fluid will be given on this hyperbola.

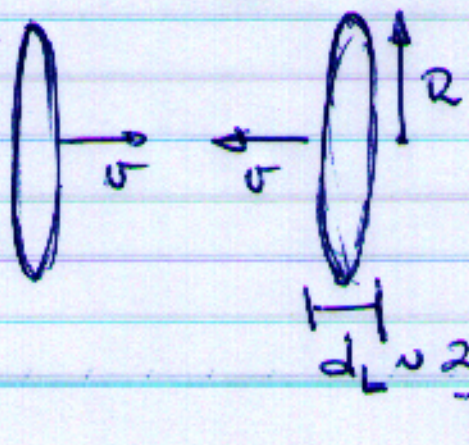
tilibra

Note that the initial conditions are not given at an initial time, but rather at an initial proper time.

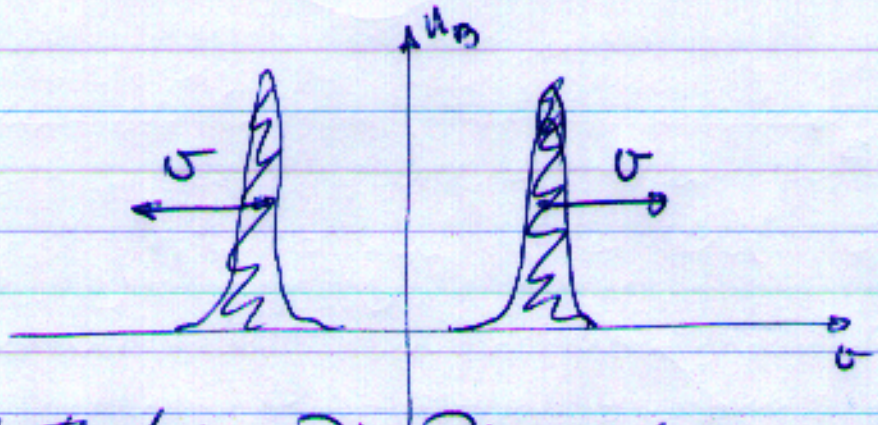


In summary the picture of the collision is as follows:

1) two Lorentz contracted nuclei with transverse radius R and longitudinal size $d_L \sim 2R m_N / E_{cm}$ collide during a time $\sim d_L / c$



2) The two nuclei cross each other and two Lorentz contracted systems recede from each other at high velocity carrying the baryonic number in opposite directions. Between them, there is baryonic matter with zero baryonic number



Note that for Pb-Pb collisions at the LHC energies, with $\sqrt{s}_{cm} \sim 2$ TeV,

$$d_L/c \sim 7 \times 10^{-3}\ fm/c \ll \tau_0$$

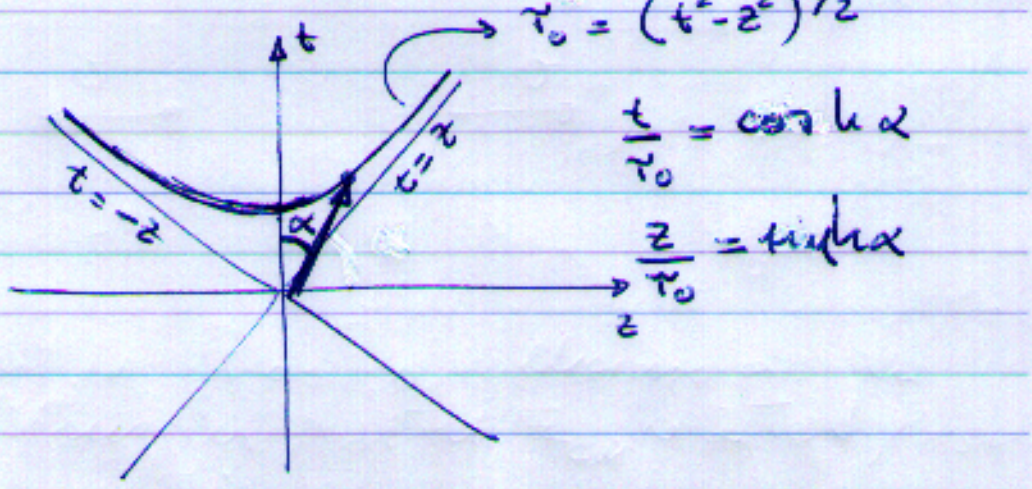
so that the duration of the collision may be neglected. For lower energies, the finite time of crossing has to be taken into account.

Let us concentrate now in the study of the central hadronic system. As said before, the central hadronic system carries zero baryonic number.

tilibra

In our picture, a collection of excited hadronic systems leaves the origin at $t=0$ and disintegrates on a hyperbola $(t^2-z^2)^{1/2}=\tau_0$. The coordinate which parametrizes a point on the hyperbola is denoted by α:

$$\alpha = \frac{1}{2} \ln \frac{t+z}{t-z}$$



The coordinate α can be identified with the rapidity.

Experimental data indicates that the particle density is approximately independent of the rapidity in the central region. Thus we can assume that the initial conditions on the hyperbola $\tau = \tau_0$ are invariant under Lorentz boosts of moderate velocity (so as to not leave the central region). These are the Bjorken's initial conditions.

tilibra

Let us assume now that we are dealing with a perfect relativistic fluid, for which we do not specify if it is a hadronic-like or plasma-like fluid.

Let us define now the rest frame of the fluid as the frame in which the energy flux is zero, and define the 4-velocity u^μ as

$$u^\mu = (1-v^2)^{-1/2}(1, \vec{v})$$

where $\vec{v}$ is the fluid velocity in the center of mass frame of the collision.

Assume now a locally conserved scalar density (like the baryon number) and its volume density measured in the rest frame of the fluid. For a perfect fluid there are no transport phenomena, so that there is no energy flux without scalar flux. This means that in the rest frame of the fluid the flux of any conserved quantity is zero:

$$\partial_\mu (n u^\mu) = 0 \qquad (1)$$

In a similar way we can write the conservation of the energy momentum

tilibra

tensor

$$\partial_\mu T^{\mu\nu} = 0 \qquad (2)$$

In the fluid rest frame we have

$$T^{00} = \varepsilon \quad ; \quad T^{ij} = P\,\delta_{ij}$$

where ε is the energy density and P the pressure. From Lorentz covariance follows that

$$T^{\mu\nu} = (\varepsilon + P)\,u^\mu u^\nu - P g^{\mu\nu} \qquad (3)$$

and contracting (2) with u^ν we obtain

$$u^\mu(\partial_\mu \varepsilon) + (\varepsilon + P)\,\partial_\mu u^\mu = 0$$

On the other hand, if there are conserved scalar quantities N_i, with associated densities n_i and chemical potentials μ_i, the following thermodynamical identities follow

$$d\varepsilon = T\,ds + \sum_i \mu_i\, dn_i \qquad (4a)$$

$$\varepsilon + P = Ts + \sum_i \mu_i n_i \qquad (4b)$$

where s is the entropy density

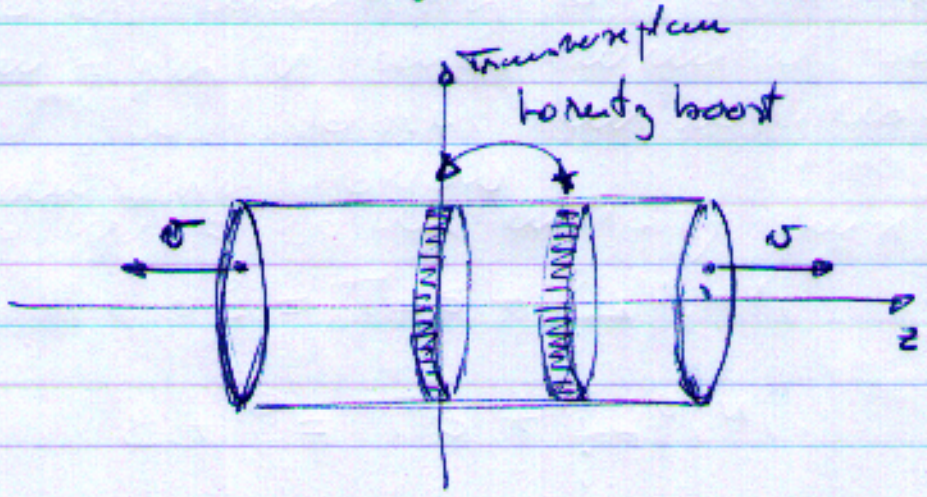
ilibra

Using now eqs (1) and (4a-4b), and assuming all the dependence to be a continuous function of space-time, the equation for entropy conservation follows:

$$\partial_\mu (s u^\mu) = 0$$

Now we can describe the longitudinal expansion in the central region, ignoring transverse expansion and using Bjorken conditions.

Due to Lorentz invariance of the hydrodynamical equations and the initial conditions, the properties of a slice of fluid around the longitudinal coordinate z can be deduced from those of the fluid at $z=0$ by a longitudinal Lorentz boost



tilibra

Let us use now the coordinates (τ, α) with

$$t = \tau \cosh\alpha$$

$$z = \tau \sinh\alpha$$

In this coordinate system, the components of a 4-vector V^μ read

$$V^\tau = V^0 \cosh\alpha - V^z \sinh\alpha$$

$$V^\alpha = -V^0 \sinh\alpha + V^z \cosh\alpha ,$$

then

$$\partial_\mu V^\mu = \frac{1}{\tau}\left(\frac{\partial(\tau V^\tau)}{\partial\tau} + \frac{\partial V^\alpha}{\partial\alpha} \right)$$

Now, the invariance of the initial conditions under Lorentz boosts, together with the Lorentz invariance of the hydrodynamical equations, requires that no quantity depends on α (as long as, for fixed τ, all points are on the same hyperbola) Then, considering a particular solution of the hydrodynamical equations given by

$$v^\alpha = 0 \; ; \; v^\tau = 1$$

the equation for entropy conservation reduces to

$$\frac{d}{d\tau}(\tau s) = 0 \qquad (5)$$

Note that for the above solution for the hydrodynamical equations, the fluid rapidity η coincides with the space-time rapidity α. On the other hand, eq. (5) implies that the entropy density decreases as the inverse of the proper time:

$$s \sim 1/\tau \qquad (6)$$

Since the system is expanding in the direction z, the volume of a slab of fluid in the rapidity range $[\eta, \eta+d\eta]$ increases with τ as

$$d^3x = \tau\, d\eta\, d^2x_\perp$$

in a frame where the fluid is at rest. Eq. (6) then means that the entropy contained in a given rapidity interval is conserved.
Assuming now that the system termalizes at a proper time $\tau_0 \simeq 1$ fm/c with an initial entropy density s_0, then

tilibra

$$s(\tau) = \frac{s_0 \tau_0}{\tau}$$

Let us turn now to numerical estimates. The total entropy in the rapidity interval $[y, y+dy]$ at a proper time τ_0 is

$$\Delta S = \pi R^2 s_0 \tau_0 \Delta y$$

Recalling from the previous section that

$$\Omega = E - TS$$

from which

$$s = \frac{S}{V} = \frac{4}{3}\frac{E}{T}$$

and

$$n = \frac{N}{V} = \frac{T^3}{\pi^2}\zeta(3)$$

which implies that

$$s = \frac{2\pi^4}{45\zeta(3)} n \simeq 3.6\, n$$

Thus

$$\Delta S \simeq 3.6\,\Delta N = \pi R^2 s_0 \tau_0 \Delta y$$

which can be written as

$$s_0 \tau_0 \simeq \frac{3.6}{\pi R^2} \frac{dN}{dy}, \qquad (7)$$

Eq (7) relates $s_0\tau_0$ to the rapidity density, which is an observable.

The rapidity density dN/dy in A-A collisions can be estimated from

$$\frac{dN}{dy} \sim A^{1.1} \frac{dN^\circ}{dy} \; ; \; \frac{dN^\circ}{dy} \simeq 0.9 \ln \frac{E_{cm}}{m_N}$$

where $\frac{dN^\circ}{dy}$ is the rapidity density in nucleon - nucleon collisions and A is the atomic number of nuclei. The exponent in A can be slightly higher than 1.1 because of multiple scattering but, 1.1 is a good estimate. With $\tau_0 \simeq 1\,fm/c$ we obtain, for Pb-Pb collisions,

$$s_0 \simeq 7.5 \ln \frac{E_{cm}}{m_N}\ fm^{-3}$$

tilibra

which for $E_{cm} \simeq 2$ TeV, and in the case of an ideal QGP with $N_f = 2$, gives a critical temperature of

$$T_0 \sim 300 \text{ MeV}$$

with an energy density

$$\varepsilon \sim 12.8 \frac{\text{GeV}}{\text{fm}^3}$$

for the plasma phase.
Note also that, as the baryonic number vanishes in the central region, the entropy is mainly carried by pions.

In the case of $\mu = 0$ we also have

$$\frac{s}{T}\frac{\partial T}{\partial s} = \frac{\partial P}{\partial \varepsilon} = c_s^2$$

where c_s is the velocity of sound ($c_s = 1/\sqrt{3}$ for an ideal ultra-relativistic gas).
Then, from entropy conservation

$$T = T_0 \left(\frac{\tau_0}{\tau}\right)^{c_s^2}$$

which shows that the temperature drops more slowly than the entropy density.

tilibra

From the preceding discussion we can draw the following picture of the evolution of the central region:

- At $\tau_0 \sim 1$ fm/c after the collision, the thermal equilibrium is reached and the temperature is large enough for the system to be in the plasma phase.

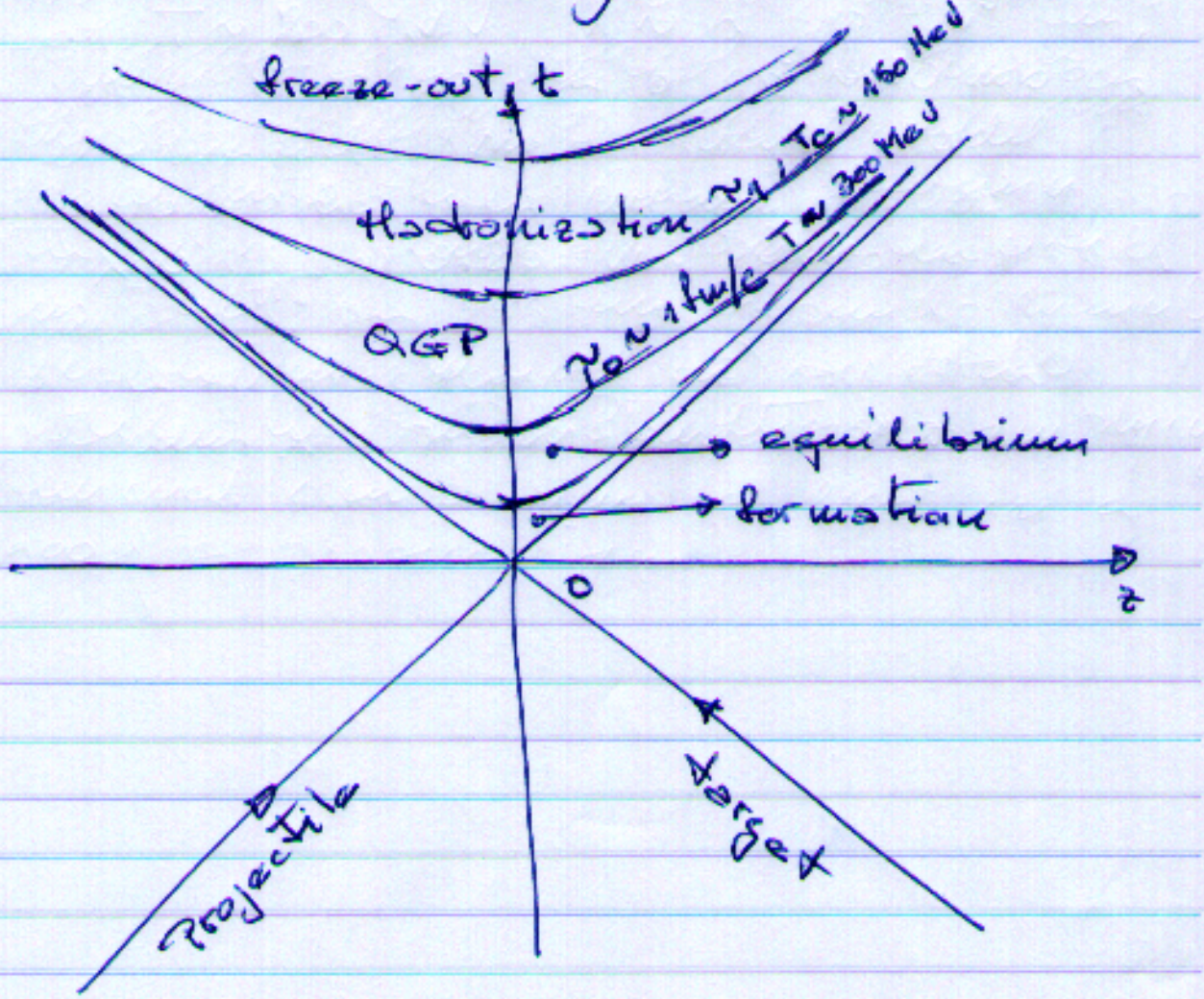
The assumption of thermal equilibrium is hard to be justified but is not unreasonable: for a QGP at $T \sim 200$ MeV, $n \sim 4$ per fm^3 then, for a cross section of $\sigma \sim 10$ mb as estimated from the quark model follows that the mean free path $\lambda \sim 1/n\sigma \sim 0.25$ fm. Then the size of the interaction region is 15-20 times λ for Pb-Pb collisions, implying thermal equilibrium (at least in a good approximation)

Thermalization justifies the use of hydrodynamics. The subsequent evolution of the system (assuming the perfect fluid approximation) tell us that the system expands mainly in the longitudinal (z) direction while the temperature T drops

until $T = T_c \sim 150$ MeV.

Thus a mixed plasma - hadronic phase occurs which lasts for some time until a pure hadronic phase is obtained.

Finally, when the mean free path is of the order of the size of the system, free particles are produced and may be observed in detectors. This is the so called freeze-out transition



tilibra

Recent data and discussions suggest that the situation can be, however, more complicated.

In fact, gluons can reach equilibrium faster than quarks. This is because the g-g cross section is much bigger than the q-g and q-q cross sections, being the mean free path for gluons $\lambda_g \sim 0.3$ fm, while for quarks $\lambda_q \sim 2$ fm.

Then, if only gluons come to thermal equilibrium, the initial temperature has to be of order $T \sim 400$ MeV, instead of the 300 MeV found earlier.

III) Hydrodynamics

In the previous section we discussed the main reasons because heavy ion collisions are also to produce the QGP. In doing that, we have introduced several concepts coming from hydrodynamical models. For that reason, and since the hydrodynamical picture is widely used in the study of the QGP, we will present now the equations of hydrodynamics and

tilibra

discuss their domain of validity.

To estimate the domain of validity of hydrodynamic equations one must known first the mean free path of a particle in a medium.

For orientation purposes, the mean free path of a high energy proton with a cross section

$$\sigma = 40\,mb$$

in nuclear matter with a density

$$\rho = 0.15\ \text{nucleon}/fm^3$$

is given by

$$\lambda = \frac{1}{\rho\sigma} = 1.7\,fm$$

If the mean free path is larger than the size L of the medium, one would expect only single collision to occur after which the particle leaves the medium. On the other hand, if

$$\lambda \sim L$$

several collisions can occur before the

particle leaves the medium, leading to the multiple scattering models. The extreme situation is when

$$\lambda \ll L$$

so that many collisions occur and it is no longer possible to discuss the interaction of the particle with the medium in terms of a succession of single collisions. In that case, the hydrodynamical equations are called for.

Roughly speaking, the hydrodynamical equations result from the constraints of energy conservation and momentum conservation applied to a gas. In order to describe a gas one needs quantities like the energy density, the local pressure and the baryonic content. The hydrodynamical equations will describe the evolution of the gas in time and space. Crucial to this is a realistic input as to what the initial conditions are.

One of the quantities which we need to estimate for the initial conditions is the energy density. In the first applications of the hydrodynamical model it was

assumed that in the center of mass frame, the nuclear matter would be stopped, leading to a gigantic energy density. In fact, for a simple p-p collision with a center of mass energy E_{cm}, the energy density was estimated to be

$$\varepsilon = \frac{2E_{cm}}{\frac{4}{3}\pi R_p^3 \frac{m_p}{E_{cm}}}$$

(Landau: L.D. Landau, Izv. Akad. Nauk. 17, 51 (1953))

which for a $E_{cm} = 250$ GeV gives $\varepsilon = 620$ GeV/fm^3, using a proton radius of 0.8 fm.

Current estimates, as we shall discuss in the following, give a energy density of about 2-3 GeV/fm^3.

The main difference between the Landau estimate and the current ones is that, on the basis of studies of hadronic interactions, today it is believed that nuclear matter is not completely stopped in the collision.

There are two main reasons for the absorb.

1) The nuclear matter has a minimum thickness, the boosting a nucleon

to a frame where it has infinite momentum does not produce a nucleus with vanishing thickness but a nucleus with an extension in the boosted direction of about 1 fm.
This is because a nucleon seen in the infinite momentum frame contains a large amount of partons with almost zero momentum (i.e. wee partons).
Thus whether we are in the rest frame of the nucleus or in the infinite momentum frame, there are always constituents (partons) approximately at rest. Since these are not influenced by the boost, the spatial extension of a nucleon will be the same in the rest frame or in the infinite momentum frame.
Since a nucleus is a collection of nucleons, this implies a limiting thickness, reducing the energy density estimate to

$$\varepsilon = \frac{2E_{cm}}{\frac{4}{3}\pi R_p^3} \sim 23 \text{ GeV/fm}^3$$

for a $E_{cm} \sim 250$ GeV.

2.) The inside - outside cascade:
When a hadronic collisions takes place one needs a proper time $\tau_0 \sim 1$ fm/c

tilibra

before the constituents hadronize.
Consequently, because of time dilation, fast partons will hadronize later than slow ones. This is the so-called inside-outside cascade.

A consequence of this picture is that, in a high energy proton-nucleus collision, the fast partons will hadronize outside of the nucleus thereby limiting the number of collisions and reducing the energy density reached in the hadronic collision.

The way to estimate the energy density taking into account both of the above effects is to start with the energy contained in a thin slab of rapidity space

$$E = N \frac{d\langle E \rangle}{dy} \Delta y$$

where N is the number of particles and $\langle E \rangle$ their average energy. Remember that $\mathcal{E} = E/V$, with V given by

$$d^3x = \tau \, dy \, d^2y$$

at the proper time τ_0 when hadronization

occurs. Integrating over the transverse direction gives

$$V = \tau_0 \Delta y A_\perp \quad ; \quad A_\perp = \pi R^2$$

and the energy density at the proper time τ_0 reads

$$\varepsilon_0 = N \frac{d\langle E \rangle}{dy} \Delta y = N \frac{d\langle E \rangle}{dy} \frac{1}{\tau_0 A_\perp}$$

or, replacing the average energy times N by

$$N \frac{d\langle E \rangle}{dy} \simeq \frac{dN}{dy} \langle m_\perp \rangle$$

where $m_\perp^2 = m^2 + p_\perp^2$ is the transverse mass,

$$\varepsilon_0 = \frac{\langle m_\perp \rangle}{\tau_0 A_\perp} \frac{dN}{dy}$$

Then, in a p-p collision, where $\langle m_\perp \rangle \sim 0.5$ GeV, $\frac{dN}{dy} \sim 4$ and $A_\perp = 4$ fm^2 we obtain

$$\varepsilon_0 \sim 0.5 \text{ GeV/fm}^3$$

tilibra

For a Uranium - Uranium collision, taking $\langle m_\perp \rangle$ as before but

$$\frac{dN}{dy} \sim 4 \times 238$$

and

$$R = 1.2 \times (238)^{1/3} \Rightarrow A_\perp = 173 \text{ fm}^2$$

we obtain for the energy density

$$\varepsilon_0 \gtrsim 2.7 \text{ GeV/fm}^3 \quad (\text{U-U collision})$$

This estimate is still subject to uncertainties in the value of τ_0 and dN/dy which will be modified by the evolution of the system to proper times greater than 1 fm/c.

Note that the inside-outside cascade was incorporated in the calculation when the volume was considered. Fast particles are outside of the volume in the rapidity space, thus not contributing to ε.

We will now to consider the thermalization of constituents in a ion-ion collision. As a rough estimate we can consider that quarks carry on the average 300 MeV

of energy in the rest frame (as is the case when they are confined inside nucleons) then their density is about

$$n \simeq \frac{2.7}{0.3} \frac{1}{\text{fm}^3} = 9 \cdot \frac{\text{quarks}}{\text{fm}^3}$$

Since the cross section for quark-quark scattering is about 5 mb (estimated from p-p collisions), then the mean free path is

$$\lambda = \frac{1}{n\sigma} \simeq 0.22 \text{ fm}$$

which is considerably smaller than the diameter of a heavy nucleus, let say, Uranium, whose size is

$$L_U \simeq 15 \text{ fm}$$

Thus, one of the conditions for the validity of hydrodynamics is satisfied, namely

$$0.22 \text{ fm} \simeq \lambda \ll L_U \simeq 15 \text{ fm}$$

We now turn our attention to the derivation of hydrodynamic equations.

tilibra

a- Derivation of hydrodynamic Equations

let us start by considering a gas in its rest frame. Let us assume also that we are dealing with a perfect gas and that we can neglect the effect of finite gradients of temperature, that is, we are going to consider a gas which is in every where at the same temperature. Then the time component of the energy-momentum tensor is the energy density of the medium:

$$T^{00} = \varepsilon$$

Since the pressure is the same in all directions, according to the hypothesis of a perfect fluid, the space components are

$$T^{ij} = P\delta^{ij}$$

where P is the pressure. Thus, in the rest frame

$$T^{\mu\nu}_{rest} = \begin{pmatrix} \varepsilon & 0 & 0 & 0 \\ 0 & P & 0 & 0 \\ 0 & 0 & P & 0 \\ 0 & 0 & 0 & P \end{pmatrix}$$

tilibra

Consider now the gas moving with 4-velocity u^μ and boost the energy-momentum tensor to this frame. This can be done by means of a simple Lorentz transformation

$$u^\mu = \Lambda^\mu_\nu u^\nu_{rest}$$

with $u^\nu_{rest} = (1,0,0,0)$, so that

$$\Lambda^\mu_0 = u^\mu$$

and the other components given by

$$g^{\mu\nu}\Lambda^\sigma_\mu \Lambda^\rho_\nu = g^{\sigma\rho}$$

then $\left(g^{00}\Lambda^\sigma_0\Lambda^\rho_0 - g^{ii}\Lambda^\sigma_i\Lambda^\rho_i = g^{\sigma\rho} \right)$

$$\Lambda^\rho_i \Lambda^\sigma_i = \Lambda^\rho_0\Lambda^\sigma_0 - g^{\rho\sigma} = u^\rho u^\sigma - g^{\rho\sigma}$$

Then

$$T^{\rho\sigma} = \Lambda^\rho_\mu \Lambda^\sigma_\nu T^{\mu\nu}_{rest} = \Lambda^\rho_0\Lambda^\sigma_0 \varepsilon + \Lambda^\rho_i\Lambda^\sigma_i P$$

and finally

$$T^{\rho\sigma} = u^\rho u^\sigma \varepsilon + \left(u^\rho u^\sigma - g^{\rho\sigma}\right) P$$

$$= (\varepsilon + P) u^\rho u^\sigma - P g^{\rho\sigma}$$

tilibra

In the rest frame of the fluid, the equation for energy and momentum conservation

$$\partial_\mu T^{\mu\nu} = 0$$

becomes extremely simple

$$\frac{\partial \epsilon}{\partial t} = 0$$

$$\frac{\partial P}{\partial x_i} = 0$$

which means that the energy does not change with time and no local gradients of pressure exists.
Note however that the energy does not need to be the same in the whole volume neither the pressure has to be constant in time.

Since we are interested in more general situations in which the fluid is not at rest, we will describe now the hydrodynamic equations in a more general frame.

In order to do so, let us start from the expression of the energy momentum tensor for a perfect fluid in pag 2-28, together with the constraints in pag 2-29 and the baryon number conservation

$$\partial_\mu \left(n_0(\vec{x},t)\, u^\mu \right) = 0 ,$$

where $n_0(\vec{x},t)$ is the local baryon number density.

Let us proceed by first contracting the equation for energy-momentum conservation with the 4-velocity

$$u_\nu \partial_\mu T^{\mu\nu} = 0 .$$

From the equation above follow that

$$u_\nu \partial_\mu \left[(\varepsilon + p) u^\mu u^\nu - g^{\mu\nu} p \right] = 0$$

and using that $u^\mu u_\mu = 1$ and $u_\nu \partial_\mu u^\nu = 0$ one obtains

$$u^\nu \partial_\nu \varepsilon + (\varepsilon + p) \partial_\nu u^\nu = 0 \qquad (2\text{-}30)$$

as the first hydrodynamic equation. The first hydrodynamic equation can be rewritten in terms of the entropy density, chemical potential and temperature

tilibra

using the relations valid for a grand canonical ensemble:

$$\varepsilon + P = Ts + \mu n_B \qquad (2\text{-}31)$$

$$d\varepsilon = T ds + \mu dn_B$$

The eq. (2-30) reduces to

$$u^\nu T \partial_\nu s + u^\nu \mu \partial_\nu n_B + (Ts + \mu n_B)\partial_\nu u^\nu = 0$$

or equivalently

$$T \partial_\nu (u^\nu s) + \mu \partial_\nu (n_B u^\nu) = 0$$

which, in view of the baryon number conservation leads to the conservation of the entropy density:

$$\partial_\nu (u^\nu s) = 0$$

A second set of hydrodynamic equations is obtained when contracting the energy momentum conservation equation with the tensor

$$g_{\nu\lambda} - u_\nu u_\lambda$$

This leads to

$$\left(g_{\nu\lambda} - u_\nu u_\lambda\right) \partial_\sigma \left[(\varepsilon + P) u^\sigma u^\nu - g^{\sigma\nu} P \right] = 0$$

which reduces to

$$(\varepsilon + P) u^\sigma \partial_\sigma u_\lambda - \partial_\lambda P + u_\lambda u^\sigma \partial_\sigma P = 0$$

Again it is of interest to express the result above in terms of thermodynamic quantities. Using the relations of eqn (2-37) we obtain

$$(Ts + \mu n_B) u^\sigma \partial_\sigma u_\lambda - s \partial_\lambda T - n_B \partial_\lambda \mu +$$

$$+ u_\lambda u^\sigma s \partial_\sigma T + u_\lambda u^\sigma n_B \partial_\sigma \mu = 0$$

or, grouping terms,

$$s\left[u^\sigma \partial_\sigma (u_\lambda T) - \partial_\lambda T \right] + n_B \left[u^\sigma \partial_\sigma (u_\lambda \mu) - \partial_\lambda \mu \right] = 0.$$

In the case in which the net baryon number is zero, the equation above reduces to

$$u^\sigma \partial_\sigma (u_\lambda T) - \partial_\lambda T = 0 \qquad n_B = 0$$

which can be written as

$$u^\sigma \partial_\sigma u_\lambda + u^\sigma u_\lambda \frac{1}{T} \partial_\sigma T - \frac{1}{T} \partial_\sigma T = 0$$

tilibra

or in its more compact form

$$u^\sigma \partial_\sigma u_\alpha + u^\sigma u_\alpha \partial_\sigma \ln T - \partial_\sigma \ln T = 0$$

Note also that for a baryon-number gas ($\mu = 0$) the equation for the entropy can be written as

$$\frac{\partial P}{\partial \varepsilon} = \frac{s}{T}\frac{\partial T}{\partial s} \qquad \mu = 0$$

where the left hand side is, by definition, the speed of sound in the medium, c_s:

$$\frac{s}{T}\frac{\partial T}{\partial s} = c_s^2 \quad ; \quad \mu = 0$$

or $$\frac{1}{c_s^2}\partial \ln T = \partial \ln s$$

Then, the equation for entropy conservation, $\partial_\nu (u^\nu s) = 0$ becomes

$$\partial_\nu u^\nu + u^\nu \partial_\nu \ln s = \partial_\nu u^\nu + u^\nu \frac{1}{c_s^2}\partial_\nu \ln T = 0$$

for $\mu = 0$. Then, the equation for the entropy becomes a equation for temperature

tilibra

Let us now start to discuss the solution to the hydrodynamic equations. In order to do that, let us assume that the beam direction is the z-axis and use cylindrical coordinates. Because of the rotational symmetry around the z-axis, the dependence in the azimuthal angle drops out of the equations..

In cylindrical coordinates, the 4-velocity reads

$$u^\mu = \frac{1}{\sqrt{1-v_z^2-v_r^2}}\left(1, v_z, v_r, 0\right)$$

with v_r the radial velocity and v_z the longitudinal one. In hadronic interactions

$$v_r \ll v_z$$

then in this approximation, and using that

$$u^\mu = (\cosh\theta, \sinh\theta, 0, 0)$$

where we have set $v_r = 0$, the hydrodynamic equations are

$$\cosh\theta \frac{\partial \varepsilon}{\partial t} + \sinh\theta \frac{\partial \varepsilon}{\partial z} + (\varepsilon + p)\left(\sinh\theta \frac{\partial \theta}{\partial t} + \cosh\theta \frac{\partial \theta}{\partial t}\right) = 0 \qquad (2\text{-}34\,a)$$

tilibra

$$\sinh\theta \frac{\partial P}{\partial t} + \cosh\theta \frac{\partial P}{\partial z} + (\varepsilon + P)\left(\cosh\theta \frac{\partial \theta}{\partial t} + \sinh\theta \frac{\partial \theta}{\partial z}\right) = 0 \qquad (2\text{-}34b)$$

while are the equations describing the longitudinal expansion of the gas (in our case, the hadronic matter).

Instead of working with the original z and t variables, it turns out to be much more convenient to work with the light cone variables

$$y = \frac{1}{2} \ln \frac{t+z}{t-z}$$

$$\tau = \sqrt{t^2 - z^2}$$

Note that under a Lorentz boost along the z-axis, i.e. going from the c.m. frame to the lab. frame, τ remains unchanged while y changes by a constant. In order to go back from (y, τ) to the original variables (t, z) one has to use

$$t = \tau \cosh y$$

$$z = \tau \sinh y$$

tilibra

To transform eqs (2-34a) and (2-34b) to the new set of coordinates, one uses the following matrix

$$\begin{pmatrix} \frac{\partial}{\partial \xi} \\ \frac{\partial}{\partial \tau} \end{pmatrix} = \begin{pmatrix} \cosh\gamma & -\sinh\gamma \\ -\sinh\gamma & \cosh\gamma \end{pmatrix} \begin{pmatrix} \frac{\partial}{\partial \tau} \\ \frac{1}{\tau}\frac{\partial}{\partial \gamma} \end{pmatrix}$$

and the final expression for the longitudinal hydrodynamic equations are

$$\tau \frac{\partial \varepsilon}{\partial \tau} + \tanh(\theta-\gamma)\frac{\partial \varepsilon}{\partial \gamma} + (\varepsilon+P)\left[\frac{\partial \theta}{\partial \gamma} + \tanh(\theta-\gamma)\,\tau\frac{\partial \theta}{\partial \tau}\right] = 0 \qquad (2\text{-}36a)$$

$$\frac{\partial P}{\partial \gamma} + \tanh(\theta-\gamma)\,\tau\frac{\partial P}{\partial \tau} + (\varepsilon+P)\left[\tau\frac{\partial \theta}{\partial \tau} + \tanh(\theta-\gamma)\frac{\partial \theta}{\partial \gamma}\right] = 0 \qquad (2\text{-}36b)$$

and the baryon number conservation

$$\tau\frac{\partial n_B}{\partial \tau} + n_B\frac{\partial \theta}{\partial \gamma} + \tanh(\theta-\gamma)\left(\frac{\partial n_B}{\partial \gamma} + n_B\,\tau\frac{\partial \theta}{\partial \tau}\right) = 0 \qquad (2\text{-}36c)$$

tilibra

The hydrodynamic equations (2-36) are to be invoked four functions: the energy density $\mathcal{E}$, the pressure P, the fluid velocity $\vec{v}$ and the baryon number density n_B

Since we have at our disposal three linear equations, we need to invoke an equation of state relating $\mathcal{E}$ and P to eliminate one of the unknowns. The initial conditions have also to be specified.

Using that the energy density and the pressure can be written in the alternative form

$$\mathcal{E} = \int d^4q \; q_0^2 \, N(x,q)$$

$$P = \frac{1}{3} \int d^4q \; |\vec{q}|^2 \, N(x,q)$$

where $N(x,q)$ in kinetic theory gives the distribution of 4-momenta q^μ at each space-point, then the simple relation follows:

$$P = \frac{1}{3} \mathcal{E} \qquad (2\text{-}37)$$

Note that the speed of sound in a fluid

is defined by

$$\frac{\partial P}{\partial \varepsilon} = c_s^2 \qquad (2\text{-}38)$$

and that for a free massless gas

$$c_s = 1/\sqrt{3}$$

in units in which $c=1$. This is the origin of the $1/3$ in eq. (2-37)
In the subsequent discussions we will not assume the validity of (2-37), but will work with the more general eq. (2-38), where c_s^2 may be a function of global variables like the temperature, but is taken to be independent of the space-time coordinates.

In this case, the hydrodynamic equations (2-36a) and (2-36b) reduce to a system of two coupled equations in two variables which can be solved. Then the solution for Θ can be used as input for (2-36c) and the baryonic number density may be obtained.

The major input from physics is in the initial conditions, where one can only make educated guesses. In London

tilibra

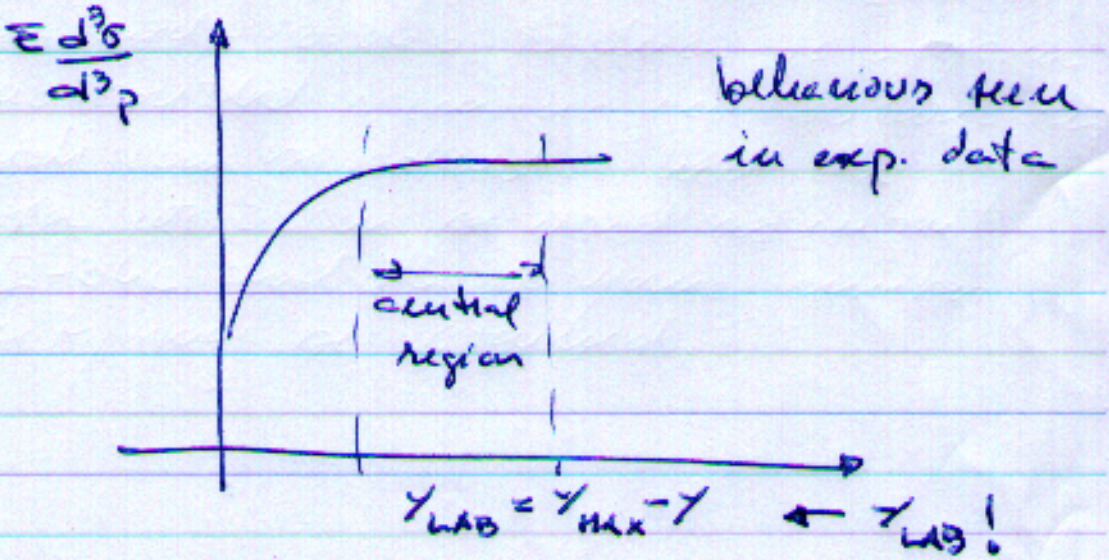
model nuclear matter is immediately stopped:

$$\vartheta(\vec{x}, t=0) = 0$$

but, as already discussed, this is unrealistic. Thus we will guide ourselves by what happens in high energy p-p collisions. In order to proceed in this direction, let us first observe that the inclusive cross section in p-p collisions, when plotted as a function of the rapidity

$$y_p = \frac{1}{2} \ln\left(\frac{E + p_z}{E - p_z}\right),$$

where p is the longitudinal momentum, exhibits a flat region for central values of y,



this is obvious from experimental data

It is therefore natural to expect a similar plateau in rapidity in very high-energy nuclear collisions. This means that there will be a region where one can perform shifts in rapidity and the differential cross-section will remains constant.

From the point of view of nuclear collisions, it means that we are allowed to make boosts in the longitudinal cross-section and the solution of the hydrodynamic equations should still be the same. Inspecting eqs (2-36) it is easy to see that the condition

$$\vartheta(y, y_0) = y \qquad (2\text{-}41)$$

provides the desired condition.

The solution characterized by the condition of eq. (2-41) has been considered by Bjorken and is known as "scaling solution", in the sense that small additive shifts to y do not change the nature of the solution.

With the above condition, the hydrodynamic equations are greatly simplified. All that remains is

tilibra

$$r\frac{\partial \mathcal{E}}{\partial r} + \mathcal{E} + P = 0 \qquad (2\text{-}42a)\ (ex\ 2\text{-}36a)$$

$$\frac{\partial P}{\partial y} = 0 \qquad (2\text{-}42b)\ (ex\ 2\text{-}36b)$$

$$r\frac{\partial u_B}{\partial r} + u_B = 0 \qquad (2\text{-}42c)\ (ex\ 2\text{-}36c)$$

The equation for the entropy takes on a similar form,

$$r\frac{\partial s}{\partial r} + s = 0 \qquad (2\text{-}42d)$$

and, for $\mu = 0$, the equation for the temperature becomes

$$c_s^2 + r\frac{\partial \ln T}{\partial r} = 0 \quad ; \mu = 0 \qquad (2\text{-}42e)$$

Solutions to eqs (2-42c) and (2-42d) are quite easy

$$s = s_0 r_0/r \qquad (2\text{-}43f)$$

$$u_B = u_B^0 r_0/r$$

Having in mind that the volume element in the light cone variables is

ulibra

$$d^3x = \tau\, d\eta\, d^2x$$

and since s and n_B are respectively the entropy and baryon number density, the solutions of eqs (2-43*) tell us that entropy and baryon number are constant in a given rapidity interval.

Integration of the eq for the temperature, eq (2-42a), gives

$$T = T_0 \left(\frac{\tau_0}{\tau}\right)^{c_s^2},$$

showing that T drops slowly than entropy and baryon number densities.

To proceed further and solve the equation for the evolution of the energy density we need a equation of state to relate ε and P. We will refuse to use the simple equation $P = c_s^2 \varepsilon$ and will look for inspiration in the Bag Model.

In the Bag Model, the energy density is given by the energy density of free quarks and gluons plus a constant B to account for the energy density of

Lilibra

the vacuum,

$$\mathcal{E} = \mathcal{E}_{\text{free gas}} + B$$

In a similar way, the pressure is

$$P = P_{\text{free gas}} - B$$

Using that for a free gas $P = c_s^2 \mathcal{E}$ we obtain

$$P = c_s^2 \left(\mathcal{E}_{\text{free gas}} + B \right) - B$$

$$= c_s^2 \mathcal{E} - \left(1 + c_s^2 \right) B$$

which we will refer to as the Bag model equation of state. Note that in order to the Bag Model equation of state to make sense, $P > 0$, then

$$\mathcal{E} > \frac{1 + c_s^2}{c_s^2} B$$

which corresponds to $\mathcal{E} > 200 \text{ MeV}/\text{fm}^3$

for $c_s^2 = 1/3$ and $B^{1/4} = 140 \text{ MeV}$

With the above relation between P and $\mathcal{E}$, the solution for the hydrodynamic equation (2-42a) is

tilibra

$$\varepsilon - B = (\varepsilon_0 - B)\left(\frac{r_0}{r}\right)^{1+c_s^2} \qquad (2\text{-}45)$$

It is interesting to note that the exponent of r_0/r is different from 1 exclusively due to the presence of P in the equation (2-42a).

Compare eqs (2-42c) - (2-42d) and their solutions with (2-42a) and its solution!

This means that the presence of the gas reflects itself in the exponent being different of one.

Let us consider now small corrections to the scaling solutions

$$\vartheta(\gamma, \tau) = \gamma + \vartheta' \quad ; \quad \vartheta' \ll 1 \,,$$

Then

$$\tanh(\vartheta - \gamma) \simeq \vartheta - \gamma = \vartheta' \,.$$

Returning to the hydrodynamic equations (2-3c) (page 2-3c) follows that the equation for the evolution of the energy remains unchanged but the equation for the pressure changes to

tilibra

$$\frac{\partial P}{\partial y} + (\varepsilon + P)\theta' = 0$$

whose solution, using the Bag Model equation of state, is

$$\varepsilon - B = (\varepsilon_0 - B)\, e^{-y \frac{1+c_s^2}{c_s^2}\theta'}$$

showing that the energy density goes to zero exponentially for large values of the rapidity y

Until now we have explored the behaviour of the time evolution of the quark-gluon-plasma phase in the longitudinal direction. In order to give a most complete picture, we will now consider the behaviour in the radial direction. To go further we recall that the scaling solution is invariant under boosts along the longitudinal direction, then it is sufficient to stand up in a point, let say $z = 0$, where the equations are simple, and construct the radial equation and solution.

In order to proceed, let us define the "radial velocity" as

$$\cosh\gamma = \frac{1}{\sqrt{1-v_r^2}}$$

Let us assume also for simplicity, that $\mu = 0$. Then the hydrodynamic equations are

$$\frac{1}{c_s}\frac{\partial \ln T}{\partial t} + v_r c_s \frac{\partial \gamma}{\partial t} + \frac{v_r}{c_s}\frac{\partial \ln T}{\partial r} +$$

$$+ c_s \frac{\partial \gamma}{\partial r} + \frac{v_r c_s}{r} + \frac{c_s}{t} = 0 \quad (2\text{-}47a)$$

$$v_r \frac{\partial \ln T}{\partial t} + \frac{\partial \gamma}{\partial t} + \frac{\partial \ln T}{\partial r} + v_r \frac{\partial \gamma}{\partial r} = 0 \quad (2\text{-}47b)$$

which, after adding and subtracting are from another gives

$$\frac{\partial}{\partial t}\left(\frac{1}{c_s}\ln T \pm \delta\right) + \frac{v_r \pm c_s}{1 \pm v_r c_s}\frac{\partial}{\partial r}\left(\frac{1}{c_s}\ln T \pm \delta\right)$$

$$+ \frac{v_r c_s}{r(1 \pm v_r c_s)} + \frac{c_s}{t(1 \pm v_r c_s)} = 0 \quad (2\text{-}47c)$$

which is the hydrodynamic equation of motion in the radial direction.

Note that the first two terms of eq (2-47c) correspond to a simple wave

tilibra

equation, with the only difference that the relevant velocity is the relativistic sum or difference of the radial velocity and the speed of sound.

The two extra terms appearing in the second line of eq. (2-47c) also imply that no solution is possible when $\frac{1}{c_s} \ln T \pm \beta$ is constant in some region of the space-time.

This has to be contrasted with the longitudinal behaviour where regions of constant Temperature are indeed possible solutions.

It is interesting to note also that solutions of eq. (2-47c) can be related to solutions of the equation

$$\frac{\partial}{\partial t}\left(\frac{1}{c_s}\ln T \pm \vartheta\right) + \frac{v \pm c_s}{1 \pm v c_s}\frac{\partial}{\partial r}\left(\frac{1}{c_s}\ln T \pm \vartheta\right) = 0$$

and that those solutions correspond to the so-called rarefaction waves propagating into the fluid.

Rarefaction waves are obtained by looking for solutions which are independent of

tilibra

the proper time. In that case, we can rewrite eqs (2-36a) and (2-36b) as

$$\tanh(\theta_r - y)\frac{\partial \varepsilon}{\partial \tau} + (\varepsilon + p)\frac{\partial \theta_r}{\partial \tau} = 0$$

$$\frac{\partial p}{\partial \tau} + (\varepsilon + p)\tanh(\theta_r - y)\frac{\partial \theta_r}{\partial \tau} = 0$$

for which we found

$$\theta_r = y \pm y_s \quad , \quad y_s = \tanh^{-1} c_s$$

The solution θ_r can be taken as an approximate solution for the radial equation (2-47c), thus

$$y \cong \frac{1}{2} \ln \frac{t+r}{t-r} \pm \tanh^{-1} c_s$$

Notice that we have limited our attention to the central region in rapidity space, where hydrodynamic equations can be solved analitically. In the fragmentation region the hydrodynamic description becomes more complex because of the presence of a net baryon number density and simultaneous production and expansion.

From the results in the fragmentation region let us only mention that because of a long production time and simultaneous expansion, the energy density is lower than in the central region. Let us also mention that in the center of mass frame, products from the central region will be more easily observed than products from the fragmentation region.

b) Relation to physical observables

The only observables in a heavy ion collision are the final state particles. From them we want to draw conclusions about the energy density, pressure, temperature, entropy and equation of state of the QGP phase which exists for a very short time after the collision.

It is clear from the beginning that it cannot be done in a unequivocal way and that we will need all the insights we can obtain to go ahead in this direction.

Clearly, the basic quantities at our disposal are the rapidity distribution, dN/dy, and the transverse momentum distribution, dN/dp_T, of the final state particles.

tilibra

Let us start first by the rapidity distribution. The logical procedure is to identify the entropy density with the particle density in the final state,

$$s(\vec{x},t) = \xi\, n(\vec{x},t)$$

where ξ is a constant whose value is $\xi = 3.92$ for a free gas of gluons and u and d quarks.

The rapidity distribution can be obtained from the particle density as follows. Let us start by considering the volume element in the 4-dimensional space-time

$$d^4x = \tau\, d\tau\, d\eta\, d^2x$$

Then, at fixed proper time τ_f (the final proper time), the rapidity distribution is given by

$$\frac{dN}{d\eta} = \int d^2x\, \tau_f\, n(\tau_f,\eta,x)$$

$$= \int d^2x\, \tau_f\, \frac{1}{\xi}\, s(\tau_f,\eta,x)$$

$$= \int d^2x\, \tau_0\, \frac{1}{\xi}\, s_0(\tau_0,\eta,x), \qquad (2\text{-}51)$$

where we have used that

tilibra

$u_0 = u_0^0 \, T_0/\tau$:

Eq (2-51) tell us that the final state distribution of particles in rapidity only depends on the initial entropy density and, if this initial entropy density is constant in the transverse direction, for a head-on ion-ion collision one obtains

$$\frac{dN}{dy} = \tau s_0 (\tau_0, y) A_\perp \qquad (2\text{-}52\,0)$$

where $A_\perp$ is the transverse size of the heavy nucleus.

Once we have related the initial entropy density with dN/dy, we can go further and extract also the initial energy density

Assuming no net baryon number the use of the equation of state and thermodynamic relations gives us

$$(\varepsilon_0 - B)(1 + c_s^2) = T_0 s_0 \qquad (2\text{-}52\,a)$$

To reach our goal we still need a relation between energy and Temperature. This relation is provided by the Bag-Model:

$$\varepsilon_0 - B = \lambda T_0^4 \qquad (2\text{-}52)$$

tilibra

where λ is a statistical factor which has into account also the degeneracy.
In the case of a gas of gluons and quarks u and d one has

$$\lambda = \frac{\pi}{30}\left(2\times 8 + 2\times 2\times 2\times 3\times\frac{7}{8}\right) = \frac{37\,\pi^2}{30} \simeq 12.17.$$

The different factor arise from number of gluons times the two polarizations (2×8) and the number of quarks times their spin from the 3 possible colors, times a factor of $7/8$ due to Fermi statistics ($2\times 2\times 3\times 7/8$). This last factor has also to be multiplied by 2 to consider particles and antiparticles

However, instead of using eq (2-52), we use a slightly more refined form coming from hydrodynamics:

$$\varepsilon_0 - B = \lambda\, T_0^{\,1+1/c_s^2}$$

so that, after combining with (2-52c) we obtain

$$s_0 = \left(\frac{\varepsilon_0 - B}{\lambda}\right)^{1/(1+c_s^2)} \lambda\,(1+c_s^2)$$

and the desired relation between the energy density and particle distribution

reads

$$\varepsilon_0 = B + \lambda \left[\frac{\xi}{A_\perp (1+c_0^2) \lambda \tau_0} \frac{dN}{dy} \right]^{(1+c_s^2)}$$

which, after using $\xi = 3.92$, $\lambda = 12.17$ and $c_s^2 = 1/3$, becomes

$$\varepsilon_0 = B + \left[\frac{1.6}{A_\perp \tau_0} \frac{dN}{dy} \right]^{4/3} \qquad (2\text{-}54)$$

which is the relation between the initial energy density and the final rapidity distribution.

Note that, in order to make (2-520) and (2-54) really useful relations, one has to further ascertain that the final rapidity distribution of quarks and gluons can be identified with the final rapidity distribution of mesons and baryons which are the particles which are detected.

Let us go now to some numerical examples of the use of eqs (2-54) and (2-520). For ordinary proton-proton collisions,

$$\frac{dN}{dy} \simeq 4 \quad ; \quad A_\perp \sim 40\,mb$$

and take $\tau_0 \sim 1\,fm$

tilibra

Then

(2-55a) $\varepsilon_0 \simeq 0.4 \frac{GeV}{fm^3} + B$ (p+p interactions)

B is of order 600 $\frac{MeV}{fm^3}$ according to low energy spectroscopy, while QCD sum rules tend to give a somewhat larger value, of order 400 MeV/fm^3

Cosmic ray events, however, give an estimate for the energy density of

(2-55b) $\varepsilon_0 = 5.1 \frac{GeV}{fm^3} + B$ (Si-Ag collisions) (silicon - silver)

Eqs (2-55a) and (2-55b) thus set the scale for the energy densities expected in heavy ion collisions. For a free gas of 2 quarks and gluons, with no chemical potential, we obtain a temperature

$$T \sim 237 \text{ MeV}$$

which according to most estimates would be sufficient to produce the plasma phase.

III Signals of QGP production

Along this section we will discuss about the signals for the production of the QGP phase and possible ways to measure the parameters of the plasma, namely its temperature, energy density and pressure. We will discuss also about possible signals of the transition from the quark-gluon to the hadronic phase.

To start with it is important to have in mind that parameters like T, ε and P are not directly measurables and all of them will vary very rapidly during the life time of the QGP phase. We will start first by discussions about the experimental accessibility of the parameters above.

a) Temperature measurements

In order to measure the temperature of the plasma phase, one wants signals produced at the early stage of the plasma which escape without interactions from the sorrounding matter. This last condition imposes severe constraints to the type of signals that could be acceptable as thermometers.

What one needs are particles with very small cross sections and large mean free paths.

inside the nuclear matter. The ideal particles to do the job are the lepton pairs, since they all have small electro-magnetic cross sections. The next to ideal are heavy resonances like the J/ψ because of the well known hierarchy of cross-sections

$$\sigma(\rho p) > \sigma(\phi p) > \sigma(J/\psi p)$$

Resonances heavier than the J/ψ are not interesting because the production rates are exceedingly small.

Let us start by discussing the production rate for lepton pairs. To simplify the discussion we will consider the plasma to be at rest and at one fixed temperature. Recall also that the standard formula for the cross section of a reaction like

$$a + b \longrightarrow \text{anything}$$

is

$$\frac{N}{tV} = \rho_a \rho_b v^{\text{relative}} \sigma(a+b)$$

where N/tV is the number of particles observed in the time interval t and produced in the volume V, ρ_a and ρ_b are the densities for particles a and b and v^{relative} is their relative velocity.

In our case the incoming particles a and b have no fixed momentum but have a specific distribution.

In the case of quarks and anti-quarks annihilating to a lepton pair l^+l^-, the above formula is modified to

$$\frac{dN}{dt\,d^3x} = \int \frac{d^3q}{(2\pi)^3} \frac{1}{e^{E_q/T}+1} \frac{d^3\bar{q}}{(2\pi)^3} \frac{1}{e^{E_{\bar{q}}/T}+1} v^{rel.} \sigma(q+\bar{q} \to l^+l^-) \tag{3-3}$$

where q ($\bar{q}$) refers to the momentum of the quark (anti-quark). The expression for the relative velocity of two equal mass particles with mass m is

$$v^{rel} = \frac{\sqrt{M^2(M^2-4m^2)}}{2E_q E_{\bar{q}}}$$

where M^2 is the invariant mass

$$M^2 = (E_q + E_{\bar{q}})^2 - (q+\bar{q})^2$$

and $\sigma(q+\bar{q} \to l^+l^-)$ is the elementary cross-section for Drell-Yan lepton pair production. The factors

$$\frac{1}{e^{E/T}+1}$$

correspond to the Fermi distribution of the

tilibra

initial quarks and anti-quarks, so that the integrals over d^3q and $d^3\bar{q}$ account for the fact that the incoming particles (fermions) have a momentum distribution.
Compare with the formulae for l^+l^- dell'Yan production in ordinary p-p collisions:

$$\frac{d\sigma}{dQ^2}^{pp\to l^+l^-+x} = \frac{1}{3}\sum_q \int dx_1 dx_2 \, f_q(x) f_{\bar{q}}(x) \frac{d\hat{\sigma}}{d\Theta^2}^{q\bar{q}\to l^+l^-}.$$

The expression of eq. (3-3) can be calculated analitically if

i) the invariant mass M is such that

$$M \gg m_{q,\bar{q}} \quad , \quad M \gg m_{l^+,l^-} \,,$$

which is the usual ultrarelativistic limit.

ii) The temperature is so large that the Fermi-Dirac distribution can be approximated by a Boltzmann distribution (high temperature limit)

$$\frac{1}{e^{+E/T}+1} \longrightarrow e^{-E/T}$$

Under these two conditions, the number of dileptons with a given invariant mass and momentum $P = q + \bar{q}$ is

tilibra

$$\frac{dN}{dt\,d^3x\,dM^2\,d^3p} = \int \frac{d^3q}{(2\pi)^3} e^{-E_q/T} \int \frac{d^3\bar{q}}{(2\pi)^3} e^{-E_{\bar{q}}/T} \frac{M^2}{2E_q E_{\bar{q}}} \times$$

$$\times \sigma(q\bar{q} \to \ell^+\ell^-)\, \delta^3(p - q - \bar{q})\, \delta\left(M^2 - (E_q + E_{\bar{q}})^2 + (q+\bar{q})^2\right) \qquad (3\text{-}5)$$

To the lowest order in α_{em}, $\sigma(q\bar{q} \to \ell^+\ell^-)$ is

$$\sigma(q\bar{q} \to \ell^+\ell^-) = \frac{4\pi\alpha_{em}^2}{9M^2}$$

after averaging over color and added a factor of $1/3$ because only color singlets contribute.

The integration of eq (3-5) over $\bar{q}$ gives us

$$\frac{dN}{dt\,d^3x\,dM^2\,d^3p} = \int \frac{d^3q}{(2\pi)^3} e^{-(E_q + E_{\bar{q}})/T} \frac{M^2}{2E_q E_{\bar{q}}} \sigma(M^2) \times$$

$$\times \delta\left(M^2 - (E_q + E_{\bar{q}})^2 + p^2\right) \qquad (3\text{-}5a)$$

with $E_{\bar{q}} = p - q$. By using the mass shell constraint and the expression

$$\frac{1}{2E_{\bar{q}}} = \int dE_{\bar{q}}\, \delta\left(E_{\bar{q}}^2 - \bar{q}^2\right) \theta(E_{\bar{q}}),$$

the 3 dimensional integral in (3-5a) can be rewritten as a 4-dimensional integral. Performing then the integral over $E_{\bar{q}}$ using the delta function we obtain

tilibra

$$\frac{dN}{dt\,d^3x\,dM^2\,d^3p} = \int \frac{d^3q}{(2\pi)^6}\,\frac{1}{E_q}\,e^{-(E_q+E_{\bar q})/T}\,\sigma(M^2)\,\times$$

$$\times\,\frac{1}{2(E_q+E_{\bar q})}\,\delta\left(\left(\sqrt{M^2+p^2}-E_q\right)^2-|\vec p-\vec q|^2\right)$$

Since $d^3q = q^2\,dq\,\sin\theta\,d\theta\,d\phi$ we let the integral over ϕ is trivial giving a factor of 2π and the integral over θ can be done by using the remaining δ-function, whose argument can be written as

$$\left(\sqrt{M^2+p^2}-q\right)^2 - p^2 - q^2 + 2pq\cos\theta,$$

and since $-1 \le \cos\theta \le 1$, giving the constraint on the q integration region

$$-1 \le \frac{2q\sqrt{M^2+p^2}-M^2}{2pq} \le 1$$

or

$$\frac{1}{2}\left(\sqrt{M^2+p^2}-p\right) \le q \le \frac{1}{2}\left(\sqrt{M^2+p^2}+p\right),$$

and finally using $E_q+E_{\bar q} = \sqrt{M^2+p^2} = E$, we obtain

$$E\,\frac{dN}{dt\,d^3x\,dM^2\,d^3p} = \frac{1}{4(2\pi)^5}\,M^2\,\sigma(M^2)\,e^{-E/T} \qquad (3\text{-}6)$$

tilibra

as the result for the production of lepton pairs in the ultra-relativistic high temperature limit.

Note that the expression of eq. (3-6) has still to be integrated over the space-time volume of the plasma. For this one should know the space time dependency of the temperature, and is in this point where hydrodynamic enters.

The integration over the space time is better performed in the light cone variables,

$$dt\,d^3x = \tau\,d\tau\,dy\,d\tau\,d\phi$$

One more or less natural choice (but by no means the only one) for the limits on the integration variables is as follow:

i) <u>proper time</u>

Start at $\tau = 1\,fm/c$, which is the time at which the first hadrons are formed. The evolution law for the temperature will give us the final proper time as the time when the plasma is cooled down to $T \sim 140$ MeV, corresponding to the pion mass,

tilibra

$$\tau_{final} = \tau_0 \left(\frac{T_0}{140\,MeV} \right)^{1/c_s^2}$$

with T_0 being the initial temperature which one would like to determine from the dilepton spectrum.

ii) <u>rapidity</u>

The limits on the rapidity can be taken as being the corresponding limits in the rapidity space,

$$-\ln \frac{\sqrt{s}}{m_p} \leq y \leq \ln \frac{\sqrt{s}}{m_p}$$

with $\sqrt{s}$ the invariant energy per nucleon and m_p the proton mass

iii) <u>r and ϕ</u>

The limits should correspond to the geometric limits of the nucleus.

Once eq. (3-6) has been integrated over the space-time volume, it may be compared with the corresponding result for lepton pair production within the standard Drell-Yan mechanism.

tilibra

The rate for Drell-Yan pair production,

$$\frac{d\sigma}{dM^2} \sim \frac{1}{M^2} d\left(\frac{M^2}{s}\right)$$

has an approximate scaling behaviour which implies a polinomical decrement with the increase of M^2. The lepton pair production in a quark-gluon-plasma is also polinomial with a power depending on the velocity of sound in the plasma. For $c_s^2 = 1/3$ the rate of thermal production has the same dependence on the invariant mass as the leading term in usual D-Y production. However, the normalization of the rate depends on the formation time of the hadronic matter and on the multiplicity. By using conservative values for these quantities, the lepton pair production within the plasma is estimated to be a factor of 3-5 smaller than that in ordinary p-p collisions.

Then: if the production rate of lepton pairs in heavy ion collisions goes down with the energy of the collision or the mass of the heavy nucleus, one has an indication that the QGP might be produced

b) Enthalpy measurements

Here we will focus in the transverse direction of the QGP. We will assume that the transverse motion is described by a rarefaction wave of the type discussed earlier.

Using the solution for $\tanh(\Theta_+ - \eta)$ we are left with two differential equations relating the transverse motion, the pressure and the energy density

$$c_s \frac{\partial \varepsilon}{\partial \eta} + (\varepsilon + P) \frac{\partial \Theta_R}{\partial \eta} = 0$$

$$\frac{\partial P}{\partial \eta} + c_s (\varepsilon + P) \frac{\partial \Theta_R}{\partial \eta} = 0$$

Dividing the first one by c_s and adding the two equations we get

$$\frac{\partial (\varepsilon + P)}{\partial \eta} + (\varepsilon + P) \frac{1 + c_s^2}{c_s} \frac{\partial \Theta_R}{\partial \eta} = 0$$

whose solution is

$$\Theta_R = \frac{c_s}{1 + c_s^2} \ln \left(\frac{\varepsilon_0 + P_0}{\varepsilon + P} \right)$$

This can be related to the transverse momentum by

$$p_T = m_L \sinh \theta_2$$

where

$$m_L = \sqrt{m^2 + p_L^2}$$

is the so called longitudinal mass. We choose now $p_L = 0$ (since other values of p_L can be obtained by boosts in the longitudinal direction) then

$$\text{are sinh } \frac{p_T}{m} = \frac{c_s}{1+c_s^2} \ln\left(\frac{\varepsilon_0 + P_0}{\varepsilon + P}\right)$$

which for large p_T gives

$$p_T \simeq \frac{m}{2}\left(\frac{\varepsilon_0 + P_0}{\varepsilon + P}\right)^{c_s/(1+c_s^2)}$$

with $\varepsilon_0 + P_0$ the initial enthalpy. Using previous relations we obtain

$$\varepsilon_0 + P_0 = \lambda \left[\frac{\xi}{A_\perp (1+c_s^2)\lambda \tau_0} \frac{dN}{dy}\right]^{1+c_s^2}$$

which relates the initial enthalpy to

tilibra

the multiplicity in rapidity space.

c) Signals associated with a First Order Phase Transition

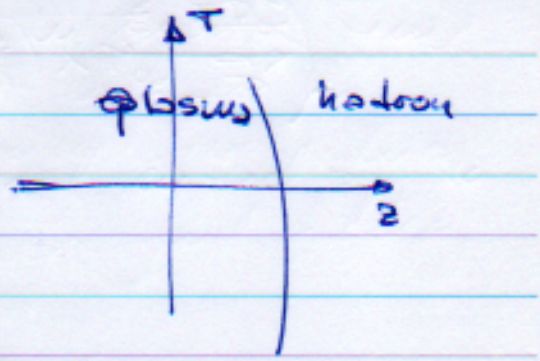
Let us start by considering a reference frame in which the boundary separating the two phases is at rest. Then, the hydrodynamic equation

$$\partial_\mu T^{\mu\nu} = 0$$

reduces to a continuity equation across the boundary

$$\frac{\partial}{\partial z} T^{zz} = 0$$

$$\frac{\partial}{\partial z} T^{z0} = 0$$



so that, after integration

$$T^{zz} = cte$$
$$T^{z0} = cte$$

across the boundary. These two equations imply

$$(\varepsilon + P) v_z^2 + P = cte$$
$$(\varepsilon + P) v_0 v_z = cte$$

dlibra

Using $v_0 = \cosh\theta$ and $v_2 = \sinh\theta$, one obtains upon comparing both sides of the boundary

$$(\varepsilon_h + p_h)\sinh^2\theta_h + p_h = (\varepsilon_q + p_q)\sinh^2\theta_q + p_q$$

$$(\varepsilon_h + p_h)\sinh\theta_h\cosh\theta_h = (\varepsilon_q + p_q)\sinh\theta_q\cosh\theta_q$$

where indexe h and q refer to the hadronic and plasma phases.
Eliminating θ_h and θ_q one obtains:

$$\tanh^2\theta_h = \frac{(p_h + \varepsilon_q)(p_q - p_h)}{(\varepsilon_q - \varepsilon_h)(\varepsilon_h + p_q)}$$

$$\tanh^2\theta_q = \frac{(p_q - p_h)(\varepsilon_h + p_q)}{(\varepsilon_q - \varepsilon_h)(\varepsilon_q + p_h)}$$

We will call deflagration to the situation in which

$$\tanh\theta_h > \tanh\theta_q$$

and detonation to

$$\tanh\theta_h < \tanh\theta_q$$

Then, deflagration requires

tilibra

$$\varepsilon_q - P_q > \varepsilon_h - P_h \qquad (3\text{-}14a)$$

while detonation means

$$\varepsilon_q - P_q < \varepsilon_h - P_h \qquad (3\text{-}14b)$$

Note that in the case of a deflagration, hadrons start to form in the surface of the plasma, while in a detonation hadrons form from a bubble inside the plasma. The case of a deflagration occurs when the velocity of hadrons exceeds the velocity of the plasma.

To gain some insight from the inequalities (3-14a) and (3-14b), let us impose the bag equation of state with $c_s^2 = 1/3$ and $P_h = \frac{1}{3}\varepsilon_h$, then

$$\varepsilon_q + 2B > \varepsilon_h \qquad \text{deflagration}$$

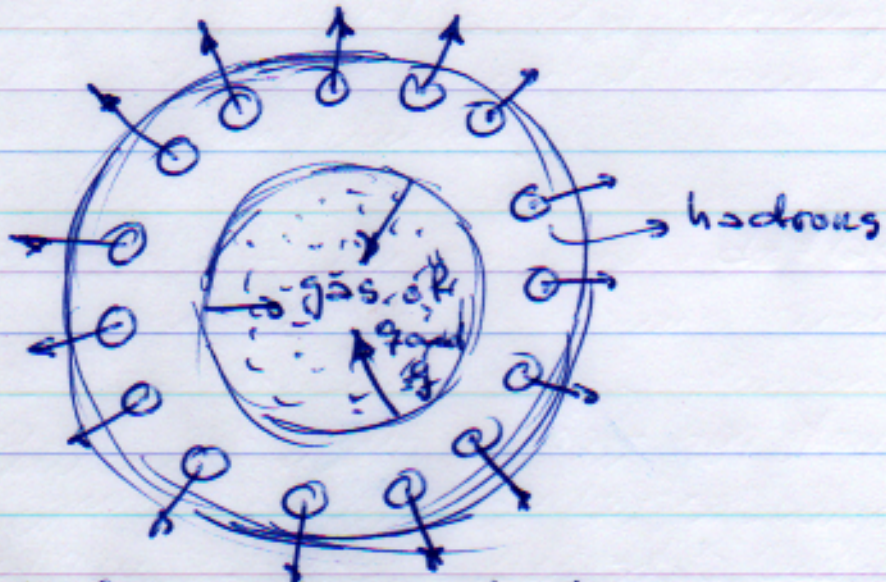
$$\varepsilon_q + 2B < \varepsilon_h \qquad \text{detonation}$$

From these last unequalities one can conclude that detonation is very unlikely to occur

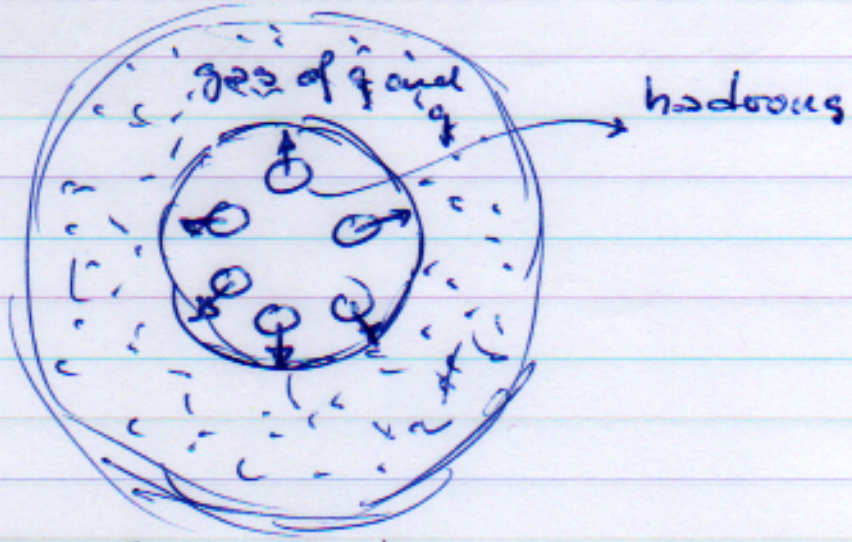
In addition from the conservation of entropy follows that, across the body



free gas of quarks and gluons



deflagration starting in the surface



detonation starting as a bubble inside the plasma

tilibra

$$\frac{\partial}{\partial z}\left(sv^2\right) = 0$$

which integrates to

$$sv^2 = \text{cte}$$

so that

$$s_q \sinh\theta_q = s_h \sinh\theta_h$$

In more general situations, when the chemical potential is non-zero, the above identity translates into

$$s_q \sinh\theta_q \leq s_h \sinh\theta_h$$

or

$$\frac{s_h^2}{s_q^2} \geq \frac{(\varepsilon_h + P_h)(\varepsilon_h + P_q)}{(\varepsilon_q + P_q)(\varepsilon_q + P_h)}$$

The Bag Model gives us

$$T_q s_q = \varepsilon_q + P_q = \frac{4}{3}\left(\varepsilon_q - B\right)$$

while, assuming that the hadronic phase is a free gas of pions,

$$T_h s_h = \frac{4}{3}\varepsilon_h$$

tilibra

Then the condition over the entropies becomes

$$\frac{\varepsilon_h}{\varepsilon_q - B} \geq \frac{3\varepsilon_h + \varepsilon_q - 4B}{3\varepsilon_q + \varepsilon_h} \frac{T_h^2}{T_q^2}$$

In order to extract useful information from the inequality above, let us replace the temperature by the corresponding energy densities

$$\varepsilon_q = \frac{37\pi^2}{30} T_q^4 + B$$

$$\varepsilon_h = \frac{\pi^2}{10} T_h^4$$

Then

$$\frac{T_h^2}{T_q^2} = \left[\frac{\varepsilon_h}{\varepsilon_q - B} \frac{37\pi^2/30}{\pi^2/10} \right]^{1/2}$$

so that

$$\left(\frac{\pi^2/10}{37\pi^2/30} \frac{\varepsilon_h}{\varepsilon_q - B} \right)^{1/2} \geq \frac{3\varepsilon_h + \varepsilon_q - 4B}{3\varepsilon_q + \varepsilon_h}$$

This last inequality restricts severely the values of ε_h and ε_q. In fact, once combining this with the inequalities resulting from

$$0 \leq \tanh^2 \theta_{u,q} \leq 1$$

we see that ε_q cannot be much larger than ε_H or, in other words, ε_q cannot be much larger than 4B because it requires that the pressure of the plasma phase be close to zero.

In sum, from detailed numerical analysis follows that

i) detonations are not possible
ii) the velocity in the plasma phase is very small
iii) the velocity in the hadron phase can be appreciably large

d) Strangeness and charm production

One interesting feature of the production of the quark-gluon-plasma is the enhancement in the production of strange quarks, leading thus to an enhancement in the production of strange hadrons which will be observed in the hadron phase.

The basis to understand the enhancement in the production of strange quarks ~~is based~~ are the following two principles:

i) in an environment rich in u, d quarks, the Pauli exclusion principle

tilibra

will prohibit the further appearance of $u\bar{u}$ and $d\bar{d}$ pairs, but no $s\bar{s}$ pairs

ii) The probability of $\bar{u}$ and $\bar{d}$ quarks to recombine with u and d quarks to produce a gluon is very large while for strange quarks is zero.

It has to be noted that the above arguments require an environment rich in baryons, i.e. a chemical potential different from zero.

The above arguments can be made more qualitative by looking at the number of $\bar{u}$ and $\bar{s}$ quarks in a freezer

$$n_{\bar{u}} = 6 \int \frac{d^3p}{(2\pi)^3} \frac{1}{e^{(p+\mu)/T} + 1}$$

$$n_{\bar{s}} = 6 \int \frac{d^3p}{(2\pi)^3} \frac{1}{e^{(p^2+m_s^2)^{1/2}/T} + 1}$$

The number of s-quarks is suppressed by the mass of the s quark in the exponential, while the number of $\bar{u}$ quarks is suppressed by the chemical potential μ.

It means that in a baryon rich environment, where μ is large, the ratio of s to $\bar{s}$ quarks will be substantially large.

It has also been shown that strange quarks only need a few fermis in time to reach chemical equilibrium with the other quarks.

The role of c-quark can be contrasted with the role of strange quarks. If the Temperature of the plasma phase is of order 200 - 400 MeV, and having in mind that the charm mass is about 1.2 - 1.5 GeV, charm production will be a rare process! Moreover, once produced charm quarks will never reach chemical equilibrium, unlike strangeness!

This means that charm will very likely escape from the plasma without interacting (the charm also has a small cross section with other quarks) and thus could serve as a thermometer of the initial stages of the QGP production. In this respect it is similar to the production of heavy lepton-pairs!

tilibra

it is necessary to trigger on them, but they are good thermometers.

a) Anomalous freeze-out volume

In a first-order phase transition, the energy density and pressure change abruptly from the plasma to the hadron phase. Consequently, the pressure changes abruptly as a function of the local number of collisions, when the collision number passes the critical value N_c. Note that we are thinking here in a ion-ion collision as a set of individual nucleon-nucleon collisions. Thus, the number of nucleon-nucleon collisions in a ion-ion collision scales as the number of nucleons in the nucleus.

As we have already seen, the pressure in the plasma phase is

$$P_{QGP} \sim \frac{37\pi^2}{90} T^4$$

which is much greater than the pressure of a pion gas

$$P_\pi \sim \frac{6\pi^2}{90} T^4$$

Thus the pressure of the plasma phase

is characterized by a region of very high pressure. The large pressure of the plasma can be detected by a large freeze-out volume. The argument is as follows.

In the Bjorken hydrodynamics the matter produced in a high energy heavy ion collision experiences longitudinal expansion. Let us consider then a plateau distribution of matter within the rapidity range $|Y| < Y_0$ and longitudinal coordinates $|z| < |z_0|$. The initial proper time is then

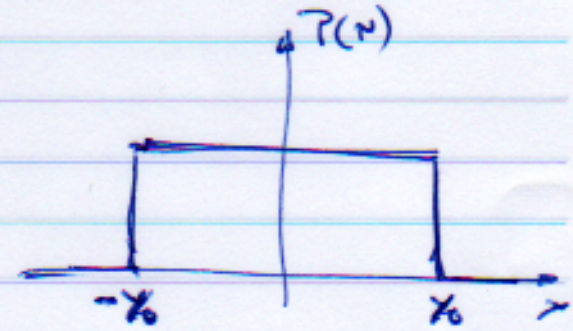
$$\tau_0 = |z_0| / \sinh Y_0$$

and the solution for the pressure in Bjorken hydrodynamics is

$$P(\tau, Y) = P(\tau)\,\theta(Y_0 - |Y|)$$

where

$$\frac{P(\tau)}{P(\tau_0)} = \left(\frac{\tau_0}{\tau}\right)^{4/3}$$



At the proper time τ, the boundary of the matter has expanded up to

$$z_\tau = \pm \tau \sinh y_0$$

and thus the ratio

$$\frac{|z_\tau|}{|z_0|} = \left(\frac{P(\tau_0)}{P(\tau)} \right)^{3/4}$$

As the matter expands, there will be a pressure $P(\tau_f)$, the freeze-out pressure, at which particles will not longer interact. Because the volume of matter, V, is proportional to $|z_\tau|$, as long as the expansion is only in the longitudinal direction, the ratio of the freeze-out volume to the initial one $V(\tau_0)$ is

$$\frac{V(\tau_f)}{V(\tau_0)} = \left(\frac{P(\tau_0)}{P(\tau_f)} \right)^{3/4}, \qquad (3\text{-}22)$$

Hence, the freeze-out volume varies with the initial pressure as $(P(\tau_0))^{3/4}$

The eq. (3-22) is applicable to hadron matter. It can also be applicable approximately to the QGP undergoing

strong longitudinal expansion for which, the temperature of the QGP is lowered so rapidly that the expansion drives the system below the critical temperature. When the energy density and pressure of the super cooled plasma drop down to the same level than those of the hadron matter, spontaneous transition from the plasma to the hadron phase takes place at a time τ_H resulting in a hadron matter volume $V(\tau_H)$. The hadron matter then undergoes further longitudinal expansion to reach the freeze-out volume $V(\tau_f)$ at T_c. For the plasma phase subject to a strong longitudinal expansion then we have

$$\frac{V(\tau_f)}{V(\tau_0)} = \frac{V(\tau_f)}{V(\tau_H)} \frac{V(\tau_H)}{V(\tau_0)} \sim \left(\frac{P(\tau_H)}{P(\tau_f)}\right)^{3/4} \left(\frac{P(\tau_0)}{P(\tau_H)}\right)^{3/4} =$$

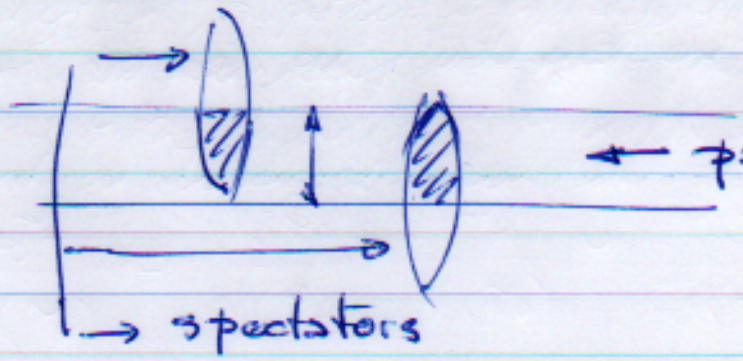
$$= \left(\frac{P(\tau_0)}{P(\tau_f)}\right)^{3/4}$$

showing that the freeze-out volume varies approximately with the initial QGP pressure as $(P(\tau_0))^{3/4}$.

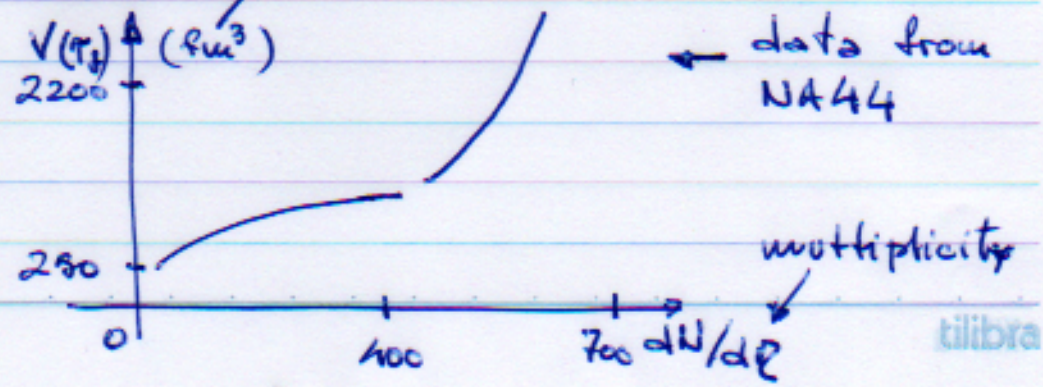
Based on the above, the large pressure of the

quark-gluon-plasma will lead to a large freeze-out volume, and a first order phase transition will be indicated by an anomalous increase of the freeze-out volume due to the increase in the pressure of the plasma phase.

We expect that the anomalous increase in the freeze-out volume occur when the average number of nucleon-nucleon collisions passes through the critical value N_c
Note also that the average number of nucleon-nucleon collisions increases with centrality



indicating that the freeze-out volume should also increase anomalously with centrality.



tilibra

IV Quark-hadron phase transition in cosmology

a) The early universe

The standard Big Bang model is based on the Einstein equations which give, for a homogeneous and isotropic universe,

$$\left(\frac{dR}{d\tau}\right)^2 = \frac{8\pi G}{3} R^2 \varepsilon \qquad (4\text{-}1a)$$

$$R^3 d\varepsilon + (\varepsilon + P) dR^3 = 0 \qquad (4\text{-}1b)$$

where R is the scale factor, ε the energy density, G is the gravitational constant and τ is the proper time measured by a comoving observer. We are not considering the curvature terms, which is negligible at high energy densities.

Eq (4-1b) can be written in the form

$$-\frac{dR}{R} = \frac{d\varepsilon}{3(\varepsilon + P)} \,. \qquad (4\text{-}1c)$$

At early times, the universe is dominated by ultra-relativistic matter, then the pressure and energy are given by

$$P = \frac{1}{3}\varepsilon = g\frac{\pi^2}{90}T^4 \qquad (4\text{-}1d)$$

with g the number of degrees of freedom,

$$g = g_b + \frac{7}{4}g_f \,.$$

(Remember the bag model).

In the QGP phase, neglecting perturbative QCD and intermediate interactions, taken into account the energy density associated with the vacuum, we have

$$P_{QGP} = \frac{1}{3}\left(\varepsilon_{QGP} - 4B\right) = g_{QGP}\frac{\pi^2}{90}T^4 - B$$

Now using (4-1a) and (4-1b) to eliminate dR/R, we obtain

$$-\frac{d\varepsilon}{3\sqrt{\varepsilon}(\varepsilon+P)} = \sqrt{\frac{8\pi G}{3}}\,dt \qquad (4\text{-}2)$$

Then, using (4-2) together with the eq. of state (4-1d) we obtain for the energy density

$$\varepsilon_{QGP} = B\coth^2\left[2\sqrt{\frac{8\pi G B}{3}}\,t\right] \qquad T > T_c$$

tilibra

If we now assume that the phase transition is adiabatic and occurs at a constant Pressure, we can rewrite eq (4-1b) as

$$R^3 d\left(\varepsilon + P(T_c)\right) + \left(\varepsilon + P(T_c)\right) dR = 0$$

which implies that

$$\left[\varepsilon + P(T_c)\right] R^3 = \text{cte} \quad ; \quad T = T_c$$

Using eq (4-2) together with the result above, we can estimate the duration of the phase transition:

$$\tau_h(T_c) - \tau_{QGP}(T_c) = \frac{2}{3}\sqrt{\frac{3}{8\pi G P(T_c)}}\left[\operatorname{arcth}\sqrt{\frac{\varepsilon_{QGP}(T_c)}{P(T_c)}} - \operatorname{arcth}\sqrt{\frac{\varepsilon_h(T_c)}{P(T_c)}}\right] \qquad (4-3)$$

Then, the universe is in the plasma phase until $\tau_{QGP}(T_c)$, in the mixed phase from $\tau_{QGP}(T_c)$ until $\tau_h(T_c)$, and in the hadronic phase since $\tau_h(T_c)$.

The solution of eq (4-2) in the hadronic phase, with the equation of state (4-1d) is

$$t = \tau_h(T_0) + \frac{1}{2}\sqrt{\frac{3}{8\pi G \varepsilon_u(T_0)}}\left[\left[\frac{\varepsilon_h}{\varepsilon_h(T_0)}\right]^{-1}\right] \quad T < T_c \qquad (4\text{-}4)$$

Now we can calculate the cooling rate of the universe. To proceed, we need to specify the constituent gases.

At the temperatures of interest, the ultra-relativistic particles present are γ^0, $e^{\pm}$, $\mu^{\pm}$, ν_e, $\bar{\nu}_e$, ν_μ, $\bar{\nu}_\mu$, ν_τ, $\bar{\nu}_\tau$ in both phases and in addition, gluons and $u, \bar{u}, d, \bar{d}$ quarks in the plasma phase.

From the above we have the following degeneracy factors:

$$g_{QGP} = 37 + 14.25$$

where 37 is from quarks and gluons (ie $4 \times 2 \times 3 \times \frac{7}{8} + 2 \times 8$), 2 photons plus 12.25 from leptons (6 neutrinos + 4×2 leptons charged)

$$g_h = 3 + 14.25$$

where the 3 is for the 3 different pions.
So the ratio is

$$r = \frac{g_{QGP}}{g_h} = \frac{51.25}{17.25} \simeq 3$$

tilibra

The condition for the phase transition

$$P_{QGP}(T_c) = P_h(T_c)$$

defines the critical Temperature:

$$g_h \frac{\pi^2}{90} T_c^4 = g_{QGP} \frac{\pi^2}{90} T_c^4 - B \equiv P(T_c)$$

and introducing the ratio $r = g_{QGP}/g_h$ we can rewrite the two eqs above as

$$g_h \frac{\pi^2}{90} T_c^4 - P(T_c) = 0 \qquad (4\text{-}5a)$$

$$g_{QGP} \frac{\pi^2}{90} T_c^4 - P(T_c) = B$$

and summing

$$\frac{\pi^2}{90} T_c^4 \left(g_h + g_{QGP}\right) - 2P(T_c) = B$$

or

$$g_h \frac{\pi^2}{90} T_c^4 \left(1 + r\right) - 2P(T_c) = B$$

and using again (4-5a)

$$(r-1) P(T_c) = B$$

Now we can use eq (4-3) to estimate the duration of the phase transition:

tilibra

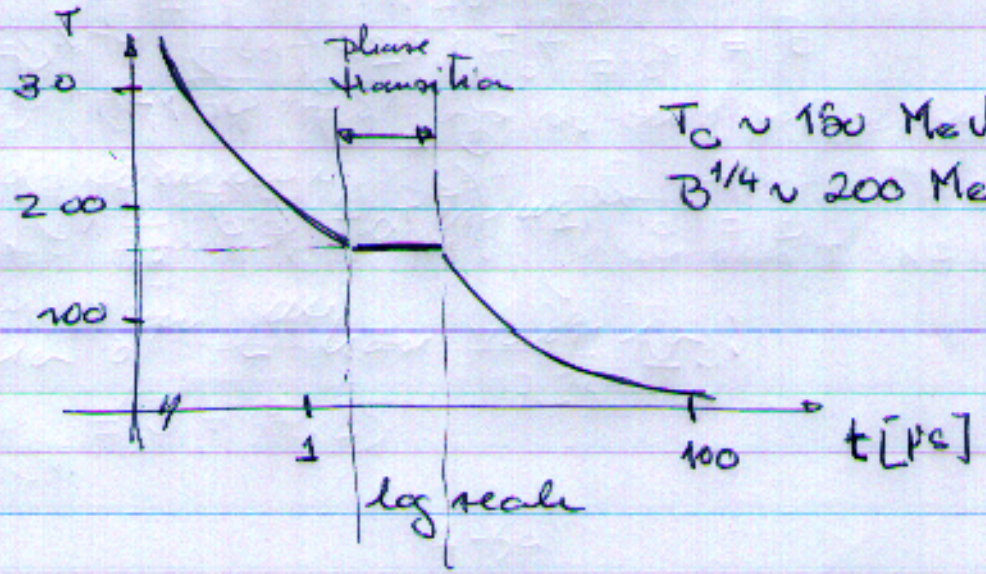
$$\tau_h(T_c) - \tau_{QGP}(T_c) = \frac{2}{3}\sqrt{\frac{3(r-1)}{8\pi G B}}\left[\operatorname{arcth}\left(\sqrt{4r-1}\right) - \operatorname{arcth}\left(\sqrt{3}\right)\right]$$

$$\simeq 30.9\left(\frac{100\,MeV}{T_c}\right)^2 \mu sec.$$

and from (4-4) the relation between time and temperature;

$$t = \tau_h(T_c) + \frac{1}{2\sqrt{3}}\sqrt{\frac{3(r-1)}{8\pi G B}}\left[\left(\frac{T_c}{T}\right)^2 - 1\right]; \quad T < T_c$$

which looks like



tilibra

V - Experimental Results

Experimental attempts to create the QGP in the laboratory and measure its properties have been carried out for more than 20 years, by studying collisions of heavy nuclei.

During that period, the center of mass energy per pair of colliding nucleon has risen steadily from $\sqrt{s_{NN}} \sim 1$ GeV in Bevalac at LNBL, to energies of $\sqrt{s_{NN}} = 5$ GeV in AGS at BNL, to $\sqrt{s_{NN}} = 17$ GeV in SPS at CERN. No decisive proof of QGP formation was found in those experiments, although a number of signals suggesting the formation of a very dense state of matter, probably partonic were found at the SPS.

With the Relativistic Heavy Ion Collider, RHIC, at BNL, the center of mass energy in central collisions between gold nuclei has been raised at $\sqrt{s_{NN}} = 200$ GeV, meaning a total center of mass energy of about 40 TeV, having in mind that the atomic number of gold is $A = 197$ (ie ~ 200 GeV $\times$ 200 nucleon-nucleon interactions $= 40.000$ GeV $= 40$ TeV). The center of mass energy will be rised even more in Alice, at CERN corresponding to $\sqrt{s_{NN}} = 14$ TeV, giving a total c.m. energy of 14 TeV $\times 207$

~ 2900 TeV.

That energies are so large that the conversion of a sizable fraction of the initial kinetic energy into matter production creates many thousands of particles in a limited volume, leading to unprecedented large energy densities and thus presumably ideal conditions for the formation of the quark-gluon plasma.

Since there is no available data coming from ALICE, we will restrict in the following to the discussion about the experimental conditions of the four RHIC experiments (STAR, PHOBOS, PHENIX BRAHMS) to produce and measure the QGP and its properties.

RHIC started regular beam operations in the year of 2000, with a short run of gold-gold collisions at $\sqrt{s_{NN}} = 130$ GeV. The first full run at the design energy $\sqrt{s_{NN}} = 200$ GeV, was in the fall/winter 2001/2002. During the almost 8 years in operation, RHIC has been producing Au+Au, d+Au and p-p collisions and the collected data has been published in a large number of scientific articles.

tilibra

a) Experimental conditions at RHIC

i) Beam energy

The kinetic energy removed from the beam in the collision is available for the production of the QGP. It depends on the amount of stopping between the colliding ions.

The stopping can be estimated from the rapidity loss experienced by the baryons in the colliding nuclei.

If the incoming beam baryons have rapidity y_b relative to the c.m. (which has $y=0$), and average rapidity

$$\langle y \rangle = \frac{\int_0^{y_b} y \frac{dN}{dy} dy}{\int_0^{y_b} \frac{dN}{dy} dy}$$

after the collision, the average rapidity loss is

$$\delta y = y_b - \langle y \rangle$$

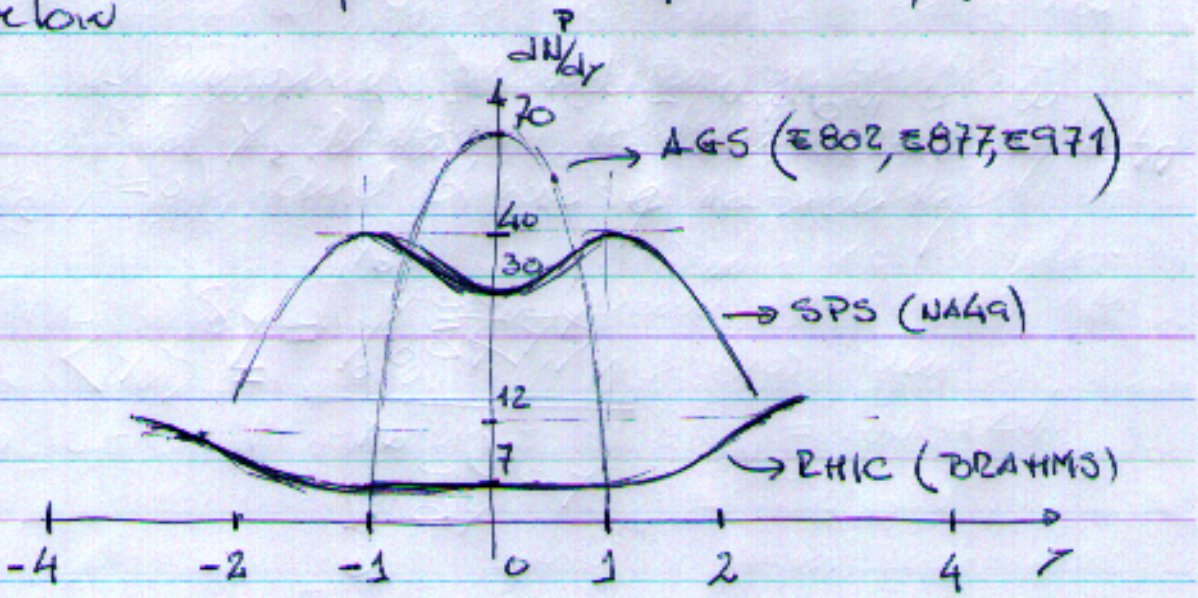
and where dN/dy is the number of net

baryons (baryon - antibaryons) per unit of rapidity. Thus, for the case of full stopping, $\delta y = y_b$ (meaning $\langle y \rangle = 0$)

BRAHMS has measured the net proton rapidity distribution at RHIC. The beam rapidity at RHIC is

$$y_b \sim 5.4$$

The results by BRAHMS, together with previous results from AGS and SPS are shown schematically in the figure below



In RHIC, the net number of protons per unit rapidity is about 7 and approximately constant in the interval $(-1, 1)$. It shows a rising up to $dN/dy \sim 12$ in the interval $y = 2-3$ in Au+Au collisions at $\sqrt{s_{NN}} = 200$ GeV.

tilibra

Note that, in contrast, the net number of protons per unit rapidity shows a peak at $y=0$ in AGS, while in SPS $dN/dy \sim 30$ at $y=0$ and rising up to $\frac{dN}{dy} \sim 30$ at $y \simeq \pm 1$.

The distribution measured at RHIC is qualitative and quantitatively different to those measured at AGS and SPS, indicating that a significantly different system is formed at mid-rapidities.

The conclusion is that the absolute rapidity loss at RHIC,

$$\delta y = 2.0 \pm 0.1$$

meaning that the average energy loss of the colliding nuclei is about

$$\varepsilon^{\text{Loss}}_{\text{Nucleon}} = 73 \pm 6 \text{ GeV}$$

per nucleon. This also corresponds to something about 26 TeV of kinetic energy removed from the beam per central Au+Au collision, which is available for particle productions immediately after the collision.

tilibra

b) Energy density

The collision scenario described in the past section indicates that the collision at RHIC can be conceptually divided in two regions: 1) the so-called fragmentation region, corresponding to the remnants of the colliding nucleus and 2) the central region in which the baryon number is comparatively small, but where significant energy density is collected. This picture is in qualitative agreement with the Bjorken regime which has been described at the beginning of the course.

The central region is decoupled of the fragmentation ones and, in that scenario, the kinetic energy removed from the fragments is stored in a color field existing between the receding partons. The linear increase of the color potential with distance eventually leads to the production of $q-\bar{q}$ pairs which may be produced anywhere between the fragments, leading to an approximately uniform particle production as a function of the rapidity.

Data from BRAHMS show that the multiplicity at RHIC is about

$$\frac{dN}{d\eta} = 625$$

particles per unit rapidity (charged) around $\eta = 0$, which is about 40-50% bigger than the multiplicity observed in p-p collisions at the same energy when the yields seen in Au+Au collisions is divided by the number of binary collisions (binary collision = nucleon-nucleon collisions, thus, the number of binary collisions scales as the atomic number A). Remember that the pseudorapidity η is defined as

$$\eta = -\ln\left[\tan\left(\frac{\theta}{2}\right)\right]$$

where θ is the angle between the beam and the produced particle, then

$$\eta = \frac{1}{2}\ln\left(\frac{\vec{p} + p_{\parallel}}{\vec{p} - p_{\parallel}}\right)$$

Integration over the charged particle pseudorapidity distributions at RHIC tell us that about 4600 charged particles are produced in (0-6%) central collisions. Since only charged particles are measured, the total number of particles produced at central collisions

is about 3/2 the number of charged particles, giving a total of about 7000 particles (charged + neutrals) produced.

From the measured spectra of pions, kaons and protons as a function of transverse momentum, the energy density can be estimated "à la Bjorken":

$$\varepsilon = \frac{1}{\pi R^2 \tau} \frac{d\langle E_T \rangle}{dy} = \frac{1}{\pi R^2 \tau} \langle m_\perp \rangle \frac{dN}{dy}$$

$$\simeq 5 \text{ GeV/fm}^3$$

for a formation time $\tau \sim 1 \text{ fm/c}$ and R the size of the overlapping region for the colliding nuclei. This value for the energy density is large enough to expect the production of the QGP.

c) Thermodynamic and chemical equilibrium at RHIC

It has been considered crucial to determine where there is thermodynamical equilibration of the "fireball" in relativistic collisions.
The main reason, as discussed in the derivation of the hydrodynamic equations is just the applicability of hydrodynamics itself.
In nuclear collisions, however, the time

tilibra

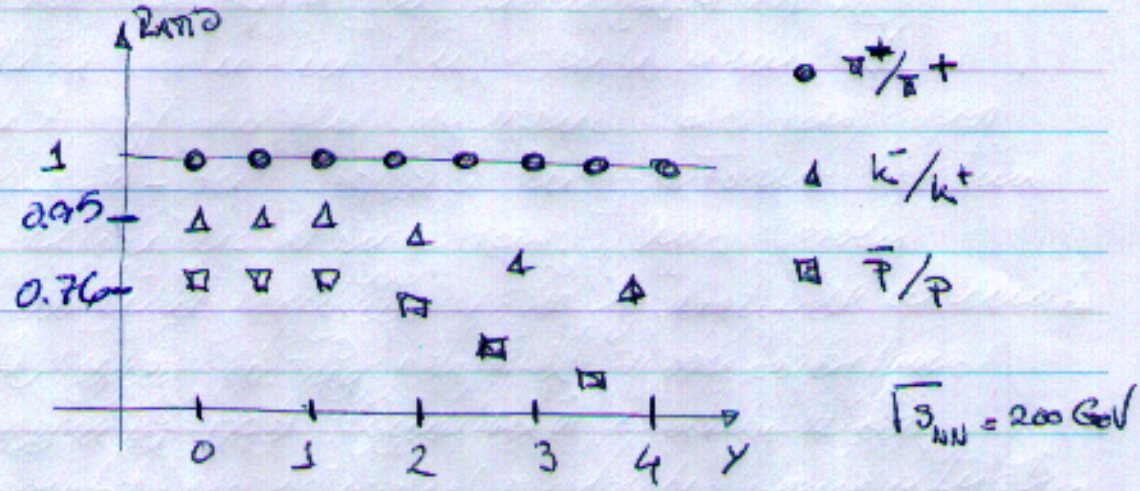
scale available is too short and the entire system only lives during the order of 10 fm/c. Consequently is not clear that the system evolves through equilibrated states. On the other hand, if equilibrium is reached, it suggest that the system lives for a very short period of time in a state with sufficiently short mean free path.

A central point in the discussion is to establish whether the equilibrium is reached, if in the hadronic gas just prior to freeze-out or in the partonic system just before hadronization. Thus, even when equilibrium is, per se, not a requirement for defining QGP, it may prove to be an important tool to identify the QGP.

i) chemical equilibrium

Whether the system is at chemical equilibrium or not at the partonic level can be studied from the ratio of the production of charged particles coming from the central rapidity region.
For a u, d gas (with its corresponding antiquarks) at chemical equilibrium we would expect the ratio of the production of π^+ to π^- to be close to 1. It means that

in the central region, at $\langle n_0 \rangle \simeq 0$, the production rate of $u/\bar{u}$ and $d/\bar{d}$ quarks is the same, leading to a π^+/π^- production ratio equal to one at mid rapidity.
The same should be true for charged K-ons and for proton anti-proton production, and in fact this is observed experimentaly at the RHIC experiments, at least approximately, as displayed schematically in the figure



The experimental results from RHIC really show that the π^-/π^+ ratio is equal to one all over the range of rapidity from 0 to 4.
For K^+/K^+ the ratio is equal to 0.95 and constant over the range 0 – 1.5 units of rapidity while for $\bar{p}/p$ the ratio is constant and equal to 0.76 over the rapidity range 0 – 1.5.

tilibra

One important process that leads to a K^-/K^+ ratio slightly lower than 1 at mid rapidity is the associated production mechanism (e.g. $p+p \rightarrow p+\Lambda+K^+$) which leads to an enrichment of positive kaons in regions where there is an excess of baryons. This means that the number of K^+ has to increase over the number of K^- at large rapidities where the net baryon number is not longer approximately zero.

A similar argument applies to the $\bar{p}/p$ ratio. As long as you get closer to the fragmentation regions, the average baryon number ceases to be zero and there is an excess of protons over anti-protons.

In sum, the ratios of anti-particle to particle production at RHIC seems to indicate that the fireball is in chemical equilibrium.

In order to give quantitative arguments we can use statistical models to obtain

$$\frac{\rho(\bar{p})}{\rho(p)} = \exp\left(-\frac{6\mu_{u,d}}{T}\right) \qquad (3)$$

for the $\bar{p}/p$ density ratio as a function of

tilibra

the chemical potential and temperature at the quark level. The same statistical argument, together with arguments including associated production lead to

$$\frac{\rho(\bar{k})}{\rho(k^+)} = \exp\left(\frac{-2(\mu_{0,N} - \mu_S)}{T}\right) =$$

$$= \exp\left(\frac{2\mu_S}{T}\right) \times \left[\frac{\rho(\bar{p})}{\rho(p)}\right]^{1/3} \qquad (4)$$

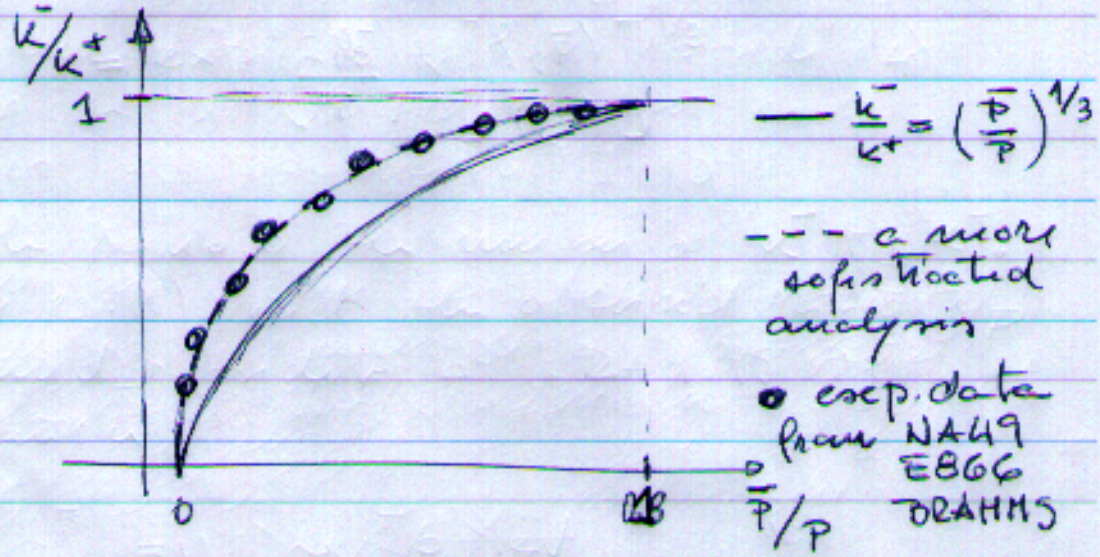
for the ratio of the number of $\bar{k}^-$ to k^+. From eq. (3) and the observed ratio $\bar{p}/p$ at mid rapidity at BRAHMS we obtain

$$\mu_{0,d} \sim 25 \text{ MeV}$$

Eq (4) tell us that at vanishing μ_S there is a power law between the two ratios with exponent $1/3$. The observed correlation deviates from the naive expectation suggesting a finite value for μ_S. However, a more detailed analysis assuming a grand canonical ensemble ~~with~~ with charge, baryon and strangeness conservation fitting these and other particle ratios measured at RHIC can be performed in order to obtain the chemical potentials and Temperature.

tilibra

Using the results of this analysis, it has been found that a large collection of such particle ratios are extremely well described by a statistical approach as the are leading to eqs (3) and (4) as show schematically in the figure below



This suggest that the system is at chemical equilibrium over the range of $\sqrt{s_{NN}}$ from AGS to RHIC and the observed rapidity ranges.

ii) Thermal equilibrium

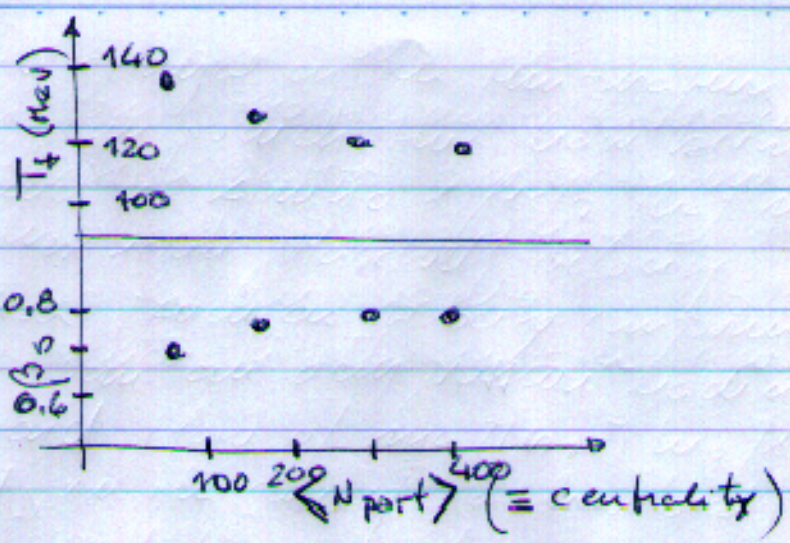
The properties of the expanding matter in the later stages of the collision up to the moment of the freeze-out, when all interactions cease, can be studied from the momentum distribution of the emitted particles. The slopes of the spectra of emitted particles

depends in general on the temperature of the source from which they have been created and on kinetic effects that may alter the expected Maxwell velocity distribution, such as velocity components resulting from an overpressure leading to an outward flow of matter. This flow is expected, in the case of (at least local) thermical equilibrium and sufficient density, to be describable by concept derived from fluid dynamics.

One should note, however, that the slope of the spectra reflects the particle distributions at the time of the freeze-out, when interactions have ceased.

In the so called blastwave approach, the spectrum shape is parametrized by a function depending on the temperature and on the transverse expansion velocity, which in turns depends on the radius. The results of such analyses for several particle/antiparticle species indicates that the thermal freeze-out temperature is in the range $T = 120-140$ MeV and that the maximum flow velocity is about $0.7c - 0.75c$ as shown in the figure above.

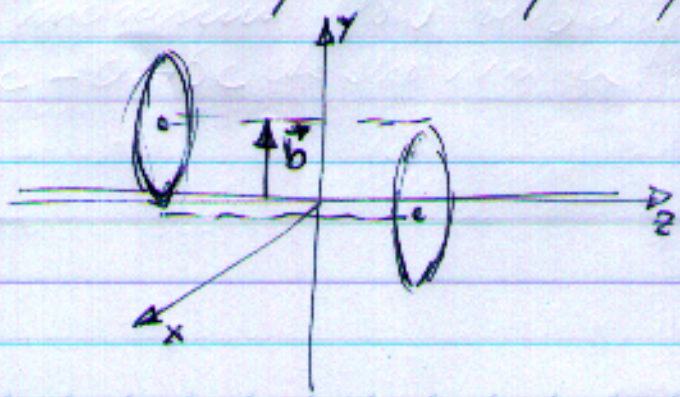
tilibra



$\beta_s \equiv$ transverse flow velocity
$T_f \equiv$ freeze-out temperature

These results are consistent with a large gradient of pressure in the transverse direction resulting from a large density.

Another powerful tool to study the thermodinamic properties of the source is the analysis of the azimutal momentum distribution of the emited particles relative to the event plane, defined as the direction of the impact parameter:



if $\vec{b}$ is along $\hat{y}$, the event (reaction) plane is x-z.

This distribution is usually parametrized as a series of terms depending on

$$\cos\left(n(\phi-\phi_r)\right)$$

where ϕ is the azimutal angle of the emited particle and ϕ_r is the angle of the reaction plane respectively (in the ~~coll~~ reference frame)
The coefficient v_1 of the term with $n=1$ measures the so-called directed flow, while the coefficient v_2 of the term in $n=2$ measures the elliptic flow. As a matter of fact, we can write

$$E\frac{dN^3}{d^3p} = \frac{1}{2\pi}\frac{d^2N}{dp_z dy}\left(1 + 2v_1\cos(\phi-\phi_r) + 2v_2\cos\left(2(\phi-\phi_r)\right) + \dots\right)$$

with $$v_1 = \langle p_x/p_\perp \rangle \; ; \; \phi \equiv \arctan\frac{p_x}{p_y}$$

$$v_2 = \left\langle \frac{p_y^2 - p_x^2}{p_x^2 + p_y^2} \right\rangle$$

where the "1" indicates that the particle production is isotropic, $v_2 \neq 0$ indicates that flow is

an asymmetry in the transverse plane (with respect to the collision axis) meaning that the "plasma" region is of the form of an almond expanding in different form in the transverse plane.

Elliptic flow has been measured at RHIC and has been found large v_2 values for many hadron species, which is consistent with hydrodynamics and thus with thermal equilibrium.

d) high $p_\perp$ suppression at mid-rapidity

RHIC data exhibits a suppression of the high $p_\perp$ transverse momentum component of hadron spectra in Au+Au central collisions as compared to the scaled momentum spectra in p+p collisions. This suppression is quantitatively accounted for the so called nuclear modification factor R_{AA},

$$R_{AA} = \frac{d^2N^{AA}/dp_\perp d\eta}{\langle N_{bin}\rangle\, d^2N^{pp}/dp_\perp d\eta}$$

ilibria

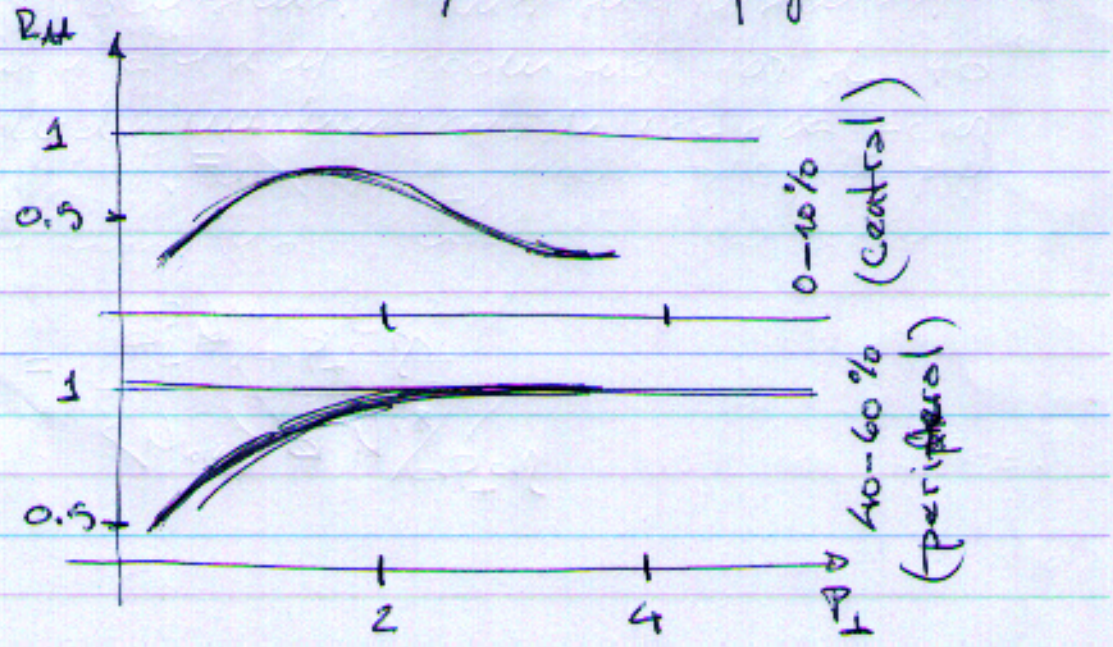
where $\langle N_{bin} \rangle$ is the number of binary collisions ($\langle N_{bin} \rangle = A$ for the collision of identical nucleus at $\vec{b} = 0$)

In the absence of medium effects, nuclear collisions at high $p_\perp$ can be viewed as a superposition of hard nucleon - nucleon collisions. Thus we expect $R_{AA} = 1$ at high $p_\perp$

At low $p_\perp$, where particle production follows a scaling with the number of participants, the above definition leads to

$$R_{AA} < 1 \quad \text{for} \quad p_\perp < 2\ \text{GeV/c}$$

Results found at RHIC behave as show schematically in the figure bellow



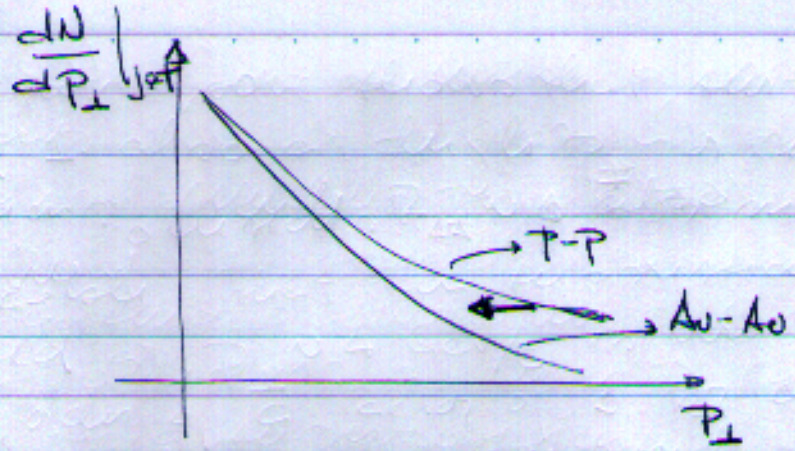
tilibra

The figure above shows that, surprisingly, $R_{AA} < 1$ also at high p_T for central collisions, while $R_{AA} \sim 1$ for more peripheral collisions. It is also remarkable that the suppression observed at $p_T \sim 4$ GeV/c is very large, of the order of a factor of 3 for central Au+Au collisions as compared to p+p

These results can be understood in terms of large energy loss of high momentum partons inside the medium. In fact, it has been shown that energy loss by radiation (quark radiate gluons inside the medium) together with multiple scattering can explain the effect, although not in full details. It has to be noted that the above interpretation in terms of parton energy loss comes from hard particle interactions inside the plasma, instead of the usual view in terms of hydrodynamics.

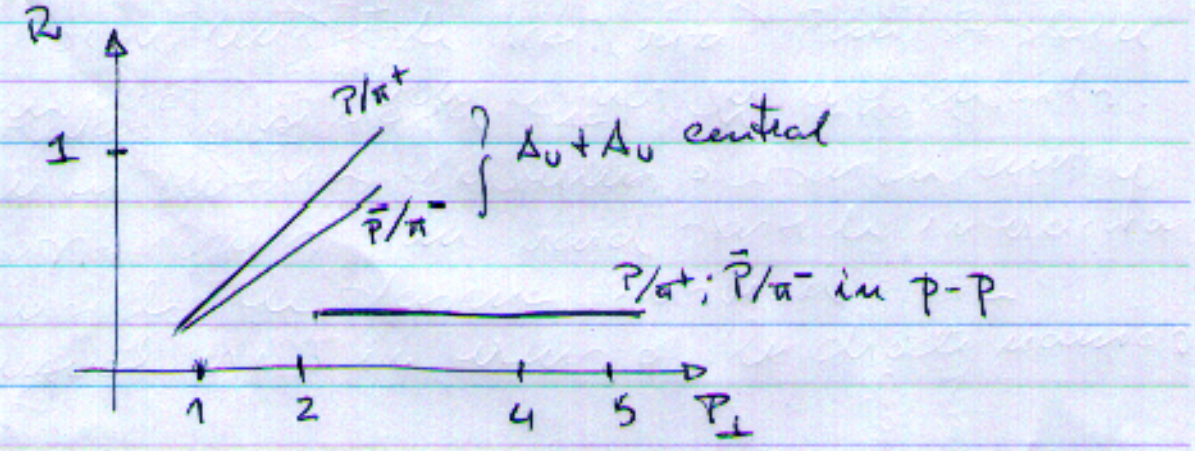
The effect of jet-suppression observed at STAR it is also understood in terms of parton energy loss:

tilibra



Jet-quenching

The high $p_\perp$ suppression has been also studied for different particle species. The ratios of particle yields for p/π^+ and $\bar{p}/\pi^-$ have been measured at BRAHMS. They are as show in the figure below



The reason for the differences of the p/π^+ and $\bar{p}/\pi^-$ ratios in central d+Au collisions as compared to p-p collisions are not understood at present.

tilibra

Available online at www.sciencedirect.com
SCIENCE DIRECT®
Physics Letters B 634 (2006) 200–204
PHYSICS LETTERS B
www.elsevier.com/locate/physletb

Finite size effects on pion spectra in relativistic heavy-ion collisions

Alejandro Ayala [a,*], Eleazar Cuautle [a], J. Magnin [b], Luis Manuel Montaño [c], Alfredo Raya [a]

[a] *Instituto de Ciencias Nucleares, Universidad Nacional Autónoma de México, Apartado Postal 70-543, México Distrito Federal 04510, Mexico*
[b] *Centro Brasileiro de Pesquisas Fisicas, Rua Dr. Xavier Sigaud 150-Urca CEP 22290-180, Rio de Janeiro, Brazil*
[c] *Centro de Investigación y de Estudios Avanzados del IPN, Apartado Postal 14-740, México Distrito Federal 07000, Mexico*

Received 18 October 2005; received in revised form 18 January 2006; accepted 26 January 2006

Available online 3 February 2006

Editor: W. Haxton

Abstract

We compute the pion inclusive transverse momentum distribution assuming thermal equilibrium together with transverse flow and accounting for finite size effects and energy loss at the time of decoupling. We compare to data on mid-rapidity pions produced in central collisions in RHIC at $\sqrt{s_{NN}} = 200$ GeV. We find that a finite size for the system of emitting particles results in a power-like fall-off of the spectra that follows the data up to larger p_t values, as compared to a simple thermal model.
© 2006 Elsevier B.V. All rights reserved.

PACS: 25.75.-q

1. Introduction

In recent years, strong evidence has been found in favor of the production of matter composed of the fundamental QCD degrees of freedom in central Au + Au collisions at the relativistic heavy-ion collider (RHIC) [1,2]. Some of the quantitative understanding about the signals supporting these findings are associated to intermediate or high p_t phenomena in particle spectra. Among these, the depletion in the production of large p_t charged hadrons and neutral pions, as compared to extrapolations of data on p + p collisions to RHIC energies [3], suggests that the fragmenting partons that give rise to final hadrons, loose energy on their way through the dense partonic matter believed to be formed during the early stages of the reaction. This phenomenon has been named jet quenching [4] and has received stronger experimental support from the results of the d + Au mode at RHIC [5]. Moreover, the behavior of the proton to pion ratio for intermediate $p_t \sim 2$ GeV [6] suggests that an important mechanism of hadron production at RHIC is the thermal recombination of free quarks [7] during the evolution of the collision.

In spite of the success of this conceptual framework to interpret RHIC data, there is an ingredient commonly overlooked: the fact that all these phenomena take place during small time scales and consequently within small volumes.

Although not commonly considered, it is certainly true that small size effects are important in the description of statistical systems. For example, finite size effects influence the late-stage growth of nucleated bubbles during a first order phase transition [8]. Also, in the statistical hadronization model, the states used for the description are in general different to the observed asymptotic ones but such difference is not an issue unless the volume of the system is small, typically of order $\mathcal{O}(10\ \text{fm})^3$ [9]. Finite size effects are also known to influence the interpretation of the correlation lengths in Hanbury Brown–Twiss analysis in the context of relativistic heavy-ion collisions [10,11].

Finite size effects on particle spectra have also been recently investigated in Refs. [12–14], where these were referred to as *boundary effects*. The scenario considered in the last two of these studies resorts to a mean field treatment of the interactions affecting the most abundantly produced particles in the reactions, namely pions. It was argued that prior to kinetic freeze-out, the pion mean free path is smaller than the pion

* Corresponding author.
E-mail address: ayala@nucleares.unam.mx (A. Ayala).

0370-2693/$ – see front matter © 2006 Elsevier B.V. All rights reserved.
doi:10.1016/j.physletb.2006.01.063

interaction range and therefore that during this stage, pions are still strongly interacting, mainly attractively, among themselves. The system resembles more a liquid than a gas, with a surface tension acting as a reflecting boundary. When assuming thermalization at freeze-out, the pion spectrum can be computed from the sum of the square of the wave functions in momentum space weighed by the thermal occupation number for each state.

Qualitatively, the behavior of particle spectra including this finite size effects deviates from a simple exponential fall-off at high momentum since, from the Heisenberg uncertainty principle, the more localized the states are in coordinate space, the wider their spread will be in momentum space. In terms of the discrete set of energy states describing the pion system, this behavior can be understood as arising from a higher density of states at large energy as compared to a calculation without boundary.

In this Letter we compute the transverse momentum distribution for pions assuming thermal equilibrium together with transverse flow and accounting for finite size effects at decoupling. By comparing to data on pion spectra on Au + Au collisions at $\sqrt{s_{NN}} = 200$ GeV [6,15], we show that for temperatures and collective transverse flow within the commonly accepted values, the transverse momentum distributions can be described up to larger values of p_t as compared to a simple exponential fall-off.

The Letter is organized as follows: in Section 2, we present the basics of the model to compute the pion spectra including finite size effects. In Section 3, we compute the thermal pion spectrum including the effects of transverse flow together with the description of finite size effects. We carry out a systematic study of the behavior of the spectra when varying the parameters involved. In Section 4 we compare the calculation to data on pion transverse distributions from Au + Au collisions at $\sqrt{s_{NN}} = 200$ GeV and show how this model pushes the thermal component of the spectrum to larger p_t values as compared to a simple exponential description. Finally, we summarize and conclude in Section 5.

2. The model

When the system of particles can be considered as confined and their wave functions as satisfying a given condition at the boundary just before freeze out, the energy states form a discrete set. The shape of the volume within the confining boundary is certainly an important issue in case the model aims to describe transverse momentum particle distributions at all rapidities. However, in this Letter we will restrict ourselves to describe spectra at central rapidities. We thus consider a scenario in which the system of particles of a given species is in thermal equilibrium and is confined within a sphere of radius R (fireball) as viewed from the center of mass of the colliding nuclei at the time of decoupling. This time needs not be the same over the entire reaction volume. Nevertheless, in the spirit of the fireball model, we consider that decoupling takes place over a constant time surface in space–time. This assumption should be essentially correct if the freeze-out interval is short compared to the system's life time.

The solutions that incorporate the effects of a finite size system have been found in Ref. [13]. They are given as the stationary solutions to the equation

$$\left(\frac{\partial^2}{\partial t^2} - \nabla^2 + m^2\right)\psi(\mathbf{r}, t) = 0 \tag{1}$$

subject to the condition

$$\psi(|\mathbf{r}| = R, t) = 0, \tag{2}$$

and also finite at the origin. The normalized stationary states are

$$\psi_{nlm'}(\mathbf{r}, t) = \frac{1}{R\ J_{l+3/2}(k_{nl}R)}\left(\frac{1}{rE_{nl}}\right)^{1/2} \times Y_{lm'}(\hat{r})J_{l+1/2}(k_{nl}r)e^{-iE_{nl}t}, \tag{3}$$

where J_ν is a Bessel function of the first kind and $Y_{lm'}$ is a spherical harmonic. The parameters k_{nl} are related to the energy eigenvalues E_{nl} by

$$E_{nl}^2 = k_{nl}^2 + m^2 \tag{4}$$

and are given as the solutions to

$$J_{l+1/2}(k_{nl}R) = 0. \tag{5}$$

Thus, the eigenfunctions for the bound system of particles are given explicitly by Eq. (3). These are analytical, albeit given in terms of Bessel functions.

3. Thermal spectrum

The contribution to the thermal particle invariant distribution from a state with quantum numbers $\{n, l, m'\}$ is given by

$$E\frac{d^3N_{nlm'}}{d^3p} = \int \frac{d\sigma}{(2\pi)^3}(k_{nl}\cdot u)\, f(k_{nl}\cdot v)\mathcal{W}_{nlm'}(\mathbf{p}, \mathbf{r}), \tag{6}$$

where $\mathcal{W}_{nlm'}(\mathbf{p}, \mathbf{r})$ is the Wigner transform and $f(k_{nl}\cdot v)$ the thermal occupation factor of the state $\psi_{nlm'}$, respectively. The four-vectors v^μ and u^μ represent the collective flow four-velocity and a four-vector of magnitude one, normal to the freeze-out hypersurface σ, respectively.

For the system of bound bosons, the Wigner transform of a given state is defined as

$$\mathcal{W}_{nlm'}(\mathbf{p}, \mathbf{r}) = \int d^3r'\, e^{-i\mathbf{p}\cdot\mathbf{r}} \times \psi^*_{nlm'}\left(\mathbf{r} + \frac{\mathbf{r}'}{2}, t\right)\overset{\leftrightarrow}{\frac{\partial}{\partial t}}\psi_{nlm'}\left(\mathbf{r} - \frac{\mathbf{r}'}{2}, t\right). \tag{7}$$

In order to consider a situation where freeze-out happens at a fixed time and within a spherical volume of radius R, the unit four-vector u^μ can be chosen as $u^\mu = (1, \mathbf{0})$.

To keep matters simple, we consider a thermal occupation factor of the Maxwell–Boltzmann kind, namely

$$f(k_{nl}\cdot v) = e^{-k_{nl}\cdot v/T}, \tag{8}$$

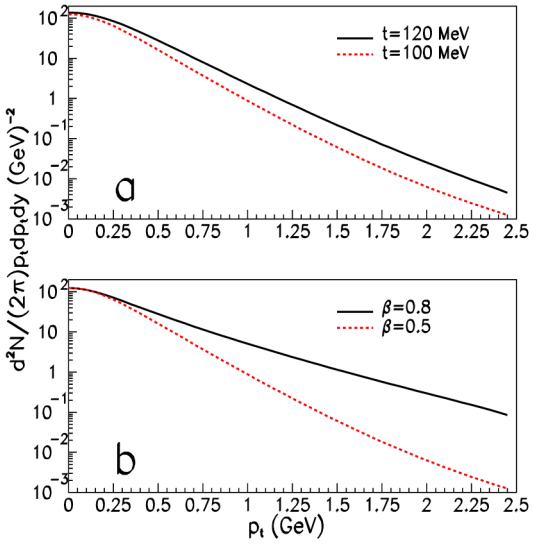


Fig. 1. Invariant pion distribution as a function of p_t for different combinations of the parameters T and β for a fixed value $R = 8$ fm. The normalization is arbitrary.

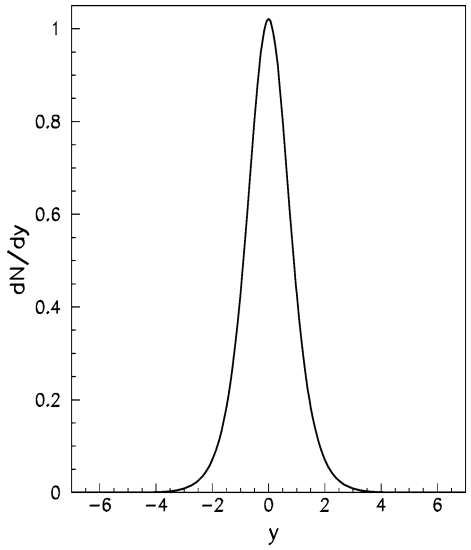


Fig. 2. Pion rapidity distribution for $T = 120$ MeV, $\beta = 0.6$ and $R = 8$ fm. The normalization is arbitrary.

where T is the system's temperature. The four-vector v^μ is parametrized as

$$v^\mu = \gamma(1, \mathbf{v}), \tag{9}$$

and we choose a radial profile for the vector $\mathbf{v}$ such as

$$\mathbf{v} = \beta \frac{\mathbf{r}}{R}, \tag{10}$$

where the parameter β represents the surface expansion velocity. Notice that the radial profile for the expansion velocity considered in Eq. (10) can be taken as the transverse component of the flow only for the description of central rapidity data. Correspondingly, the gamma factor is given by

$$\gamma = \frac{1}{\sqrt{1 - (\beta \frac{r}{R})^2}}. \tag{11}$$

Nonetheless, in order to continue to keep matters as simple as possible, and be able to analytically perform the integrations in Eq. (6), we will instead consider that the gamma factor is a constant evaluated at the average transverse expansion velocity, namely,

$$\gamma \to \bar{\gamma} = \frac{1}{\sqrt{1 - (3\beta/4)^2}}. \tag{12}$$

We take the four-vector k^μ_{nl} given by

$$k^\mu_{nl} = (E_{nl}, \mathbf{k}_{nl}), \tag{13}$$

and choose $\mathbf{k}_{nl} \parallel \mathbf{p}$. This choice is motivated from the continuum, boundless limit, where the relativistically invariant exponent in the thermal occupation factor becomes $\gamma(E - \mathbf{p}\cdot\mathbf{v})$.

Gathering the elements described in Eqs. (7) to (13), it is straightforward to evaluate the integral in Eq. (6). Summing over all the states, the invariant thermal distribution is given by

$$E\frac{d^3N}{d^3p} = \mathcal{N}\sum_{nl}\frac{(2l+1)}{(2\pi)}\frac{k^2_{nl}E_{nl}\, e^{-\bar{\gamma}E_{nl}/T}}{\sqrt{p^2 + (\frac{\bar{\gamma}\beta k_{nl}}{2RT})^2}} \times \frac{|J_{l+1/2}(pR - i\frac{\bar{\gamma}\beta k_{nl}}{2T})|^2}{[p^2 - k^2_{nl} - (\frac{\bar{\gamma}\beta k_{nl}}{2RT})^2]^2 + [\frac{\bar{\gamma}\beta p k_{nl}}{RT}]^2}, \tag{14}$$

where the factor $(2l+1)$ comes from the degeneracy of a state with a given angular momentum eigenvalue l and $\mathcal{N}$ is a normalization constant.

Fig. 1 shows the invariant pion distribution as a function of p_t for different combinations of the parameters T and β and a fixed value $R = 8$ fm. Fig. 1(a) shows the distribution for two different temperatures $T = 100$, 120 MeV and $\beta = 0.5$. As expected, the effect of increasing the temperature is to increase the inverse slope of the distribution. Fig. 1(b) shows the distribution for two different values of the surface expansion velocity, $\beta = 0.5$, 0.8 and $T = 100$ MeV. The effect of increasing the expansion velocity is also to increase the inverse slope of the distribution. Fig. 2 shows an example of the kind of rapidity distributions obtained in the model. Notice that the distribution is not as broad as data seem to indicate (see for example Ref. [16]). This is a limitation of the spherical symmetry assumed in the model emphasizing the need of restricting its applicability to the description of central rapidity data.

Fig. 3 shows the distribution for two different values of the confining radius $R = 8$, 10 fm for fixed values of $T = 120$ MeV and $\beta = 0.6$. The effect of increasing the confining radius is to increase the value of p_t for which the distribution has a point of inflexion towards a concave shape. This is to be expected since in the limit where the confining volume goes to infinity, the value of p_t for this point of inflexion should also go to infinity as the system becomes boundless.

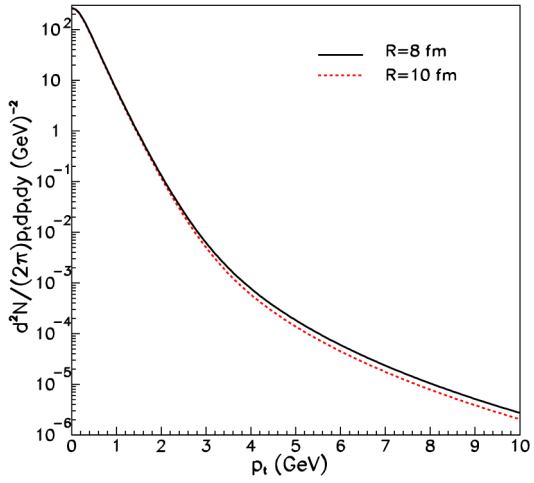


Fig. 3. Invariant pion distribution as a function of p_t for two values of the parameter R and fixed values $T = 120$ MeV and $\beta = 0.6$. The normalization is arbitrary.

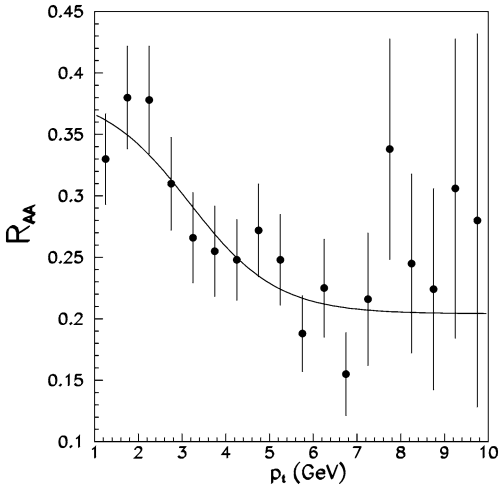


Fig. 4. Nuclear suppression factor R_{AA} for neutral pions from Ref. [15] parametrized in the interval from 1 to 10 GeV. The parametrization is chosen as to become a constant for large p_t values.

4. Pion spectra

In order to test the model, we compare the theoretical distribution to data on mid-rapidity pions produced in RHIC central collisions at $\sqrt{s_{NN}} = 200$ GeV [6,15]. Rather than performing an overall fit to find the optimum parameters, we fix them to values within the commonly accepted ones to describe freeze-out conditions.

To include the effects of parton energy loss, we resort to parametrize the data on R_{AA} for neutral pions as measured by PHENIX [15]. We use the expression

$$\frac{A}{e^{x-B}+1} + C, \tag{15}$$

and find from a fit to the data on R_{AA} the values $A = 0.18$, $B = 3.17$ and $C = 0.20$. This parametrization is taken in such a way that for large p_t the nuclear suppression factor remains a constant. This is shown in Fig. 4.

First we describe data for the low p_t part of the spectra. This is done in Fig. 5 where we show the invariant pion distribution as a function of p_t for $R = 8$ fm, $T = 120$ MeV and $\beta = 0.6$, including the energy loss effect, compared to data on π^+ from PHENIX [6]. The normalization of the model theoretical curve has been calculated from a fit to the data. We notice from Fig. 5 that the curve does a very good job describing the data for all values of p_t. In contrast, a calculation where no effects of a finite size are included, and thus the wave function of a given state is simply a plane wave, does not describe the data over the considered range when we use the same values for T and β as for the case of the calculation with a confining volume. This is also shown in Fig. 5 where we notice the more steep fall-off of the curve without finite size effects.

Next we describe data in the range 1 GeV $< p_t <$ 10 GeV. This is done in Fig. 6 where we show the invariant pion distribution as a function of p_t for $T = 120$ MeV, $\beta = 0.6$ and $R = 8$–14 fm, including the energy loss effect, compared to data on neutral pions from PHENIX [15]. The normalization of the curves has been taken from the fit to the π^+ spectrum. The

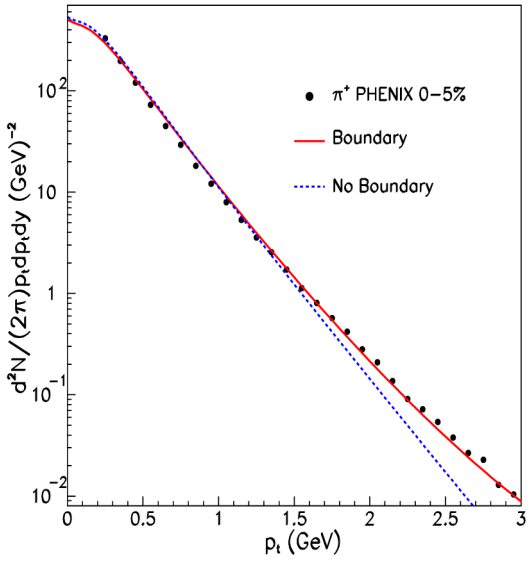


Fig. 5. Invariant pion distribution as a function of p_t for $R = 8$ fm, $T = 120$ MeV and $\beta = 0.6$ compared to data on mid rapidity positive pions from central collisions at $\sqrt{s_{NN}} = 200$ GeV measured by PHENIX. The normalization of the model theoretical curve has been fixed from a fit to the data.

model does a good description of data for values of the parameter R between 8 and 10 fm up to $p_t \sim 3$ GeV from where the curves start deviating from the data that shows a steeper fall-off. This failure is however expected since for large p_t the leading particle production mechanism is the fragmentation of fast moving partons, some of which fragment outside the fireball region and thus are not influenced by the confining boundary that the rest of the particles experience within the fireball.

5. Summary and conclusions

In this Letter we have computed the pion transverse momentum distribution in a thermal model including transverse expansion and accounting for the fact that the system of particles is produced within a small volume up to freeze-out, in

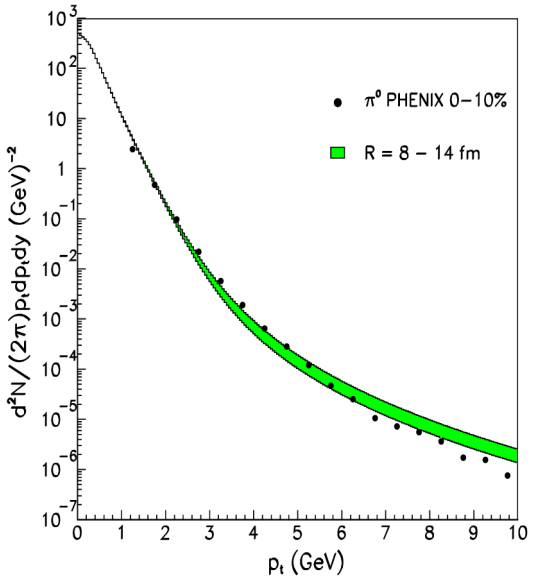


Fig. 6. Invariant pion distribution as a function of p_t for $T = 120$ MeV, $\beta = 0.6$ for values of $R = 8$ fm (upper curve) to $R = 14$ fm (lower curve), compared to data on mid rapidity neutral pions from central collisions at $\sqrt{s_{NN}} = 200$ GeV measured by PHENIX. The normalization of the curves has been taken from the fit to the π^+ spectrum.

the context of relativistic heavy-ion collisions. The finite size has been introduced by requiring that the system's wave functions vanish at the boundary but remain finite at the origin. The net effect is a broadening of the particle transverse momentum distribution with respect to a simple thermal model without a boundary. The physical origin of this broadening is the Heisenberg uncertainty principle since as the states are more localized in coordinate space, their spread is wider in momentum space. Energy loss has also been considered by a parametrization of the experimentally measured nuclear suppression factor R_{AA} where we require that this becomes constant for large p_t values.

The model does a very good job describing data for low to intermediate p_t in the range $0 < p_t \lesssim 3$ GeV for commonly accepted values of the temperature $T = 120$ MeV and the surface transverse expansion velocity $\beta = 0.6$ (corresponding to an average transverse expansion velocity $\langle\beta\rangle \simeq 0.5$) when the system's radius R at freeze-out is in the range $8\text{ fm} \lesssim R \lesssim 10$ fm. This is best seen when comparing the model to data on charged pions produced in central Au + Au collisions. The description of data for p_t in the range $3 \lesssim p_t < 10$ is not as good as can be seen from a comparison of the model to the spectrum of neutral pions produced in central Au + Au collisions. This behavior is not surprising though, since for large p_t it is well known that the leading particle production mechanism is the fragmentation of fast moving partons, some of which fragment outside the fireball region and thus are not influenced by the confining boundary, or mean field, that the rest of the particles experience within the fireball.

We thus conclude that the thermal features of the spectrum, which are obtained from the low p_t region, are best highlighted when accounting for the finite size of the system at decoupling. It is of course interesting to check the consistency of this treatment when extended to the case of fermions, and in particular protons. Finally, it is worth to note that finite size effects should also play a role during the partonic phase of the collision [17] and in particular that they can also influence the recombination scenario. This kind of analyses is for the future.

Acknowledgements

The authors thank G. Paic for his valuable comments and suggestions and I. Dominguez for having prepared a PYTHIA simulation for comparison with our work. A.A. and L.M.M. thank the staff at CBPF for their help during a summer visit when part of this work was done. Support for this work has been received in part by PAPIIT-UNAM under grant number IN107105 and CONACyT under grant numbers 40025-F and bilateral agreement CONACyT-CNPq J200.556/2004 and 491227/2004-3.

References

[1] R. Bellwied, Nucl. Phys. A 752 (2005) 398c.
[2] J. Adams, et al., STAR Collaboration, Nucl. Phys. A 757 (2005) 102.
[3] K. Adcox, et al., PHENIX Collaboration, Phys. Rev. Lett. 88 (2002) 022301;
C. Adler, et al., STAR Collaboration, Phys. Rev. Lett. 89 (2002) 202301;
B.B. Back, et al., PHOBOS Collaboration, Phys. Lett. B 578 (2004) 297.
[4] M. Gyulassy, M. Plumer, Phys. Lett. B 243 (1990) 432;
X.N. Wang, M. Gyulassy, Phys. Rev. Lett. 68 (1992) 1480.
[5] K. Adcox, et al., PHENIX Collaboration, Phys. Rev. Lett. 91 (2003) 072303;
C. Adler, et al., STAR Collaboration, Phys. Rev. Lett. 91 (2003) 072304;
B.B. Back, et al., PHOBOS Collaboration, Phys. Rev. Lett. 91 (2003) 072302.
[6] S.S. Adler, et al., PHENIX Collaboration, Phys. Rev. C 69 (2004) 034909.
[7] R.C. Hwa, C.B. Yang, Phys. Rev. C 67 (2003) 034902;
R.J. Fries, B. Müller, C. Nonaka, S.A. Bass, Phys. Rev. Lett. 90 (2003) 202303;
V. Greco, C.M. Ko, P. Lévai, Phys. Rev. Lett. 90 (2003) 202302.
[8] E.S. Fraga, R. Venugopalan, Braz. J. Phys. 34 (2004) 315;
E.S. Fraga, R. Venugopalan, Physica A 345 (2004) 121.
[9] F. Becattini, J. Phys. Conf. Ser. 5 (2005) 175.
[10] Q.H. Zhang, S.S. Padula, Phys. Rev. C 62 (2000) 024902;
Q.H. Zhang, hep-ph/0106242.
[11] A. Ayala, A. Sánchez, Phys. Rev. C 63 (2001) 064901.
[12] M. Mostafa, C.Y. Wong, Phys. Rev. C 51 (1995) 2135.
[13] A. Ayala, A. Smerzi, Phys. Lett. B 405 (1997) 20.
[14] A. Ayala, J. Barreiro, L.M. Montaño, Phys. Rev. C 60 (1999) 014904.
[15] S.S. Adler, et al., PHENIX Collaboration, Phys. Rev. Lett. 91 (2003) 072301.
[16] I.G. Bearden, et al., BRAHMS Collaboration, Phys. Rev. Lett. 94 (2005) 162301.
[17] C.-Y. Wong, Phys. Rev. C 48 (1993) 902.

Proton and pion transverse spectra at the BNL Relativistic Heavy Ion Collider from radial flow and finite size effects

Alejandro Ayala,[1] Eleazar Cuautle,[1] J. Magnin,[2] and Luis Manuel Montaño[3]
[1]*Instituto de Ciencias Nucleares, Universidad Nacional Autónoma de México, Apartado Postal 70-543, México Distrito Federal 04510, Mexico*
[2]*Centro Brasileiro de Pesquisas Fisicas, Rua Dr. Xavier Sigaud 150-Urca CEP 22290-180, Rio de Janeiro, Brazil*
[3]*Centro de Investigación y de Estudios Avanzados del IPN, Apartado Postal 14-740, México Distrito Federal 07000, Mexico*
(Received 13 March 2006; revised manuscript received 4 October 2006; published 4 December 2006)

We show that the proton and pion transverse momentum distributions measured at BNL Relativistic Heavy Ion Collider (RHIC), for all collision centralities for pions and most of the collision centralities for protons, can be simultaneously described in terms of a thermal model with common values for the radial flow and temperature, when accounting for the finite size of the interaction region at the time of decoupling. We show that this description is obtained in terms of a simple scaling law of the size of the interaction region with the number of participants in the collision. The behavior of the proton to pion ratio at mid-rapidity can also be understood as a consequence of the strength of the radial flow and system size reached at RHIC energies.

DOI: 10.1103/PhysRevC.74.064903 PACS number(s): 25.75.Ld, 24.10.Pa

I. INTRODUCTION

The unexpected behavior of the proton to pion ratio as a function of p_t has been taken as an indication of the onset of the thermal recombination of quarks as an important mechanism for hadron production at BNL Relativistic Heavy Ion Collider (RHIC) energies in Au+Au collisions [1]. In its simplest form, thermal recombination invokes a densely populated parton phase space to allow the statistical formation of hadrons from constituent quarks assigning degeneracy factors appropriate for either mesons or baryons [2].

An important shortcoming of the recombination scenario is that it ignores inelastic and elastic scattering experienced by hadrons before kinetic freeze-out and thus neither particle abundance nor their spectra are fixed right after recombination. A more appropriate description of statistical systems, which includes the fact that the detailed history is washed out by means of interactions after a long enough time, can be given in terms of global features that survive all the way to the end of the system's evolution. One of these global features is flow, in particular, radial flow.

It has been observed that the magnitude of the radial flow velocity exhibits a 50% increase from BNL Alternating Gradient Synchrotron (AGS) and CERN Super Proton Synchrotron (SPS) to RHIC energies [3]. Recall that in $p + p$ collisions, where no effects of radial flow exist, it is known that the proton to pion ratio as a function of p_t remains basically unchanged, never exceeding one, for collision energies ranging from 19.4 GeV at the Tevatron and 44.6 and 52.8 GeV at Intersecting Storage Rings (ISR) up to 200 GeV at RHIC [4]. In contrast, the proton to pion ratio in Au+Au collisions at RHIC reaches and even exceeds one for $p_t \sim 2$ GeV. Therefore, if recombination of thermal partons has anything to do with this behavior it is clear that a thermal description of the individual particle spectra must be possible at least up to such p_t values. Nevertheless, in Ref. [1], a fit to a thermal model that attempts a description of particle spectra up to $p_t \sim 2$ GeV in terms of an intrinsic freeze-out temperature T_0, together with radial flow, yields values on the order of $T_0 \sim 180$ MeV, which is closer to the hadronization temperature than to the kinetic freeze-out temperature.

Yet another intriguing behavior that concerns freeze-out temperatures and expansion velocities in thermal models is their relation as a function of the centrality of the collisions, which, within the usual thermal model calculations, can be stated as an increase in flow together with a decrease in temperature as the centrality of the collisions increases. This behavior is usually attributed to the greater amount of time spent by the system in the hadronic phase for the most central collisions, allowing for the development of flow and consequently decreasing the values for the kinetic freeze-out temperature [5,6]. However, as results from elliptic flow analyses seem to indicate [7], flow is generated early, in the partonic phase of the collision. Moreover, kinetic freeze-out temperatures can also be thought of as a global feature of strongly interacting systems that reflect the average kinetic energy needed for the system to decouple. In fact, a systematic study of Hanbury-Brown–Twiss (HBT) data and particle yields for pions at mid-rapidity from AGS to RHIC energies [8] shows that this average energy is independent of centrality and beam energy. Therefore, one can ask if an alternative description, with common values of temperature and flow velocity, reflecting the above property of strongly interacting systems can be achieved for all centralities. As we show, the key ingredient that allows a description of particle spectra in a thermal model, including radial flow, and that addresses the above-mentioned phenomena from a unifying point of view, is the realization that particle production and successive freeze-out in a relativistic heavy-ion environment takes place during small time scales, on the order of 10 fm, and consequently within small volumes.

Although not commonly considered, small size effects are important in the description of a variety of phenomena associated with statistical systems such as the late-stage growth of nucleated bubbles during a first-order phase transition [9]

 ©2006 The American Physical Society

and the statistical hadronization model [10]. Finite size effects are also known to influence the interpretation of the correlation lengths in HBT analysis in the context of relativistic heavy-ion collisions [11,12].

Recall that useful microscopical information in this kind of collision can be obtained from comparing the average interparticle separation during the collision evolution to the range of strong interactions. In the case of pions (the most copiously produced particles in the collision), right after the collision the system is better described as a liquid rather than as a gas [13]. One important consequence is the appearance of a surface tension that acts as a reflecting boundary for the particles that move toward it. The reflection details depend on the wavelength of the incident particle but the important property introduced by the reflecting surface is that it allows very little wave function leakage and, to a good approximation, the wave functions vanish outside this boundary. When the average separation of the particles in the system becomes larger than the range of the strong interaction, they become a free gas but, because of the short interaction range, the transition between the liquid and the gas stages is very rapid and the momentum distribution is determined by the distribution just before freeze-out.

To be concrete, we need to compare the pion separation d to the average range of the pion strong interaction ($d_s \sim 1.4$ fm). For typically accepted values for the density and formation times [14], it is possible to show that $d \sim 0.6$ fm $< d_s$ and the condition to regard the pion system as a liquid is met.

Qualitatively, the behavior of thermal particle spectra including finite size effects deviates from a simple exponential fall-off at high momentum because, from the Heisenberg uncertainty principle, the more localized the states are in coordinate space the wider their spread will be in momentum space. In terms of the discrete set of energy states describing the particle system, this behavior can be understood as arising from a higher density of states at large energy as compared to a calculation without finite size effects. These ideas have been applied to the description of charged and neutral pion spectra measured at RHIC with good agreement for the transverse momentum interval $0 < p_t \lesssim 3$ [15].

In this article we compute the transverse momentum distribution for pions and extend the above ideas to also include protons in the description, assuming thermal equilibrium together with radial flow and accounting for finite size effects at decoupling. By comparison with data on pion and proton spectra on Au+Au collisions at $\sqrt{s_{NN}} = 200$ GeV [1], we show that, for temperatures and collective transverse flow within values corresponding to kinetic freeze-out conditions, the transverse momentum distributions can be described with common values of temperature and expansion velocities for all collision centralities for pions and for most of the collision centralities for protons.

This work is organized as follows: In Sec. II we present the basics of the model to compute pion and proton distributions. In Sec. III we compute the transverse momentum distributions for protons and pions comparing these to data on Au+Au collisions at $\sqrt{s_{NN}} = 200$ GeV. We show that a good agreement with these data for different collision centralities can be achieved by assuming a simple scaling of the radii with the cube root of the number of participants in the collision. In Sec. IV we compute the pion correlation function and also extract the size of the system as a function of the cube root of the number of participants in the collision. We finally conclude in Sec. V.

II. THE MODEL

We consider a scenario where finite size effects are included by restricting the system of particles to be confined within a volume of the size of the fireball at freeze-out. Because we aim to describe spectra at central rapidities, it suffices to take the confining volume as a sphere of radius R (fireball) as viewed from the center of mass of the colliding nuclei at the time of decoupling [16]. This time needs not be the same over the entire reaction volume. Nevertheless, in the spirit of the fireball model we consider that decoupling takes place over a constant time surface in space-time. This assumption should be essentially correct if the freeze-out interval is short compared to the system's lifetime. Though some of the particles emitted in the central rapidity region could originate from a finite range of longitudinal positions due to thermal smearing, we consider that most of the central rapidity particles come from the central spatial region and thus neglect possible effects on these particles from a different longitudinal and transverse expansion velocities.

In the case of bosons, the wave functions that incorporate the effects of a finite size system have been found in Ref. [16], where we refer the reader for further details of the model. These wave functions are given as the stationary solutions of the wave equation for bosons, namely, the Klein-Gordon equation

$$\left(\frac{\partial^2}{\partial t^2} - \nabla^2 + m^2\right)\phi(\mathbf{r}, t) = 0 \tag{1}$$

subject to the boundary condition $\phi(|\mathbf{r}| = R, t) = 0$, and finite at the origin. The normalized stationary states are

$$\phi_{nlm'}(\mathbf{r}, t) = \frac{e^{-iE_{nl}t}}{R J_{l+3/2}(k_{nl}R)} \frac{Y_{lm'}(\hat{\mathbf{r}}) J_{l+1/2}(k_{nl}r)}{\sqrt{r E_{nl}}}. \tag{2}$$

In the case of fermions, the wave functions are found as the stationary solutions of the Dirac equation

$$\left(i\gamma^\mu \partial_\mu - m\right)\psi(\mathbf{r}, t) = 0 \tag{3}$$

subject to the the boundary condition $\psi(|\mathbf{r}| = R, t) = 0$, and also finite at the origin. It is easy to show that the normalized stationary states are

$$\psi_{nlm'}(\mathbf{r}, t) = \frac{e^{-iE_{nl}t}}{2mR J_{l+3/2}(k_{nl}R)} \begin{Bmatrix} E_{nl} + m + i\boldsymbol{\sigma}\cdot\nabla \\ -E_{nl} + m - i\boldsymbol{\sigma}\cdot\nabla \end{Bmatrix} \times \frac{Y_{lm'}(\hat{\mathbf{r}}) J_{l+1/2}(k_{nl}r)}{\sqrt{r}}. \tag{4}$$

In Eqs. (2) and (4), J_ν is a Bessel function of the first kind, $Y_{lm'}$ is a spherical harmonic, $\boldsymbol{\sigma}$ are the Pauli matrices, and the parameters k_{nl} are related to the energy eigenvalues E_{nl} by $E_{nl}^2 = k_{nl}^2 + m^2$ and are given as the solutions to $J_{l+1/2}(k_{nl}R) = 0$. The contribution to the thermal invariant

distribution from a state with quantum numbers $\{n, l, m'\}$ is given by

$$E\frac{d^3N_{nlm'}}{d^3p} = \int \frac{d\Sigma}{(2\pi)^3}(k_{nl}\cdot u) f(k_{nl}\cdot v)\mathcal{W}_{nlm'}(\mathbf{p},\mathbf{r}), \quad (5)$$

where $\mathcal{W}_{nlm'}(\mathbf{p},\mathbf{r})$ is the Wigner transform and $f(k_{nl}\cdot v)$ the thermal occupation factor of the state, respectively. The four-vectors v^μ and u^μ represent the collective flow four-velocity and a four-vector of magnitude one, normal to the freeze-out hypersurface Σ, respectively.

To consider a situation where freeze-out happens at a fixed time and within a spherical volume of radius R, the unit four-vector u^μ can be chosen as $u^\mu = (1, \mathbf{0})$. To keep matters simple, we also consider a thermal occupation factor of the Maxwell-Boltzmann kind $f(k_{nl}\cdot v) = e^{-k_{nl}\cdot v/T}$, where T is the system's temperature. The four-vector v^μ is parametrized as $v^\mu = \gamma(1, \mathbf{v})$, and we choose a radial profile for the vector $\mathbf{v}$ such as $\mathbf{v} = \beta\mathbf{r}/R$, where the parameter β represents the surface expansion velocity. Correspondingly, the γ factor is given by

$$\gamma = \frac{1}{\sqrt{1-\left(\beta\frac{r}{R}\right)^2}}. \quad (6)$$

Nonetheless, to continue to keep matters as simple as possible and to be able to analytically perform the integrations in Eq. (5), we instead consider that the γ factor is a constant evaluated at the average transverse expansion velocity, namely,

$$\gamma \to \bar{\gamma} = \frac{1}{\sqrt{1-(3\beta/4)^2}}, \quad (7)$$

where the average is computed by assuming that the matter distribution is uniform within the fireball.

We take the four-vector $k^\mu_{nl} = (E_{nl}, \mathbf{k}_{nl})$, and choose $\mathbf{k}_{nl} \parallel \mathbf{p}$. This choice is motivated from the continuum, boundless limit, where the relativistically invariant exponent in the thermal occupation factor becomes $\gamma(E - \mathbf{p}\cdot\mathbf{v})$.

Summing over all the states, the invariant thermal distributions for bosons and fermions are given by

$$E\frac{d^3N_b}{d^3p} = \mathcal{N}_b\sum_{nl}\frac{(2l+1)}{(2\pi)}\frac{k^2_{nl}E_{nl}e^{-\bar{\gamma}E_{nl}/T}}{\sqrt{p^2+\left(\frac{\bar{\gamma}\beta k_{nl}}{2RT}\right)^2}} \times \frac{\left|J_{l+1/2}\left(pR - i\frac{\bar{\gamma}\beta k_{nl}}{2T}\right)\right|^2}{\left[p^2 - k^2_{nl} - \left(\frac{\bar{\gamma}\beta k_{nl}}{2RT}\right)^2\right]^2 + \left[\frac{\bar{\gamma}\beta p k_{nl}}{RT}\right]^2}, \quad (8)$$

$$E\frac{d^3N_f}{d^3p} = \mathcal{N}_f\sum_{nl}\frac{(2l+1)}{(2\pi)} \times \left[\frac{\left(E^2_{nl}+m^2+p^2\right)+(\beta k_{nl}/2RT)^2}{m^2}\right] \times \frac{k^2_{nl}E_{nl}e^{-\bar{\gamma}E_{nl}/T}}{\sqrt{p^2+\left(\frac{\bar{\gamma}\beta k_{nl}}{2RT}\right)^2}} \times \frac{\left|J_{l+1/2}\left(pR - i\frac{\bar{\gamma}\beta k_{nl}}{2T}\right)\right|^2}{\left[p^2 - k^2_{nl} - \left(\frac{\bar{\gamma}\beta k_{nl}}{2RT}\right)^2\right]^2 + \left[\frac{\bar{\gamma}\beta p k_{nl}}{RT}\right]^2}, \quad (9)$$

respectively. The factor $(2l + 1)$ in Eqs. (8) and (9) comes from the degeneracy of a state with a given angular momentum eigenvalue l. $\mathcal{N}_b$ and $\mathcal{N}_f$ are normalization constants.

The contrast between a calculation with and without finite size effects can be appreciated by looking at Fig. 5 in Ref. [15] which shows a comparison between the invariant pion distribution as a function of p_t computed for $T = 120$ MeV, $\beta = 0.6$, with finite size effects ($R = 8$ fm) and without them. The curves are also compared to data on positive pions from PHENIX [1]. We notice from the figure that the curve with finite size effects does a very good job describing the data for all values of p_t in this range. In contrast, a calculation where no effects of a finite size are included, and thus the wave function of a given state is simply a plane wave, does not describe the data over the considered range when use is made of the same values for T and β as for the case of the calculation with a confining volume.

III. TRANSVERSE SPECTRA

We now compare the model to data on mid-rapidity positive pions together with protons from central Au+Au collisions at $\sqrt{s_{NN}} = 200$ GeV measured in RHIC [1]. We perform a χ^2 fit to each spectra. The fit parameters are the pion and proton fireball radii R_π and R_p, temperatures T_π and T_p, surface radial flow velocities β_π and β_p, and normalizations $\mathcal{N}_\pi$ and $\mathcal{N}_p$. Based on the success of the description of the central rapidity pion data obtained in Ref. [15] up to $p_t \sim 3$ GeV, we first fix the parameters describing the pion data with the minimization procedure. The parameters thus obtained are $R_\pi = 8$ fm, $T_\pi = 117$ MeV, and $\beta_\pi = 0.6$, which are basically the same as the ones obtained in Ref. [15] where only the normalization was left as a free parameter and the rest were set to reasonable values that describe freeze-out conditions at RHIC.

Next, to find the parameters that describe the proton spectrum, we fix the values of any two of the parameters R_p, T_p, and β_p to be the same as the corresponding parameters describing the pions, leaving the third parameter, along with the normalization constant $\mathcal{N}_p$, free. The optimum set of parameters obtained with this procedure corresponds to $R_p = 8$ fm, $T_p = 117$ MeV, and $\beta_p = 0.53$. Figure 1 shows the distributions for pions and protons for central collisions (0–10%) [1] compared to the theoretical calculation with the best parameters obtained. We notice that the proton data are well described by the model up to $p_t \sim 3$ GeV for a temperature and system size equal to the corresponding parameters for the pions but that the magnitude of β_p is about 10% smaller than that of β_π. We recall that to find an analytical expression for the momentum distributions, we resorted to approximating the γ factor in Eq. (6) by the average γ factor in Eq. (7). Because the effect of the same radial flow is stronger for particles with larger mass, it is therefore natural to expect that with this approximation we introduce a discrepancy in the description

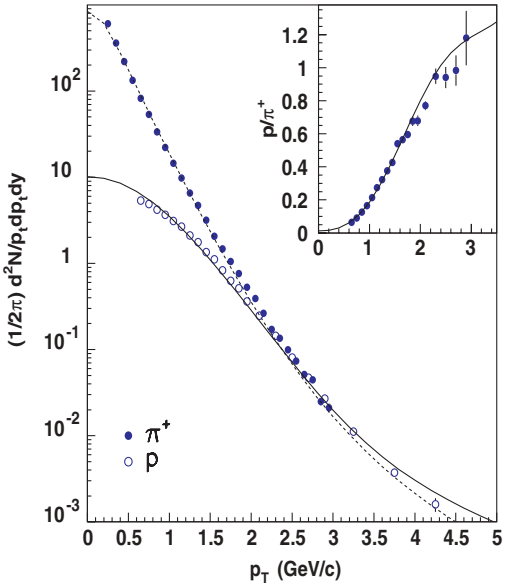


FIG. 1. (Color online) Invariant π^+ and p distributions as a function of p_t for $T = 117$ MeV, $R = 8$ fm, $\beta_\pi = 0.6$, and $\beta_p = 0.53$. Also shown in the insert is the ratio p/π^+ of these distributions. Data are from Ref. [1] for collisions with 0–10% of centrality.

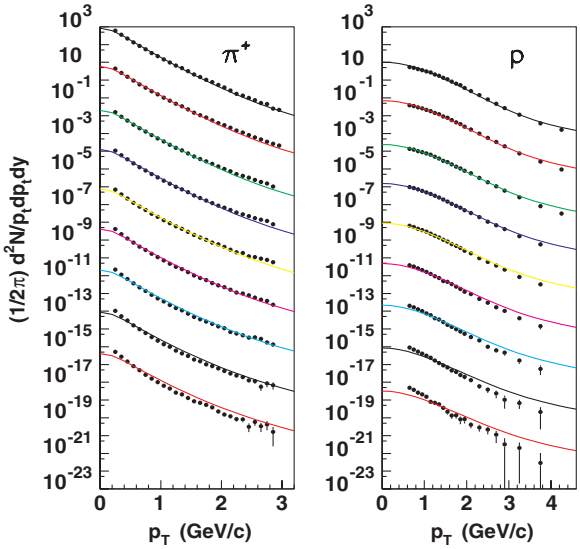


FIG. 2. (Color online) Invariant π^+ (left panel) and p (right panel) distributions as a function of p_t for different collision centralities. The uppermost curves correspond to the most central collisions, 0–10% with the centrality decreasing in intervals of 10% [1] multiplied by successive factors of 10^{-2}. The size of the equivalent spherical region is calculated according to the relation $R = R_0 + C(N_{\text{part}}/2)^{1/3}$, with $R_0 = 1$ fm and $C = 1.28$. The curves represent the theoretical calculation with $T_p, \pi = 117$ MeV, $\beta_\pi = 0.6$, and $\beta_p = 0.53$, which describe the most central collisions' data.

of the flow for particles with different masses. Nevertheless, we feel that an error on the order of 10% is acceptable considering the advantage of working with analytical expressions.

We also notice that the description of the proton data for $p_t > 3$ GeV is not as good. This can be understood by recalling that for large p_t the leading particle production mechanism is the fragmentation of fast moving partons, some of which fragment outside the fireball region and thus are not influenced by the confining boundary that the rest of the particles experience within the fireball, and, thus, that our description is not valid for these large p_t particles.

Figure 2 shows the distributions for pions and protons for different collision centralities. For the description of these data, we have fixed the values of T_p,π and β_p,π to the ones obtained from the most central collisions' analysis, leaving the normalizations to be determined by the minimization procedure. The size of the overlap region for peripheral collisions was determined from the number of participants N_{part} in the reaction [1] by a simple scaling law for the size of the equivalent spherical region according to the relation $R = R_0 + C(N_{\text{part}}/2)^{1/3}$, with $R_0 = 1$ fm and $C = 1.28$, which gives $R = 8$ fm for the most central region (0–10%) data. This relation is motivated by a similar one that gives the radius of a nucleus in terms of the mass number. The value of R_0 tries to account for the finite size of the interaction region as the number of participants takes its smallest value for the most peripheral collision, namely, $N_{\text{part}} = 2$.

The values for R and N_{part} are listed in Table I. We notice that the pion data are well described for all centralities except for those at the lower end of the spectra where a thermal calculation is expected to fail because of resonance contamination. The proton data are well described up to $p_t \sim 3$ GeV only up to centralities on the order of 40–50%; from there the quality of the description decreases as the centrality of the collisions decreases. We interpret the poor description of the proton data for $p_t > 3$ GeV for all centralities as an indication that the leading particle production is not a kind of thermal parton recombination but instead the fragmentation of fast moving partons. However, the failure to describe proton data for centralities smaller than 40–50% could be attributed to a different scaling of the effective size of the interaction region with N_{part} as compared to the one obeyed by the pions or to the fact that, for large impact parameters, the proton size becomes comparable to the size of the interaction region. An analysis exploring these possibilities will be presented elsewhere.

TABLE I. Parameters N_{part} and R for the description of the pion and proton spectra corresponding to different centralities. The radii of the equivalent spherical region has been calculated according to the relation $R = R_0 + C(N_{\text{part}}/2)^{1/3}$, with $R_0 = 1$ fm and $C = 1.28$.

Centrality (%)	N_{part}	R (fm)
0–10	234.6	7.3
20–30	166.6	6.6
30–40	114.2	5.9
40–50	74.4	5.3
50–60	45.5	4.6
60–70	25.7	4.0
70–80	13.4	3.4
80–92	6.3	2.9

IV. PARTICLE CORRELATIONS

To explore the space-time dimensions of the system created in high-energy heavy-ion collisions, one typically looks at two-particle correlation functions. In the present case, it is thus instructive to look at this function to see whether the size scale that can be extracted from a two-particle correlation is comparable to the intrinsic scale dimension used in the model formulation. We carry out the analysis for the two-pion correlation function. For the purposes of this section, we closely follow Ref. [11] to which we refer the reader for details.

Let $\psi_{nlm'}(\mathbf{p})$ represent the Fourier transform of the wave function for the state with quantum numbers n, l, m', namely,

$$\psi_{nlm'}(\mathbf{p}) = \int \frac{d^3r}{(2\pi)^3} e^{-i\mathbf{p}\cdot\mathbf{r}} \psi_{nlm'}(\mathbf{r}). \tag{10}$$

With the normalization adopted in Eq. (2), the one-pion momentum distribution can be represented as

$$P_1(\mathbf{p}) \equiv \frac{d^3N}{d^3p} = \sum_{n,l,m'} 2E_{nl} e^{-\tilde{\gamma} E_{nl}/T} \psi^*_{nlm'}(\mathbf{p}) \psi_{nlm'}(\mathbf{p}). \tag{11}$$

Similarly, and under the assumption of a complete factorization of the two-particle density matrix, the two pion momentum distribution can be written as

$$P_2(\mathbf{p}_1, \mathbf{p}_2) \equiv \frac{d^6N}{d^3p_1 d^3p_2} = P_1(\mathbf{p}_1) P_1(\mathbf{p}_2) + \left| \sum_{nlm'} 2E_{nl} e^{-\tilde{\gamma} E_{nl}/T} \psi^*_{nlm'}(\mathbf{p}_1) \psi_{nlm'}(\mathbf{p}_2) \right|^2, \tag{12}$$

where the two-pion correlation function C_2 can be written, in terms of P_1 and P_2, as

$$C_2(\mathbf{p}_1, \mathbf{p}_2) = \frac{P_2(\mathbf{p}_1, \mathbf{p}_2)}{P_1(\mathbf{p}_1) P_1(\mathbf{p}_2)}. \tag{13}$$

Notice that as a consequence of the factorization assumption, the correlation function is such that $C_2(\mathbf{p}, \mathbf{p}) = 2$.

For the spherically symmetric problem described here, the correlation function depends on the magnitude, as well as on the angle between the momenta of the two particles $\mathbf{p}_1$ and $\mathbf{p}_2$. We make the change of variables to relative $\mathbf{q} = \mathbf{p}_1 - \mathbf{p}_2$ and average $\mathbf{K} = (\mathbf{p}_1 + \mathbf{p}_2)/2$ momenta and also to the angle between these last two vectors, θ. The correlation function thus becomes a function of $K = |\mathbf{K}|$, $q = |\mathbf{q}|$, and θ. To consider the contribution from pions with different angles between their momenta, we average over θ. Figure 3 shows $C_2(q)$ averaged over θ and for a fixed value $K = 260$ MeV as a function of q for $R = 8$ fm, $T = 117$ MeV, and $\beta = 0.55$. The solid curve shows the corresponding Gaussian fit.

To extract the system's size R_{eff} from this function, we fit this curve to a Gaussian distribution of the form

$$g(q) = 1 + \rho^2(q), \qquad \rho(q) = \exp\left(-q^2 R^2_{\text{eff}}/2\right). \tag{14}$$

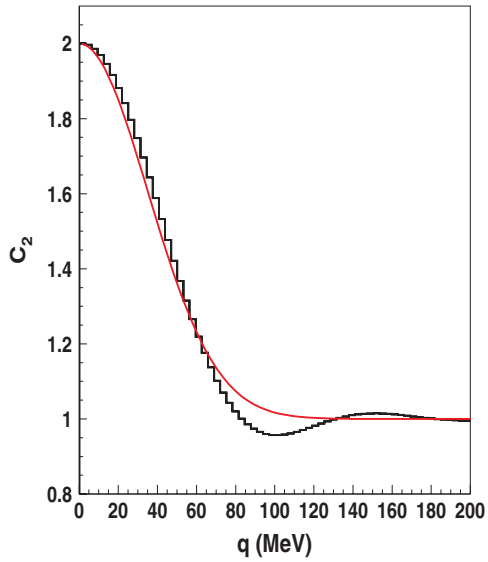


FIG. 3. (Color online) $C_2(q)$ averaged over the angle between $\mathbf{K}$ and $\mathbf{q}$ as a function of q for $K = 260$ MeV, $R = 8$ fm, $T = 117$ MeV, and $\beta = 0.55$. The histogram corresponds to the model calculation, whereas the solid curve shows the corresponding Gaussian fit.

Figure 4 shows the behavior of R_{eff} as a function of $(N_{\text{part}})^{1/3}$ using $K = 260$ MeV, compared to measured values for R_{side} [17] from Au+Au collisions at $\sqrt{s_{NN}} = 200$ GeV. The lower solid curve corresponds to our model effective radii, whereas the upper solid curve is the model curve displaced by a constant $\tilde{R} = 0.8$ fm. The dashed curve corresponds to the

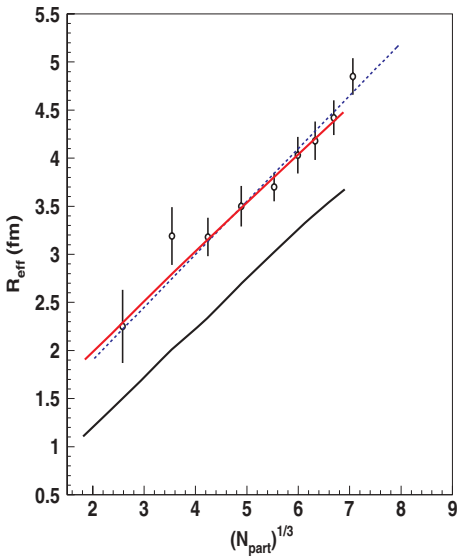


FIG. 4. (Color online) R_{eff} as a function of $(N_{\text{part}})^{1/3}$ for $K = 260$ MeV compared to measured values for R_{side} from Au+Au collisions at $\sqrt{s_{NN}} = 200$ GeV. The lower solid curve corresponds to the model effective radii, whereas the upper solid curve is the model curve displaced by the constant $R_0 = 0.8$ fm. The dashed curve is the best linear fit to the data.

best linear fit to the data. We notice that the slope of our model curve is in good agreement with the data. The fact that the intercept is different from zero may indicate the existence of correlation scales in the data that are not considered in our simple approach.

However, as a function of K, it is expected that $R_{\rm eff}$ approaches a limiting value for large K, in accordance with the analysis in Ref. [11]. This expectation is based on the findings in Ref. [15], where it is shown that the model overshoots the large p_t part of the neutral pion spectrum. A detailed analysis in this direction is being performed and will be reported elsewhere.

Finally, recall that

$$\rho(r) = \exp\left(-r^2/2R_{\rm eff}^2\right) \tag{15}$$

is the spherically symmetric three-dimensional distribution in space that gives rise to $\rho(q)$ upon Fourier transformation and that the $R_{\rm rms}$ radius from $\rho(r)$ is given by

$$R_{\rm rms} = \sqrt{3}R_{\rm eff}. \tag{16}$$

However, for a rigid sphere, such as the distribution giving rise to our model distribution, the $R_{\rm rms}$ radius is given by

$$R_{\rm rms} = \sqrt{3/5}R. \tag{17}$$

By equating these two rms radii, we see that to compare the effective radius with the model one the relation between them is given by

$$R = \sqrt{5}R_{\rm eff}. \tag{18}$$

V. CONCLUSIONS

In conclusion, we show that, by considering the finite size of the interaction region and a simple scaling law of this with the number of participants in the collision, it is possible to achieve a good description of mid-rapidity pion and proton data in Au+Au collisions at RHIC with common values of temperature and transverse expansion velocity. For central collisions, the proton to pion ratio is also well described and its behavior can be attributed to the strength of the radial flow achieved in RHIC. By performing a two-particle correlation analysis and comparing to data for $R_{\rm side}$ as a function of $(N_{\rm part})^{1/3}$ from Au+Au collisions at $\sqrt{s_{NN}} = 200$ GeV, we see that the scaling law found from the single particle spectra analysis is in good agreement provided that we displace our model curve by a constant $\tilde{R} = 0.8$ fm and we speculate that this signals the existence of an extra correlation length in data that is not accounted for in our simple model.

We should stress that the spherical symmetry assumed throughout can be thought of as a theoretical tool rather than as a realistic approximation to the actual collision geometry for the highest RHIC energies. Our intention is to provide a working model with a high degree of symmetry that can be better controlled in an actual calculation. The same is true for the treatment of the shape of the region for noncentral collisions, which one knows from elliptic flow analyses partially retains the original almond shape of the overlap region in the collision. The sizes referred to in this way reflect characteristic sizes rather than actual spherical radii. Although modifying the geometry used for the calculation will certainly give rise to a different set of quantum states, the bulk of the effect will remain because the physics that it captures is the Heisenberg uncertainty principle, whereby restricting the size of the region to become finite the momentum states become broader. As for the use of stationary states, we point out that, although the freeze-out volume is reached with a large expansion velocity, the transition from a strongly interacting system to a free gas is rapid and what matters is the distribution right before this transition and therefore the length scale associated with it.

It is important to emphasize that a description of the transverse distributions for different impact parameters can be done by considering a varying freeze-out temperature and radial velocity, but the lesson to be learned from the present analysis is that this variation can be tempered and/or even avoided by considering the finite size of the interaction region.

We point out that some hydrodynamical models without finite size effects have been able to give similarly good descriptions of data up to p_t on the order of 2–2.5 GeV [18] at the expense of introducing a large amount of parameters. What we have shown here is that it is also possible to achieve the same quality of description including a basic property of quantum systems often neglected, that is, the fact that in high energy reactions particles are produced in small space-time regions. While doing this and in this first step approach, we made use of approximations to render the calculations tractable; one such example is the treatment of the γ Lorentz factor in terms of an average one. The relaxation of these approximations is a natural step forward and we will report on the progress of this work elsewhere.

ACKNOWLEDGMENTS

The authors thank G. Paic for his valuable comments and suggestions. Support for this work has been received from PAPIIT-UNAM under Grant IN107105 and CONACyT under Grant 40025-F and from the bilateral agreement CONACyT-CNPq J200.556/2004 and 491227/2004-3.

[1] S. S. Adler *et al.* (PHENIX Collaboration), Phys. Rev. C **69**, 034909 (2004).
[2] R. C. Hwa and C. B. Yang, Phys. Rev. C **67**, 034902 (2003); R. J. Fries, B. Müller, C. Nonaka, and S. A. Bass, Phys. Rev. Lett. **90**, 202303 (2003); V. Greco, C. M. Ko, and P. Lévai, *ibid.* **90**, 202302 (2003).
[3] I. Tserruya, Pramana **60**, 577 (2003).
[4] J. Adams *et al.* (STAR Collaboration), Phys. Lett. **B637**, 161 (2006).
[5] C. M. Hung and E. Shuryak, Phys. Rev. C **57**, 1891 (1998).
[6] J. Adams *et al.* (STAR Collaboration), Nucl. Phys. **A757**, 102 (2005).

[7] K. H. Ackermann (STAR Collaboration), Phys. Rev. Lett. **86**, 402 (2001).
[8] D. Adamová *et al*. (CERES Collaboration), Phys. Rev. Lett. **90**, 022301 (2003).
[9] E. S. Fraga and R. Venugopalan, Braz. J. Phys. **34**, 315 (2004); Physica **A345**, 121 (2004).
[10] F. Becattini, J. Phys. Conf. Ser. **5**, 175 (2005).
[11] Q. H. Zhang and S. S. Padula, Phys. Rev. C **62**, 024902 (2000); Q. H. Zhang, *Constraints on the size of the quark gluon plasma*, hep-ph/0106242.
[12] A. Ayala and A. Sánchez, Phys. Rev. C **63**, 064901 (2001).
[13] E. V. Shuryak, Phys. Rev. D **42**, 1764 (1990).
[14] A. Ayala, J. Barreiro, and L. M. Montaño, Phys. Rev. C **60**, 014904 (1999).
[15] A. Ayala, E. Cuautle, J. Magnin, L. M. Montaño, and A. Raya, Phys. Lett. **B634**, 200 (2006).
[16] A. Ayala and A. Smerzi, Phys. Lett. **B405**, 20 (1997).
[17] S. Adler *et al*. (PHENIX Collaboration), Phys. Rev. Lett. **93**, 152302 (2004).
[18] E. Schnedermann, J. Sollfrank, and U. Heinz, Phys. Rev. C **48**, 2462 (1993).

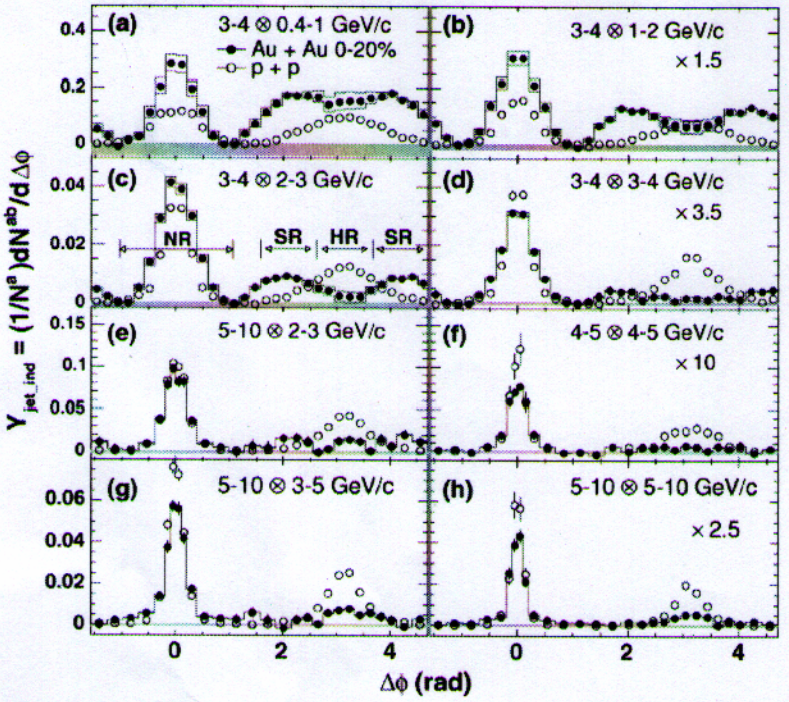


FIG. 6. (Color online) Per-trigger yield vs $\Delta\phi$ for various trigger and partner p_T ($p_T^a \otimes p_T^b$), arranged by increasing pair proxy energy (sum of p_T^a and p_T^b), in $p+p$ and 0–20% Au+Au collisions. The data in several panels are scaled as indicated. Solid histograms (shaded bands) indicate elliptic flow (ZYAM) uncertainties. Arrows in Fig. 6(c) depict the "head" region (HR), the "shoulder" region (SR) and the "near-side" region (NR).

central Au+Au collisions, there is an additional maximally 5%, centrality-dependent uncertainty due to occupancy effect.

The propagation of uncertainties arising from the single particle efficiency are different for different jet variables. For the per-trigger yield, it depends on the errors associated with the efficiency estimated for the partners (ε^b). For the hadron-pair yields, it depends on the errors related to efficiencies for both trigger (ε^a) and partner (ε^b) hadrons. Since the efficiency correction uncertainties are similar for trigger and partner hadrons in both Au+Au and $p+p$ collisions, we can use a single variable ε to represent them. If the uncertainties are independent between Au+Au and $p+p$, the total uncertainty would be $\sim\sqrt{2}\delta\varepsilon/\varepsilon$ for JPY and I_{AA} and $2\delta\varepsilon/\varepsilon$ for J_{AA}. However, some systematic errors partially cancel between Au+Au and $p+p$, especially those for the matching cut, momentum scale, and momentum resolution. The total uncertainties are estimated to be 12% for I_{AA} and JPY and 17% for J_{AA}.

The statistical uncertainties for v_2 are important in the most central and most peripheral centrality bins for $p_T > 4$ GeV/c. The systematic uncertainties are, however, driven by the uncertainty associated with the determination of the reaction plane resolution; they are estimated to be ~6% for central and midcentral collisions and ~10% for peripheral collisions [18]. This error is nearly independent of p_T, i.e., $\delta v_2^a/v_2^a \approx \delta v_2^b/v_2^b$, and the resulting error for the hadron-pair ratio is

$$\begin{aligned}\delta\mathrm{JPR}(\Delta\phi) &= 2\xi\left(\delta v_2^a v_2^b + \delta v_2^b v_2^a\right)\cos 2\Delta\phi \\ &\approx (\delta v_2/v_2) 4 v_2^a v_2^b \cos 2\Delta\phi, \end{aligned} \tag{21}$$

where the last approximation takes into account the fact that ξ is close to 1. Additional systematic errors related to v_4 and the factorization assumption that $\langle v_2^a v_2^b\rangle = \langle v_2^a\rangle\langle v_2^b\rangle$ were also estimated and found to be small [19].

The uncertainty due to ξ (ZYAM uncertainty) can be expressed as

$$\delta\mathrm{JPR}(\Delta\phi) = \delta\xi\left(1 + 2v_2^a v_2^b \cos 2\Delta\phi\right) \approx \delta\xi, \tag{22}$$

where we ignored the $\cos 2\Delta\phi$ term, since $2v_2^a v_2^b \ll 1$. The uncertainty of ξ includes both the statistical error of the data points around $\Delta\phi_{\mathrm{min}}$ and the systematic error from the fitting procedure.

Table III summarizes the systematic errors for the jet yield in 0–20% Au+Au collisions due to v_2 and ZYAM subtraction. Errors for several combinations of trigger and partner p_T (in $p_T^a \otimes p_T^b$) are given. The uncertainties are $\Delta\phi$ dependent, so we present them separately for the three regions used in this analysis: a "head" region ($|\Delta\phi - \pi| < \pi/6$, HR), a "shoulder" region ($\pi/6 < |\Delta\phi - \pi| < \pi/2$, SR), and the near-side region ($|\Delta\phi| < \pi/3$, NR). These regions are indicated in Fig. 6(c).

The three types of systematic errors impact the jet shape and jet yield differently. The single particle efficiency correction is a multiplicative factor, so its uncertainty influences the normalization of the jet yield but does not influence its shape. The uncertainties associated with the elliptic flow varies with $\Delta\phi$. It is largest for regions around 0 and π, but reaches a minimum in the shoulder region. The influence of the ξ uncertainty on the jet yield also depends on $\Delta\phi$. It is the dominant uncertainty for the away-side yield at high p_T.

IV. RESULTS

A. Jet-induced dihadron azimuthal ($\Delta\phi$) distributions

Figure 6 shows a representative subset of the per-trigger yield distributions $Y_{\mathrm{jet_ind}}(\Delta\phi)$ for various combinations of

Three and Two Hadron Correlations in $\sqrt{s_{NN}} = 200$ GeV Proton-Proton and Nucleus-Nucleus Collisions

Alejandro Ayala,[1,2] Jamal Jalilian-Marian,[3] J. Magnin,[2] Antonio Ortiz,[1] G. Paić,[1] and Maria Elena Tejeda-Yeomans[4]

[1]*Instituto de Ciencias Nucleares, Universidad Nacional Autónoma de México, Apartado Postal 70-543, México Distrito Federal 04510, México*

[2]*Centro Brasileiro de Pesquisas Físicas, CBPF, Rua Dr. Xavier Sigaud 150, 22290-180, Rio de Janeiro, Brazil*

[3]*Department of Natural Sciences, Baruch College, New York, New York 10010, USA and CUNY Graduate Center, 365 Fifth Avenue, New York, New York 10016, USA*

[4]*Departamento de Física, Universidad de Sonora, Boulevard Luis Encinas J. y Rosales, Colonia Centro, Hermosillo, Sonora 83000, México*

(Received 24 November 2009; published 25 January 2010)

We compare the azimuthal correlations arising from three and two hadron production in $p + p$ and Au + Au collisions at $\sqrt{s_{NN}} = 200$ GeV. We show that in Au + Au, the two away side partons in two-to-three processes have in average a smaller and a greater path length than the average path length of the away-side parton in two-to-two processes. Since in average the particle with the shortest path length in two-to-three processes loses less energy, with respect to the away-side particle in two-to-two processes, this effect leads to a relative enhancement of the ratio of two-to-three to two-to-two processes in Au + Au compared to $p + p$ collisions. We argue that this phenomenon may be responsible for the shape of the away side in azimuthal correlations at the Relativistic Heavy-Ion Collider.

DOI: 10.1103/PhysRevLett.104.042301 PACS numbers: 25.75.Gz

Many interesting phenomena have been observed in high energy heavy-ion collisions at the Relativistic Heavy-Ion Collider (RHIC), among them, the suppression of the single hadron transverse momentum spectra in Au + Au, as compared to normalized $p + p$ collisions. This is believed to result from the energy loss of fast partons traversing and multiply scattering from the medium [1,2]. This picture was further confirmed by azimuthal correlation studies where for certain combinations of leading and associated particles a disappearance of the away-side peak is observed. This is interpreted as the absorption of the away-side parton by the medium. Combined with an enhancement of the single hadron production in $d + \mathrm{Au}$ collisions as compared to normalized $p + p$ collisions, the above established the presence of a final state medium produced in Au + Au collisions at RHIC. Furthermore, the strong collectivity of the medium, as measured by the flow parameter v_2 has led to the consensus that this is partonic in origin as well as strongly interacting [3,4].

In spite of the success of the above interpretation of RHIC data [5], there still remain important aspects of energy loss dynamics which are poorly understood. The picture has been further complicated by the recent observation in azimuthal correlation studies in Au + Au collisions, where for the case when the magnitude of the momentum difference between leading and associated particles increases, either a double hump structure or a broadening of the away-side peak appears, while these structures are absent in $p + p$ collisions at the same energy [6,7]. This observation gave rise to a large number of theoretical explanations based on the assumption that collective phenomena are at work in $A + A$ collisions. These include conical flow that gives rise to a Mach cone [8,9], emission of Cherenkov-like gluons [10], Markovian scattering of partons [11], and more sophisticated hydrodynamical evolution scenarios [12,13].

However, one can ask whether these features are already present at the level of $p + p$ collisions, albeit obscured by the smallness of their intensity. For instance, two-to-three parton processes would lead to such a double hump structure even in $p + p$ collisions, although these would be suppressed with respect to two-to-two parton processes. The question is whether in $A + A$ collisions there exists a mechanism that amplifies hadron production from two-to-three processes with respect to that from two-to-two parton processes. This question has been recently partially investigated in Ref. [14] using the event shape analysis in $p + p$ collisions.

In this Letter, we study angular correlations between three hadrons produced both in $p + p$ and $A + A$ collisions at RHIC using the full leading order (LO) matrix elements [15] for two-to-three parton processes and compare these to angular correlations between two hadrons using also LO matrix elements for two-to-two parton processes. To the best of our knowledge, this is the first study of its kind using the complete LO matrix elements to calculate three hadron production in $A + A$ collisions. We should mention that the implementation of next-to-leading order (NLO) matrix elements for two-to-three processes requires the corresponding nuclear parton distributions and medium modified fragmentation functions to matching accuracy. The former are available in the literature [15], the latter

 © 2010 The American Physical Society

are not fully known. Therefore here we use the LO matrix elements, given that we focus on the nuclear effects. We use a medium modified fragmentation function in order to treat the medium-induced parton energy loss, following the approach of Ref. [16] where two hadron production cross section in $A + A$ collisions is studied. We argue that since in $A + A$ collisions, the final state parton with the short (long) trajectory in the away side has a large probability to punch through (get absorbed) the effect produces, on the average, a double hump in the azimuthal correlation.

Using the LO matrix elements for two-to-three parton processes, including the final state phase space factors and enforcing momentum conservation, the three hadron production cross section can be written as

$$\frac{d\sigma^{pp\to h1h2h3X}}{dy_1dy_2dy_3dh_{1t}dh_{2t}dh_{3t}d\phi_2d\phi_3} = \frac{1}{2^5}\frac{1}{(2\pi)^4}\frac{1}{h_{3t}S}\frac{|\sin\phi_2|}{[\sin\phi_2\sin^2(\phi_3/2)-\sin\phi_3\sin^2(\phi_2/2)]^2} \times \int dz_3|\mathcal{M}|^2 f_{i/p}(x_1,\mu^2)f_{j/p}(x_2,\mu^2)D^0_{h1/k}(z_1,\mu^2)D^0_{h2/m}(z_2,\mu^2)D^0_{h3/n}(z_3,\mu^2), \quad (1)$$

where y_i, h_{it} are the rapidity and magnitude of transverse momentum of the ith produced hadron, $\phi_2(\phi_3)$ is the azimuthal angle between the second (third) hadron and the first hadron, assumed to be the leading hadron, and $\sqrt{S}$ is the total center of mass energy. The parton distribution functions are denoted by $f_{i/p}(x_1, \mu^2)$ and are given by the CTEQ6 parametrization [17]. $D^0_{h/i}(z_i, \mu^2)$ are the unmodified fragmentation functions given by the KKP parametrization [18]. All along this work, the scale μ^2 is taken to be the same for all the distribution and fragmentation functions and given as the invariant mass squared of the final state hadrons, which we take as pions. We will focus on the midrapidity region and thus, hereafter, set all rapidities equal to zero. The momentum fractions x_1, x_2, z_1, z_2 are all given in terms of z_3 and the transverse momenta of the produced hadrons. Furthermore, requiring that all momentum fractions are between 0 and 1 introduces the lower and upper limits on the z_3 integration. Further details will be provided in Ref. [19].

We now use Eq. (1) to calculate the three hadron production cross section in $p + p$ for midrapidity at $\sqrt{S} = 200$ GeV. The open circles on the left panel of Fig. 1 show the differential cross section as a function of the azimuthal angle ϕ for the particular case where each of the three hadrons carry transverse momentum of $h_t = 10$ GeV/c and therefore, due to momentum conservation on partonic level, they are separated by an angle of $\Delta\phi = 2\pi/3$ radians. Only the angular distribution of the away-side hadrons (with respect to the direction of one of the hadrons—the would be leading hadron—which in the symmetric case chosen here, can be any one of them) is shown.

In order to investigate the effects of a medium on three hadron production in $A + A$ collisions, we use the modified fragmentation function proposed in [16] given by

$$D_{h/i}(z_i,\mu^2) = (1-e^{-\langle L/\lambda\rangle})\left[\frac{z_i'}{z_i}D^0_{h/i}(z_i',\mu^2) + \left\langle\frac{L}{\lambda}\right\rangle\frac{z_g'}{z_i}D^0_{h/g}(z_g',\mu^2)\right] + e^{-\langle L/\lambda\rangle}D^0_{h/i}(z_i,\mu^2), \quad (2)$$

where $z_i' = \frac{h_t}{(b_{ti}-\Delta E_i)}$ is the rescaled momentum fraction of the leading parton with flavor i, $z_g' = \langle\frac{L}{\lambda}\rangle\frac{b_t}{\Delta E_i}$ is the rescaled momentum fraction of the radiated gluon, ΔE_i is the average radiative parton energy loss, and $\langle\frac{L}{\lambda}\rangle$ is the average number of scatterings. The energy loss ΔE_i is related to the gluon density of the produced medium via

$$\Delta E = \left\langle\frac{dE}{dL}\right\rangle_{1d}\int_{\tau_0}^{\infty}d\tau\frac{\tau-\tau_0}{\tau_0\rho_0}\rho_g(\tau,\vec{b}_\perp,\vec{r}_t+\vec{n}\tau), \quad (3)$$

where $\vec{b}_\perp$ is the impact parameter of the collision. Since here we consider the most central collisions, we set $\vec{b}_\perp = 0$ in the rest of the Letter. $\vec{r}_t$ is the transverse plane location of the hard scattering where the partons are produced and $\vec{n}$ is the direction in which the produced hard parton travels in the medium. The average number of scatterings $\langle\frac{L}{\lambda}\rangle$, the one-dimensional energy loss $\langle\frac{dE}{dL}\rangle_{1d}$, and the gluon density of the medium ρ_g—which is related to the geometry of the produced medium—are taken from Ref. [16] where we refer the reader for details.

The three produced partons will in general travel through the medium at different angles with respect to the direction of $\vec{r}_t$ until they leave the medium after which they hadronize. Therefore, the fragmentation function for

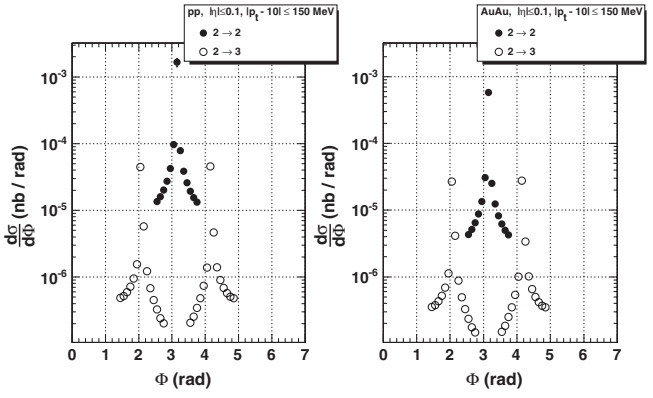


FIG. 1. Comparison of the differential cross sections for two-to-two (full circles) and two-to-three (open circles) processes in $p + p$ (left panel) and $A + A$ (right panel) collisions.

each produced parton will have a different dependence on the path length traveled through the medium. Based on simple geometry one can show that out of the three angles involved, only one is independent which we take to be the angle that the direction of motion of particle 1 makes with the position vector of the scattering center. The normalized cross section is obtained from Eq. (1) using the modified fragmentation functions given by Eq. (2), integrating over the location of the hard scatterings and dividing by the nuclear overlap area. Because of the kinematics involved in midrapidity collisions, we expect the nuclear modification of parton distribution functions to be small [20,21] and therefore ignore them.

The open circles on the right panel of Fig. 1 show the results of the above analysis for the three hadron production differential cross section as a function of azimuthal angle ϕ for midrapidity Au + Au collisions at $\sqrt{S_{\rm NN}} = 200$ GeV. As in the $p + p$ case, we also consider that each of the three hadrons carry momentum with magnitude $h_t = 10$ GeV/c. Since in our picture fragmentation occurs collinear to the direction of the original parton, the final hadrons are separated by an angle $\Delta\phi = 2\pi/3$ radians. One can check that the ratio of the distributions in the Au + Au to the $p + p$ case is as a function of ϕ approximately constant ~0.7.

In order to compare the three hadron to the two hadron production differential cross section in the $p + p$ and the $A + A$ cases, we now compute the latter as a function of the azimuthal angle ϕ. To this end we use the LO DIPHOX algorithm [22]. We use CTEQ6 distribution functions and in the $p + p$ case, unmodified fragmentation functions given by the Kniehl-Kramer-Potter parametrization. For the $A + A$ case, we use the modified fragmentation functions in Eq. (2) integrating over the location of the hard scatterings and dividing by the nuclear overlap area. To have a fair comparison to the already calculated cross section for two-to-three processes, and similar to the experimental situation, we take the leading and away-side particles also having $h_t = 10$ GeV/c. The full circles in Fig. 1 show this cross section. On the left panel we show the results for $p + p$ collisions and on the right panel, the results of Au + Au, both for $\sqrt{S_{\rm NN}} = 200$ GeV collisions at midrapidity. Notice that in both cases the two-to-three hadron production cross section is suppressed with respect to the two-to-two result. However, and this is the main result of our work, this suppression is smaller in $A + A$ collisions than in $p + p$ collisions. Dividing this ratio in $A + A$ to that in $p + p$, we get as a function of ϕ approximately a constant ~2.26.

Since in the present analysis, the sole ingredient that distinguishes between the $p + p$ and the $A + A$ cases is the energy loss of partons that hadronize collinearly, then the only reason for the cross sections in two-to-three processes to be less suppressed in $A + A$ than in $p + p$, when compared to the two-to-two processes, is the different geometry for the trajectories of three as opposed to two particles in the final state.

To test this idea, we compute the distribution of path lengths with two and three hadrons in the final state. We take a nuclear overlap area with a distribution of scattering centers denser in the middle and decreasing toward the edge. In each case we disregard the shortest path length (the one that would correspond to the trigger particle) and compute the distribution of the other path lengths (the ones corresponding to the away-side particles). This is shown in Fig. 2. Notice that indeed, when there are three hadrons in the final state, the large (short) path length in the away side is greater (smaller) than the case of the away-side particle when there are two hadrons in the final state. This means that for the case of three particles in the final state, even if one of the nonleading particles gets absorbed by the medium (the one with the largest path length), the remaining particle has a large probability of punching through than in the case when one has two particles in the final state. We interpret this as signaling that in two-to-three processes, there is a large probability to have one of the two away-side particles being absorbed an the other randomly getting out, producing on the average, a double hump.

In conclusion, we have presented a LO calculation in $p + p$ collisions for the cross section of two-to-three processes and compared to the corresponding cross sections for two-to-two processes, using the same approximations. We have also computed the same processes in $A + A$ collisions taking into account a detailed Glauber approach, similar to the one employed in Ref. [23]. The results show that the cross section in two-to-three processes in $A + A$ is less suppressed—with respect to two-to-two processes—than in the case of $p + p$. We attribute this result to a purely geometrical effect associated with the differences in the path lengths of three as opposed to two particles in the final state in the case of $A + A$ collisions. These results

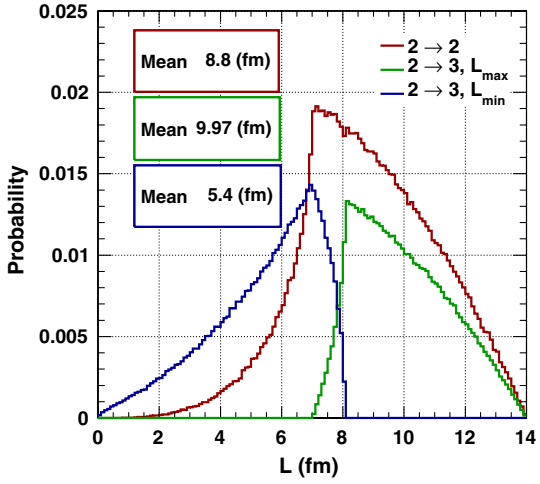


FIG. 2 (color online). Distribution of path lengths for two-to-two and two-to-three processes for the away-side partons, obtained by discarding the shortest of the path lengths in each case.

raise several interesting possibilities that need to be addressed, among them we can point out the following: (1) two-to-three processes are naturally expected and the strength of their signal is not beyond the capabilities of current experiments; (2) considering that two-to-three processes exist in $p + p$ collisions, as suggested also in Ref. [14], our work shows that their observation in $A + A$ should be enhanced with respect to the strongly energy-loss suppressed two-to-two processes and thus, that this effect may have a bearing on the shape of the away side for different kinematical cuts in azimuthal correlations in $A + A$. The work highlights the importance of carrying out three-particle correlation measurements (see Ref. [7]) which will help to distinguish between different scenarios that might be responsible for the shape of the away side in two-particle correlation studies. In this context, our work shows that two-to-three processes should contribute with a non-negligible intensity to the strength of these correlations. In order to contrast this effect to others arising from collective behavior, a detailed study, that includes determining the position of the peaks originated in these processes in a three-particle correlation analysis, is currently under way and will be reported elsewhere.

A. A. and J. J-M. thank CBPF for their hospitality and financial support during a visit when this work was initiated. A. A. thanks support by PAPIIT Grant No. IN116008. J. J-M. thanks A. Dumitru for discussions and is supported by The City University of New York through a PSC-CUNY research grant and by the Office of Nuclear Physics, US-DOE Grant DE-FG02-09ER41620. J. M. is supported by FAPERJ, under Proj. No. E-26/110.266/2009 and CNPq, the Brazilian Council for Science and Technology. M. E. T.-Y. thanks the Programa de Intercambio UNAM-UNISON for support.

[1] M. Gyulassy and X. N. Wang, Nucl. Phys. **B420**, 583 (1994); R. Baier, Y. L. Dokshitzer, A. H. Mueller, S. Peigne, and D. Schiff, Nucl. Phys. **B484**, 265 (1997); M. Gyulassy, P. Levai, and I. Vitev, Nucl. Phys. **B594**, 371 (2001); U. A. Wiedemann, Nucl. Phys. **B588**, 303 (2000); S. Wicks, W. Horowitz, M. Djordjevic, and M. Gyulassy, Nucl. Phys. A **784**, 426 (2007).

[2] For a recent review, see U. A. Wiedemann, arXiv:0908.2306.

[3] I. Arsene *et al.* (BRAHMS Collaboration), Nucl. Phys. **A757**, 1 (2005); B. B. Back *et al.*, Nucl. Phys. **A757**, 28 (2005); K. Adcox *et al.* (PHENIX Collaboration), Nucl. Phys. **A757**, 184 (2005); J. Adams *et al.* (STAR Collaboration), Nucl. Phys. **A757**, 102 (2005).

[4] M. Gyulassy and L. McLerran, Nucl. Phys. **A750**, 30 (2005).

[5] S. Jeon, J. Jalilian-Marian, and I. Sarcevic, Phys. Lett. B **562**, 45 (2003); Nucl. Phys. **A723**, 467 (2003).

[6] A. Adare *et al.* (PHENIX Collaboration), Phys. Rev. C **78**, 014901 (2008).

[7] F. Wang *et al.* (STAR Collaboration), Nucl. Phys. **A774**, 129 (2006).

[8] J. Casalderrey-Solana, E. V. Shuryak, and D. Teaney, J. Phys. Conf. Ser. **27**, 22 (2005).

[9] G. Torrieri, B. Betz, J. Noronha, and M. Gyulassy, Acta Phys. Pol. B **39**, 3281 (2008).

[10] A. Majumder and X.-N. Wang, Phys. Rev. C **73**, 051901 (R) (2006).

[11] C. B. Chiu and R. C. Hwa, Phys. Rev. C **74**, 064909 (2006).

[12] A. K. Chaudhuri, Phys. Rev. C **77**, 027901 (2008).

[13] J. Takahashi *et al.*, Phys. Rev. Lett. **103**, 242301 (2009).

[14] A. Ayala, E. Cuautle, I. Domínguez, A. Ortíz, and G. Paić, Eur. Phys. J. C **62**, 535 (2009).

[15] R. K. Ellis and J. C. Sexton, Nucl. Phys. **B269**, 445 (1986); F. A. Berends, R. Kleiss, P. De Causmaecker, R. Gastmans, and T. T. Wu, Phys. Lett. B **103**, 124 (1981).

[16] H. Zhang, J. F. Owens, E. Wang, and X. N. Wang, Phys. Rev. Lett. **98**, 212301 (2007).

[17] J. Pumplin, D. R. Stump, J. Huston, H. L. Lai, P. Nadolsky, and W. K. Tung, J. High Energy Phys. 07 (2002) 012.

[18] B. A. Kniehl, G. Kramer, and B. Potter, Nucl. Phys. **B582**, 514 (2000).

[19] A. Ayala, J. Jalilian-Marian, J. Magnin, A. Ortíz, G. Paić, and M. E. Tejeda-Yeomans (to be published).

[20] M. Arneodo *et al.* (New Muon Collaboration), Nucl. Phys. **B481**, 23 (1996); **B441**, 12 (1995); **B481**, 3 (1996).

[21] M. R. Adams *et al.* (E665 Collaboration), Phys. Rev. D **54**, 3006 (1996).

[22] T. Binoth, J. Ph. Guillet, E. Pilon, and M. Werlen, Eur. Phys. J. C **24**, 245 (2002).

[23] A. Dainese, C. Loizides, and G. Paić, Eur. Phys. J. C **38**, 461 (2005).

Eur. Phys. J. C 39, 95–99 (2005)
Digital Object Identifier (DOI) 10.1140/epjc/s2004-02073-2

THE EUROPEAN PHYSICAL JOURNAL C

Longitudinal $\bar{\Lambda}_0$ polarization in heavy-ion collisions as a probe for QGP formation

G. Herrera[1,a], J. Magnin[2,b], L.M. Montaño[1,c]

[1] Depto. de Física del Centro de Investigación y de Estudios Avanzados del IPN, Apartado postal 14-740, México D.F. 07000, México
[2] Centro Brasileiro de Pesquisas Físicas, Rua Dr. Xavier Sigaud 150 – CEP 22290-180, Rio de Janeiro, Brazil

Received: 21 September 2004 / Revised version: 25 October 2004 /
Published online: 17 December 2004 – © Springer-Verlag / Società Italiana di Fisica 2004

Abstract. We present an analysis of the longitudinal $\bar{\Lambda}_0$ polarization in ultrarelativistic heavy-ion collisions. The polarization of $\bar{\Lambda}_0$'s coming from the decay chain $\bar{\Xi} \to \bar{\Lambda}_0 + \pi$ exhibits a very well differentiated behavior depending on the production region of the primordial $\bar{\Xi}$'s. This effect reflects the different values of the $N_{\bar{\Xi}}/N_{\bar{\Lambda}_0}$ ratio in the QGP region, where nucleon–nucleon interactions take place in a hot and dense environment, and the peripherical region, in which ordinary nucleon–nucleon interactions occur. An increase in the longitudinal $\bar{\Lambda}_0$ polarization signals a strangeness enhancement which is thought of as a property of the QGP phase.

1 Introduction

In nuclear collisions at relativistic and ultrarelativistic energies, a phase transition from ordinary nuclear matter to a quark gluon plasma (QGP) is expected, which should be observed when sufficiently high baryonic densities and/or temperatures are achieved in the collision. In order to identify this phase transition, a number of experimental observables, namely J/Ψ suppression, strangeness enhancement, fluctuations in particle ratios, flow patterns, etc. have been proposed [1].

In particular, it has been argued that the strangeness enhancement in hot and dense regions of nuclear matter would lead to an abundant formation of multistrange baryons and antibaryons, providing thus key information about the QGP formation [2]. Indeed, detailed calculations [3] predict that the abundance of $\bar{\Xi}(\bar{s}\bar{s}\bar{q})$ should be enriched to about half the abundance of antihyperons $\bar{Y}(\bar{s}\bar{q}\bar{q})$ as compared to the $\bar{\Xi}/\bar{Y}$ ratio seen in nucleon–nucleon interactions. Considering that at $\sqrt{s} = 63\,\mathrm{GeV}$, $\bar{\Xi}/\bar{\Lambda}_0 = 0.06 \pm 0.02$ [5] in the central rapidity region, then in the presence of QGP, the $\bar{\Xi}/\bar{\Lambda}_0$ would be 10 times greater. However, although the $\bar{\Xi}/\bar{\Lambda}_0$ ratio is a quantity which is difficult to establish experimentally, the longitudinal $\bar{\Lambda}_0$ polarization is not and can be used to get a measurement of the above mentioned ratio [2].

At this point it is useful to remember that $\bar{\Xi}$ decays into $\bar{\Lambda}_0 + \pi$ with a branching fraction of about 99% and that the weak decay polarizes the $\bar{\Lambda}_0$ spin longitudinally. This means that all the longitudinally polarized $\bar{\Lambda}_0$ are associated with the primordial abundance of $\bar{\Xi}$. Note also that the $\bar{\Omega}^+$ have little influence on the particle abundances and, in particular, on their polarizations [2]. In fact, the STAR Collaboration [4] measured $N_{\Omega}/N_{\bar{\Xi}^+} \sim 0.16$, where N_{Ω} refers to the total number of $\Omega^- + \bar{\Omega}^+$. Furthermore, the polarization of $\bar{\Lambda}_0$'s coming from $\bar{\Omega}^+ \to \Lambda_0 + K^+$ (BR $\sim 68\%$) is a factor of 5 lower than the polarization of $\bar{\Lambda}_0$'s coming from $\bar{\Xi} \to \bar{\Lambda}_0 + \pi$ while the polarization of the $\bar{\Lambda}_0$'s coming from the decay $\bar{\Omega}^+ \to \bar{\Xi} + \pi$ (BR $\sim 23\%$ and BR $\sim 9\%$ for the $\bar{\Xi}^0$ and the $\bar{\Xi}^+$ decay modes respectively) and the subsequent decay of the $\bar{\Xi}$ into $\bar{\Lambda}_0 + \pi$ is still lower by a factor of ~ 20. This situation is expected to be maintained at the energy where QGP formation takes place (see also the discussions in [2,3]).

The $\bar{\Lambda}_0$ polarization can be defined in terms of the so called up–down asymmetry of the $\bar{\Lambda}_0$ decay with reference to the plane normal to the $\bar{\Lambda}_0$ momentum. Thus [2]

$$\frac{N_u - N_d}{N_u + N_d} = \frac{1}{2}\alpha_{\bar{\Lambda}} p_{\bar{\Lambda}}\,, \tag{1}$$

where $p_{\bar{\Lambda}} = \alpha_{\bar{\Xi}} = -\alpha_{\Xi}$ is the $\bar{\Lambda}_0$ polarization and $\alpha_{\bar{\Lambda}}$ is the $\bar{\Lambda}$ decay parameter. From data tables $\alpha_{\bar{\Lambda}} = -\alpha_{\Lambda} = 0.642 \pm 0.013$ and $\alpha_{\bar{\Xi}} = 0.413 \pm 0.022$ (0.455 ± 0.015) for $\bar{\Xi}^0$ $(\bar{\Xi}^-)$. Hence the total up–down asymmetry for all the neutral $\bar{\Lambda}_0$ events is

$$\frac{N_u - N_d}{N_u + N_d} = \gamma\frac{1}{2}\alpha_{\bar{\Lambda}}\alpha_{\bar{\Xi}}\,, \tag{2}$$

where $\gamma = N_{\bar{\Xi}}/N_{\bar{\Lambda}_0}$.

Equation (2) shows that in ordinary nucleon–nucleon interactions at the ISR energies, the up–down asymmetry

[a] e-mail: gherrera@fis.cinvestav.mx
[b] e-mail: jmagnin@cbpf.br
[c] e-mail: lmontano@fis.cinvestav.mx

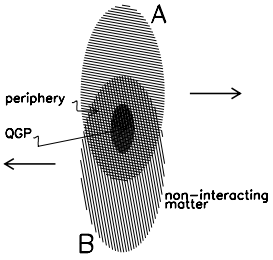


Fig. 1. Schematic representation of the reaction $A + B$ and the regions in which Ξ's are produced. In the hot and dense (QGP) region, $\gamma_{\rm QGP} \sim 0.5$ while in the periphery, in which ordinary nucleon–nucleon interactions take place, $\gamma_{\rm periph.} \ll \gamma_{\rm QGP}$

should be of the order of -0.008 while in hot and dense nuclear matter it should amount to something of about -0.07, which is an effect of one order of magnitude and one that could be measured in experiments.

Of course, all of the above argumentation can be applied to Λ_0 and the Ξ's, but in this case, many of the Λ_0's should be mere fragments of nucleons going into $\Lambda_0 K$, giving a less clear signal.

In the interaction region of a heavy-ion collision it is expected that one has a core of hot and dense nuclear matter – possibly QGP – surrounded by a region in which ordinary nucleon–nucleon interactions take place (see Fig. 1). These regions, as it is shown in the following sections, can be mapped by measuring the $\bar{\Lambda}_0$ polarization as a function of the impact parameter, b, and transverse momentum, $p_{\rm T}$. What is expected is a plot displaying a polarization approximately constant and of the order of -0.07 in the hot and dense region surrounded by a region in which the polarization is again constant, and of the order of -0.008, corresponding to the periphery, where ordinary nucleon–nucleon interactions occur.

This paper is organized as follows. In Sect. 2 we study the behavior of the $N_{\bar{\Xi}}/N_{\bar{\Lambda}_0}$ ratio in both the low and high nuclear density regions. In Sect. 3 we calculate the $\bar{\Lambda}_0$ polarization as a function of the impact parameter and transverse momentum, and Sect. 4 is devoted to conclusions and final remarks.

2 The $N_{\bar{\Xi}}/N_{\bar{\Lambda}}$ ratio in heavy-ion collisions

In the interaction region of the collision of nucleus A and B, when QGP coexists with the ordinary nuclear matter, the ratio of the number of $\bar{\Xi}$ to the number of $\bar{\Lambda}_0$ baryons is given by

$$\gamma_{A+B} = \frac{N_{\bar{\Xi}}^{\rm periph.} + N_{\bar{\Xi}}^{\rm QGP}}{N_{\bar{\Lambda}_0}^{\rm periph.} + N_{\bar{\Lambda}_0}^{\rm QGP}} = \frac{N_{\bar{\Lambda}_0}^{\rm periph.}\gamma_{\rm periph.} + N_{\bar{\Lambda}_0}^{\rm QGP}\gamma_{\rm QGP}}{N_{\bar{\Lambda}_0}^{\rm periph.} + N_{\bar{\Lambda}_0}^{\rm QGP}}\,, \qquad (3)$$

where the quantities labeled $^{\rm periph.}$ and $^{\rm QGP}$ refer respectively to the number of $\bar{\Lambda}_0$ and $\bar{\Xi}$ in each region. As long as the dependence on the impact parameter, b, and transverse momentum, $p_{\rm T}$, of $N_{\bar{\Lambda}_0}$ is different in the QGP from the peripherical region, γ_{A+B} must be also dependent on b and $p_{\rm T}$. In fact, in the same way as the longitudinal polarization of the $\bar{\Lambda}_0$'s does, it should provide a map of the interacting region in which the peripherical and QGP zones are displayed. Note, however, that the only dependence on b and $p_{\rm T}$ in γ_{A+B} arises from the dependence on b and $p_{\rm T}$ in $N_{\bar{\Lambda}_0}^{\rm periph.}$ and $N_{\bar{\Lambda}_0}^{\rm QGP}$ since $\gamma_{\rm periph.}$ and $\gamma_{\rm QGP}$ are expected to be approximately constant [5].

2.1 $N_{\bar{\Lambda}_0}(b, p_{\rm T})$ in the peripherical region

The $N_{\bar{\Lambda}_0}^{\rm periph.}$ can be estimated along the lines in [6]. As stated in [6], and remembering that in ordinary nucleon–nucleon interactions the typical behavior of the production cross section as a function of $p_{\rm T}$ is an exponential in $p_{\rm T}^2$, the number of produced $\bar{\Lambda}_0$'s as a function of the impact parameter and $p_{\rm T}$ in the collision of nucleus A and B can be written as

$$\frac{{\rm d}^4 N_{\bar{\Lambda}_0}^{\rm periph.}}{{\rm d}^2 b\ {\rm d}p_{\rm T}^2} = \frac{1}{2} C {\rm e}^{-a p_{\rm T}^2} T_{AB}(b)\,, \qquad (4)$$

where the $1/2$ is because the number of $\bar{\Lambda}_0$'s is approximately half the number of neutral hyperons, C is a constant which normalizes the integral over the transverse momentum to unity, and T_{AB} is

$$T_{AB}(z, \mathbf{b}) = \int {\rm d}^2 s\ T_A(z, \mathbf{b}) T_B(z, \mathbf{s} - \mathbf{b})\,, \qquad (5)$$

with T_A and T_B given by

$$T_A(z, \mathbf{s}) = \int_{-z/2}^{z/2} {\rm d}z'\ \rho_A(z', \mathbf{s})\,, \qquad (6)$$

and where the limits of integration over z have to be extended to $[-\infty, +\infty]$. For ρ_A, which is the nucleon density per unit area in the transverse plane with respect to the collision axis, we use the standard Woods–Saxon density profile

$$\rho_A(\mathbf{r}) = \frac{\rho_0}{1 + {\rm e}^{(r - R_A)/d}}\,, \qquad (7)$$

with $R_A = 1.1 A^{1/3}\,{\rm fm}$, $d = 0.53\,{\rm fm}$ [7] and ρ_0 fixed by normalization:

$$\int {\rm d}\mathbf{r}\ \rho_A(\mathbf{r}) = A\,, \qquad (8)$$

giving $\rho_0 = 0.17\,{\rm fm}^{-3}$ in the case of ^{197}Au, which we shall consider as an example in the following.

We are assuming that each peripheral collision produces final state particles in the same way as in free nucleon reactions. However, in order to exclude the zone where the density of participants n_p is above the critical density n_c to produce QGP, we rewrite (4) as

$$\frac{{\rm d}^4 N_{\bar{\Lambda}_0}^{\rm periph.}}{{\rm d}^2 b\ {\rm d}p_{\rm T}^2} = \frac{1}{2} C {\rm e}^{-a p_{\rm T}^2} \int {\rm d}^2 s\, T_A(z, \mathbf{b}) T_B(z, \mathbf{s} - \mathbf{b}) \Theta\left[n_c - n_p(\mathbf{s}, \mathbf{b})\right]\,, \qquad (9)$$

where $n_p(\mathbf{s},\mathbf{b})$ is the density of participants at the point $\mathbf{s}$ and Θ is the step function. The density of participants per unit transverse area in the collision of nucleus A with nucleus B at an impact parameter $\mathbf{b}$ has a profile given by [8]

$$n_p(s,\mathbf{b}) = \tag{10}$$
$$T_A(\mathbf{s})\left[1-\mathrm{e}^{-\sigma_{\mathrm{NN}}T_B(\mathbf{s}-\mathbf{b})}\right]+T_B(\mathbf{s}-\mathbf{b})\left[1-\mathrm{e}^{-\sigma_{\mathrm{NN}}T_A(\mathbf{s})}\right],$$

where σ_{NN} is the nucleon–nucleon inelastic cross section which we take as $\sigma_{\mathrm{NN}} = 32\,\mathrm{mb}$. The total number of participants N_p at impact parameter b is

$$N_p(b) = \int \mathrm{d}^2 s\; n_p(\mathbf{s},\mathbf{b})\,. \tag{11}$$

From (9), the number of $\bar{\Lambda}_0$'s coming from the decay chain $\bar{\Xi} \to \bar{\Lambda}_0 + \pi$ is then given by

$$\frac{\mathrm{d}^4 N^{\mathrm{periph.}}_{\bar{\Xi}\to\bar{\Lambda}_0+\pi}}{\mathrm{d}^2 b\;\mathrm{d}p_{\mathrm{T}}^2} = \gamma_{\mathrm{periph.}}\,\frac{\mathrm{d}^4 N^{\mathrm{periph.}}_{\bar{\Lambda}_0}}{\mathrm{d}^2 b\;\mathrm{d}p_{\mathrm{T}}^2}\,. \tag{12}$$

Following [8], we choose $n_c = 3.3\,\mathrm{fm}^{-2}$ for the critical density. This number results from the observation of a substantial reduction of the J/Ψ yield in Pb–Pb collisions at the SPS. For the parameter a in (4) and (9) there are no published data at the relevant energies, which for LHC should be about 5 TeV per nucleon. Then we use the value measured by the Hera-B Collaboration [9] in proton–nucleus interactions at 920 GeV, $a = 2.2 \pm 0.3\,\mathrm{GeV}^{-2}$.

2.2 $N_{\bar{\Lambda}}(b, p_{\mathrm{T}})$ in the QGP region

In QGP, the average number of produced antistrange quarks scales with the number of participants N_p^{QGP} in the collision roughly as [11]

$$\frac{\langle\bar{s}\rangle}{N_p^{\mathrm{QGP}}} = cN_p^{\mathrm{QGP}}\,. \tag{13}$$

Assuming that a $\bar{s}$ quark will produce $\bar{\Xi}$, $\bar{\Lambda}_0$ or $\bar{\Sigma}_0$, and taken the number of $\bar{\Lambda}_0$ approximately equal to the number of produced $\bar{\Sigma}_0$, we have

$$\langle\bar{s}\rangle = 2N_{\bar{\Xi}}^{\mathrm{QGP}} + 2N_{\bar{\Lambda}_0}^{\mathrm{QGP}} = [2\gamma_{\mathrm{QGP}}+2]\,N_{\bar{\Lambda}_0}^{\mathrm{QGP}}\,. \tag{14}$$

Combining (13) and (14) we obtain

$$N_{\bar{\Lambda}_0}^{\mathrm{QGP}} = \frac{c}{2\gamma_{\mathrm{QGP}}+2}\left[N_p^{\mathrm{QGP}}\right]^2\,. \tag{15}$$

N_p^{QGP} as a function of the impact parameter is given, using (11), as

$$N_p^{\mathrm{QGP}}(b) = \int \mathrm{d}^2 s\; n_p(\mathbf{s},\mathbf{b})\theta\left[n_p(\mathbf{s},\mathbf{b})-n_c\right]. \tag{16}$$

Equation (15) represents the behavior of the number of $\bar{\Lambda}_0$ as a function of the impact parameter; then we use

$$\frac{\mathrm{d}^4 N_{\bar{\Lambda}_0}^{\mathrm{QGP}}}{\mathrm{d}^2 b\;\mathrm{d}p_{\mathrm{T}}^2} = \frac{c}{2\gamma_{\mathrm{QGP}}+2}\left[N_p^{\mathrm{QGP}}(b)\right]^2 C'\mathrm{e}^{-a' p_{\mathrm{T}}^2}\,, \tag{17}$$

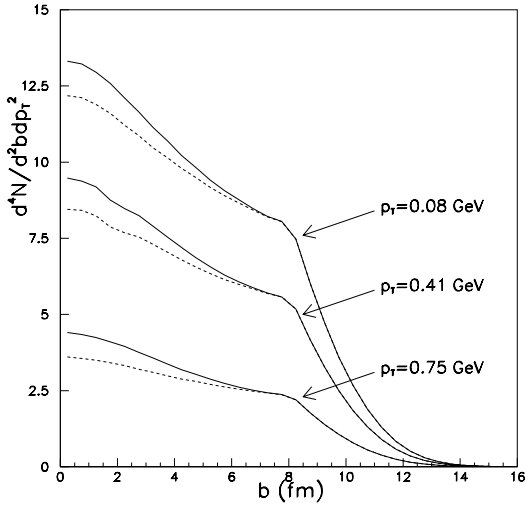


Fig. 2. Number of $\bar{\Lambda}_0$'s as a function of the impact parameter for fixed values of p_{T}. A full line shows the total (peripherical + QGP) number. A dashed line is the peripherical contribution

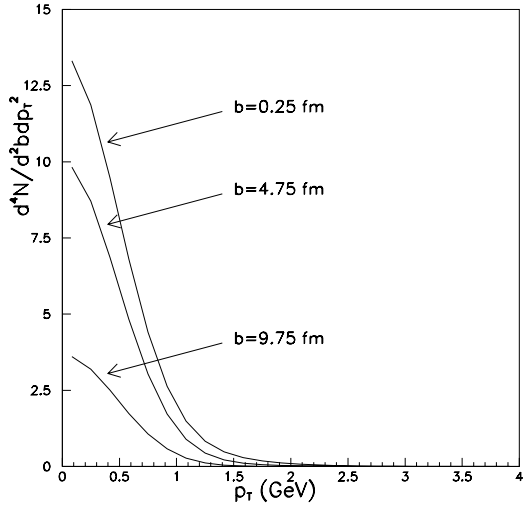


Fig. 3. Number of $\bar{\Lambda}_0$'s as a function of p_{T} at fixed values of b

assuming an exponential dependence in p_{T}^2 for $\bar{\Lambda}_0$ production [10]. As for the peripherical $\bar{\Lambda}_0$'s, (17) times γ_{QGP} gives the number of $\bar{\Lambda}_0$'s as a function of b and p_{T} coming from the decay chain $\bar{\Xi} \to \bar{\Lambda}_0 + \pi$ in the QGP phase. We use $c = 0.005$ [6] and read $a' = 0.67$ from [10].

In Figs. 2 and 3 we show the behavior of the total (peripherical + QGP) number of $\bar{\Lambda}_0$'s as a function of the impact parameter for different values of p_{T} and as a function of p_{T} for several values of b respectively.

3 $\bar{\Lambda}$ polarization in heavy-ion interactions

The up–down asymmetry is then given by (2) with γ_{eff} as given in (3) and shown in the left side of Fig. 4 as a function of b and p_{T}. The right side of Fig. 4 shows the behavior of $\gamma_{\mathrm{eff}} = N(\bar{\Xi})/N(\bar{\Lambda}_0)$ defined in (3) as a function of b and p_{T}. As can be seen, the $\bar{\Lambda}_0$ polarization exhibits a dramatical change as the impact parameter becomes bigger

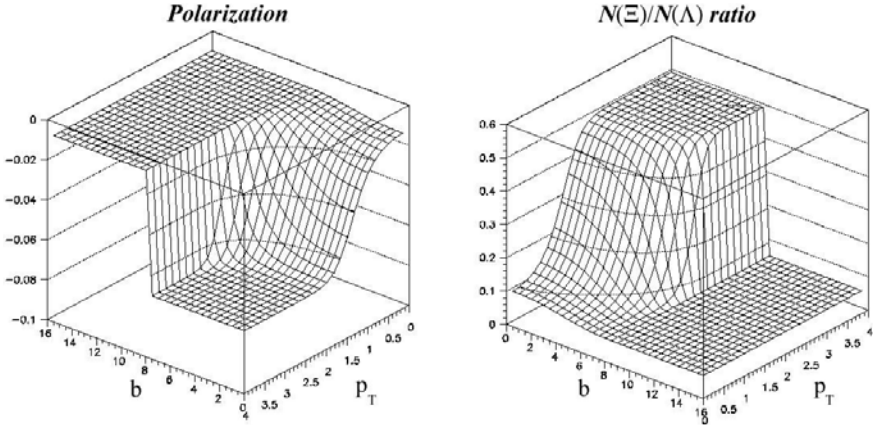


Fig. 4. Left: $\bar{\Lambda}_0$ polarization as a function of b and p_{T} as defined in (2). We used $\gamma^{\mathrm{periph.}} = 0.06$ and $\gamma^{\mathrm{QGP}} = 0.5$ to obtain the plot. Right: $\gamma_{\mathrm{eff}} = N(\bar{\Xi})/N(\bar{\Lambda}_0)$ as a function of b and p_{T} as defined in (3). Note that this plot is rotated by 180° with respect to the plot of the polarization for a better visualization. The maximum of γ_{eff} corresponds to the minimum of the $\bar{\Lambda}_0$ polarization

than a critical value, starting from which the QGP region suddenly vanishes. From this value on the polarization reaches the characteristic value seen in ordinary nucleon–nucleon interactions. Conversely, at high p_{T} and low b, the polarization shows the behavior expected in the hot and high density region where QGP takes place. This reflects the characteristic increase in the $N_{\bar{\Xi}}/N_{\bar{\Lambda}_0}$ expected when QGP be formed. Another interesting feature of the longitudinal $\bar{\Lambda}_0$ polarization is the dependence on p_{T} due to the different p_{T} dependence of $\bar{\Lambda}_0$ production in the peripherical and QGP region.

However, in relativistic heavy-ion collisions, there are several effects which can modify the $\bar{\Lambda}_0$ polarization and have to be taken properly into account. These are
(i) $\bar{\Lambda}_0$'s produced by secondary pion–nucleon scattering,
(ii) secondary scattering of $\bar{\Lambda}_0$'s with nucleons in the interaction region and
(iii) spin-flip in secondary interactions of the $\bar{\Lambda}_0$'s. $\bar{\Lambda}_0$'s coming from secondary pion–nucleon interactions will have a characteristic low momentum signature and can be eliminated from the analysis by setting kinematical constrains in the reconstruction of the data, therefore excluding them from the polarization analysis. Spin-flip effects in polarization, which are associated to spin–spin interactions among the $\bar{\Lambda}_0$ and the surrounding particles, are characterized by a polarization transfer coefficient which expresses the final polarization in terms of the initial one as

$$P' = DP\,. \tag{18}$$

However, due to the lack of experimental information at the range of energies of interest, we will omit this effect from our analysis (for a more detailed analysis and references, see [6]). Secondary scattering of the $\bar{\Lambda}_0$'s with nucleons in the surrounding nuclear environment will produce a momentum shift that can be characterized in terms of a sequential model. The final effect will be that a $\bar{\Lambda}_0$ produced with an initial $(p_{\mathrm{L}}, p_{\mathrm{T}})$, after multiple scattering, in the high energy limit, will have an average momentum [6]

$$\begin{aligned}\langle p_{\mathrm{L}}(b)\rangle &= p_{\mathrm{L}}\ \mathrm{e}^{-I\bar{N}(b)}\,,\\ \langle p_{\mathrm{T}}(b)\rangle &= p_{\mathrm{T}}\ \mathrm{e}^{-I\bar{N}(b)}\cos\left[\Gamma\sqrt{\bar{N}(b)}\right],\end{aligned} \tag{19}$$

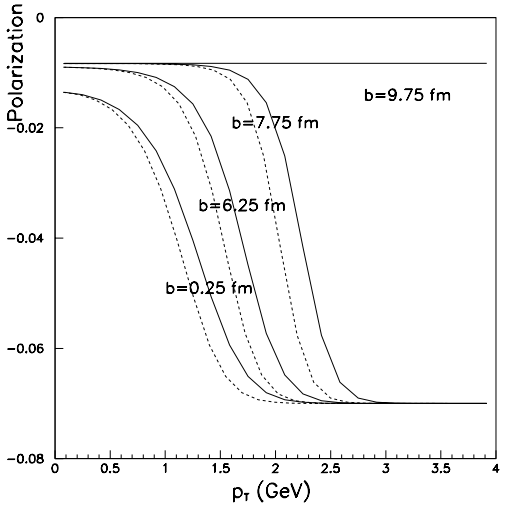


Fig. 5. $\bar{\Lambda}_0$ polarization as a function of p_{T} at several values of the impact parameter. A full line shows the polarization before the momentum shift due to multiple scattering in the nuclear medium, a dashed line shows the polarization after the momentum shift

where $I = 0.2$ is the inelasticity coefficient, $\Gamma = 0.01$ is the average dispersion angle in each collision and $\bar{N}(b)$ is the average number of $\bar{\Lambda}_0$ collisions in the nuclear medium,

$$\bar{N}(b) = \sigma^{\mathrm{tot}}_{\bar{\Lambda}_0 N}\ T_A(b/2)\,, \tag{20}$$

where $\sigma^{\mathrm{tot}}_{\bar{\Lambda}_0 N} = 1.4\,\mathrm{mb}$ [9], taken from proton–nucleus interactions at 920 GeV. This effect is shown in Fig. 5 where the polarization as a function of p_{T} is displayed for several values of b before and after the momentum shift due to multiple scattering. Note also that, for low p_{T}, the polarization takes the value corresponding to that expected in ordinary nucleon–nucleon interactions, a behavior which is more evident as b grows. Conversely, at high p_{T} and low b, the polarization reaches the value expected in the QGP phase.

4 Final remarks and conclusions

In conclusion, we have shown that the longitudinal polarization of $\bar{\Lambda}_0$ in heavy-ion relativistic interactions presents

a dramatical change with $N_{\bar{\Xi}}/N_{\bar{\Lambda}_0}$ in the transition from the expected QGP region to the peripherical one. This effect, which can be easily measured in the laboratory, can help to unveil one of the signals of the transition to the QGP phase, namely the strangeness enhancement and the consequent increase in the multistrange baryon formation. Notice that the longitudinal polarization of the $\bar{\Lambda}_0$ in the low b, high p_{T} region gives direct access to the measurement of the γ_{QGP} ratio. It is simply the quotient of the polarization by $\alpha_{\bar{\Lambda}}\alpha_{\bar{\Xi}}/2$. Conversely, in the high b, high p_{T} region, the $\bar{\Lambda}_0$ longitudinal polarization gives the $\gamma_{\mathrm{periph.}}$ ratio, which is not easily measured in experiments. It is interesting to note that the momentum shift due to multiple scattering of $\bar{\Lambda}_0$'s in the nuclear medium produces a small increase in the polarization as a function of p_{T} in the low momentum region.

Another possible observable which would exhibit strong changes in the presence of the QGP phase is the transverse polarization of the Λ_0's [6, 12]. However, in this case a decrease is expected of its value with respect to what happens in p–p interactions since the transverse polarization is related to the production mechanisms of the Λ_0.

Acknowledgements. This work was supported by a binational research agreement CNPq/CONACYT under grant numbers 690176/02-3 and J200-652. J.M. is grateful for the warm hospitality at the Physics Department of CINVESTAV, where part of this work was done. L.M.M. is grateful for the kind hospitality at CBPF during the completion of this work

References

1. For a recent review on the suject, see U.W. Heinz, Hunting down the Quark Gluon Plasma in relativistic heavy-ion collisions, Proceedings of the Conference on Strong and Electroweak Matter (SEWM 98), Copenhagen, Denmark, edited by J. Ambjorn, P. Damgaard, K. Kainulainen, R. Rummukainen (World Scientific Publ. Co., Singapore 1999), p. 81
2. M. Jacob, J. Rafelski, Phys. Lett. B **190**, 173 (1987); M. Jacob, Z. Phys. C **38**, 273 (1988)
3. P. Koch, B. Müller, J. Rafelski, Phys. Rep. **142**, 167 (1986)
4. J. Adams et al. (STAR Collaboration), Phys. Rev. Lett. **92**, 182301 (2004)
5. T. Äkesson et al. (ISR-Axial-Field Spectrometer Collaboration), Nucl. Phys. B **246**, 1 (1984)
6. A. Ayala, E. Cuautle, G. Herrera, L.M. Montaño, Phys. Rev. C **65**, 024902 (2002); Rev. Mex. Fis. **48**, 549 (2002)
7. B. Povh, C. Scholz, K. Rith, F. Zersche, Particles and nuclei: an introduction to the physical concepts, p. 65 (Springer, Berlin 1995)
8. J.P. Blaizot, J.Y. Ollitrault, Phys. Rev. Lett. **77**, 1703 (1996)
9. I. Abt et al. (Hera-B Collaboration), Eur. Phys. J. C **29**, 181 (2003)
10. C. Adler et al. (STAR Collaboration), Phys. Rev. Lett. **89**, 092301-1 (2002)
11. J. Letessier, J. Rafelski, A. Tounsi, Phys. Lett. B **389**, 586 (1996)
12. A.D. Panagiotou, Phys. Rev. C **6**, 1999 (1986)